Dynamics and Stability of Pulses and Pulse Trains in Excitable Media

vorgelegt von Diplom-Physiker
Grigory Bordyugov
aus Saratov

Von der Fakultät II - Mathematik und Naturwissenschaften
der Technischen Universität Berlin
zur Erlangung des akademischen Grades
Doktor der Naturwissenschaft
- Dr. rer. nat. -
genehmigte Dissertation

Promotionsausschuss:
Vorsitzender: Prof. Dr. C. Thomsen
Berichter: Prof. Dr. H. Engel
Berichter: Prof. Dr. A. Pikovsky
Zusätzlicher Gutachter: Prof. Dr. B. Sandstede
Tag der wissenschaftlichen Aussprache: 20.10.2006

Berlin 2006
D 83

Abstract

The present Thesis deals with the dynamics and stability of pulses and spatially periodic pulse trains in excitable media. Such pulses represent nonlinear waves in active systems far from the thermodynamic equilibrium. They are very important for the understanding of such phenomena as the conduction of excitation in neuronal systems, intracellular calcium dynamics, electrical activity in the heart muscle, structure formation in the Belousov-Zhabotinsky reaction and many others.

We analyze two qualitatively different types of solitary pulses. The first one has a monotonous decay behind the high-amplitude pulse head and the second one decays in an oscillatory manner. This difference in the decay essentially influences the interaction between pulses in a spatially periodic pulse train or in a pulse pair.

The presence of the tail oscillations leads to the so far unknown coexistence of pulse trains of the same wavelength and different velocities. This coexistence is reflected in the bistable domains in the dispersion relation of spatially periodic pulse trains. A large part of the dissertation addresses the stability of the pulse trains in such bistable domains.

We show that oscillatory decay is typical for excitation pulses close to the transition between trigger and phase waves and describe several stages of the transition. First, we observe the emergence of small-amplitude damped oscillations in the wake of the solitary pulse under increase of the excitability of the system. Further increase of the excitability results in the emergence of undamped tail oscillations. Dispersion curve of spatially periodic pulse trains displays damped and undamped oscillations as well in accordance to the decay type behind the solitary pulse. The depiction of the transition between trigger and phase waves demanded a detailed analysis of the stability of the waves in the transition region.

We also studied pulses with monotonous tails under influence of non-local coupling. In numerous systems nonlocal coupling must be considered besides local diffusive coupling. Examples for such systems include brain tissue and electro-chemical reactions. We show that an arbitrary small, exponentially decaying nonlocal coupling leads to the emergence of bound states. The emergence of bound states is model-independent given that the model supports propagation of stable solitary pulses.

Zusammenfassung

Die vorliegende Dissertation handelt von der Dynamik und Stabilität von Pulsen und Pulsfolgen in erregbaren Medien. Diese Pulse stellen nichtlineare Wellen in aktiven Systemen fern vom thermodynamischen Gleichgewicht dar und sind wichtig für das Verständnis solcher Phänomene wie die Erregungsleitung in neuronalen Systemen, intrazelluläre Kalziumwellen, elektrische Erregungswellen im Herzmuskel, Musterbildung in der Belousov-Zhabotinsky Reaktion und viele andere.

Zwei qualitativ verschiedene Pulstypen werden untersucht. Bei dem ersten hat der Einzelpuls einen monotonen Ausläufer, während der zweite Typ kleinamplitudige Oszillationen im Ausläufer besitzt. Dieser Unterschied im Ausläufer des Einzelpulses beeinflusst wesentlich die Wechselwirkung zwischen Pulsen innerhalb einer räumlich periodischen Pulsfolge oder eines Pulspaares.

Die Oszillationen im Ausläufer verursachen die bislang unbekannte Koexistenz von Pulsfolgen mit gleicher Wellenlänge aber unterschiedlichen Ausbreitungsgeschwindigkeiten. Diese Koexistenz findet ihren Ausdruck in bistabilen Bereichen in der Dispersionskurve von räumlich periodischen Pulsfolgen. Ein grosser Teil der Dissertation befasst sich mit der Untersuchung der Stabilität der Pulsfolgen in den bistabilen Bereichen der Dispersionskurve.

Wir zeigen, dass Pulse mit oszillatorischen Ausläufern typischerweise in der Nähe des Übergangsbereiches zwischen Trigger- und Phasenwellen existieren und beschreiben mehrere Stufen dieses Überganges. Mit zunehmender Erregbarkeit entstehen zunächst gedämpfte Oszillationen im Ausläufer des Einzelpulses, die mit weiterer Zunahme der Erregbarkeit ungedämpft werden. In Übereinstimmung damit zeigen die räumlich periodischen Pulsfolgen gedämpfte bzw. ungedämpfte Oszillationen in der Dispersionskurve. Der Übergang wird durch eine Kollision der Dispersionkurven von Phasen- und Triggerwellen abgeschlossen. Die Beschreibung des Überganges erforderte Stabilitätsuntersuchungen von Trigger- und Phasenwellen im Übergangsbereich.

Pulse mit monotonen Ausläufern unter dem Einfluss von nichtlokaler Kopplung werden auch untersucht. In zahlreichen Systemen wie in neuronalen Geweben oder bei elektrochemischen Reaktionen sind neben kurzreichweitigen auch langreichweitige räumliche

Kopplungen zu berücksichtigen. Es wurde gezeigt, dass eine beliebig schwache, exponentiell abklingende nichtlokale Kopplung zur Ausbildung von Pulspaaren führt. Die Entstehung von Pulspaaren ist unabhängig vom verwendeten Modell, vorausgesetzt, dieses besitzt ohne nichtlokale Kopplung stabile Einzelpulse.

Acknowledgments

I am very thankful to Prof. Dr. Harald Engel for the possibility to complete my PhD Thesis in his group. He provided me with excellent working conditions for my research, and his professional help and guidance during the whole time can be hardly overestimated.

I would like to thank mathematicians Prof. Dr. Björn Sandstede, Prof. Dr. Arnd Scheel and Dr. Jens Rademacher since I really learned a lot from their papers and from our private communications.

Also I am very grateful to Georg Röder and Nils Fischer for their readiness to discuss and to continue some common research projects further.

For the nice working atmosphere in the group I would like to thank Jan Schlesner, Valentina Beato, Vladimir Zykov, Hermann Brandtstädter, Ingeborg Gerdes and Martin Braune.

The acknowledgment list would not be complete without Alexander Balanov, Natalia Janson, Olexandr Popovich, Markus Bär, Lutz Brusch, Oliver Rudzick, Vanessa Casagrande, Martin Falcke, Oliver Steinbock, Dmitry Turaev and Ernesto Nicola.

Contents

Chapter 1

Introduction

1.1 Overview of nonlinear wave phenomena

In 2002, a short article about the Mexican wave (or *La Ola*) was published by Nature [1]. The name of the phenomenon originates from the 1986 World Football Cup in Mexico. The Mexican wave represents a surge of people, rapidly rising from their seats; the wave propagates through the rows of audience in a stadium at an average speed 12 metres (or 20 seats) per second. Usually, one needs no more than a few dozens of people to ignite such a wave. This wave is essentially nonlinear, i.e. two Mexican waves do not interfere and cannot run through each other, which can be easily seen from the unwillingness of the participators to get up again immediately after the first wave. A quantitative treatment for this phenomenon was developed, and this treatment could accurately reproduce the details of the wave activity. On the homepage of the project[1] one can start an interactive simulation of the Mexican wave and play with the parameters, which are responsible for the propagation of the wave.

The apparent simplicity of the Mexican wave assumes a simple model, which can describe the phenomenon qualitatively. The audience, or the *medium*, consists of the individuals which need to be connected somehow in order to provide the wave propagation. Since the wave can propagate in both directions (clock-wise as well as counter clock-wise) around the football field, we can assume that the connection between the viewers is symmetric with respect to the left and right. A short consideration shows that the connection between the viewers is of the diffusional type: it means that the difference

[1] `http://angel.elte.hu/wave/`

Figure 1.1: Mexican Wave, Copyright: Walter Späth, http://photopage.de

between the own state and the states around is important. Small perturbations of the homogeneous background of sitting (standing) people in the form of a lonely standing (sitting) spectator tend to vanish.

The momentary status of a given viewer can be modeled by three qualitatively different states:

1. *Excitable*, or *inactive* state. In this state the spectator sits quiescently (also possibly after the previous wave) and is ready to get up. Upon seeing a number of rapidly rising neighbors, the spectator stands up as well and thus passes into the

2. *Excited* or *active* state. In this state the spectator can in turn to pass her/his excitation further, making the next people stand up.

3. After a pretty short period of the active state, the spectator sits down, and remains *refracter* for some time. Typically, people do not like to get up every second, so we have to wait some certain time before trying to ignite the next wave. The characteristic time that the spectator needs to take a breath is called the *refractory period* of the medium.

From this scheme we can deduce that the possible quantitative description of the current state must involve at least two variables, one of which has to be slow in order to account for the refractory period. One can consider the slow variable as the representation of the memory effect of the spectator.

The authors of the article stress that the emergence and propagation of the Mexican wave perfectly fits in the more general theory of the so-called *excitable media*, which describes nonlinear phenomena in many physical, chemical and biological systems [2, 3]. We would like to note that the term "excitable" is perhaps the most telling description of the Mexican wave phenomenon, since the audience in a football match is typically very emotional.

Plenty of interest in the phenomenon of excitability was triggered in the fifties of the twentieth century by the discovery of the famous auto-catalytic Belousov-Zhabotinsky reaction [4]. This reaction was first discovered to be oscillatory, i.e. the result of the reaction was the establishment of temporally periodic concentrations of the reagents. Sometimes the reaction is referred to as "chemical clocks". Under a certain choice of the chemical parameters, the homogeneous stationary state can be stable; however, the reaction can respond to small perturbations with a burst of activity, this is exactly what one refers to as excitability. The small perturbation can come, for instance, from the neighborhood of a given point through the diffusive flow of the reagents in the case if the solution is not stirred so that the gradients of concentrations can appear.

The Belousov-Zhabotinsky reaction has proven to be an excellent experimental model for studies of waves in reaction-diffusion systems. There are a number of particular versions of the reaction, the most important element of them is the presence of an acid and bromine. Usually, the experiments with the reaction are carried out either in a Petri dish or in the so-called open reactors, where it is possibly to keep the concentration of the reagents on the appropriate level. The reaction occurs under common laboratory conditions. The solution has different color and transparency depending on the concentration of the oxidized form of the catalyst. Typical timescales of the reaction can vary from a few dozens of second to several minutes and typical wavelengths of the patterns are several millimeters, which advantageously distinguishes this reaction from the Mexican wave in connection to the experiments and observations. The more recent versions of the Belousov-Zhabotinsky use a photo-sensitive catalyst, which make possible to control the reaction by means of light. A typical experimental set-up is thus pretty simple and consist of an open reaction together with a video camera and a beamer or a comparable device which can throw a given light pattern upon the medium. Characteristic wave patterns in the Belousov-Zhabotinsky reaction include solitary waves, wave trains, two-dimensional target patterns, spiral waves and scroll waves in three dimensions.

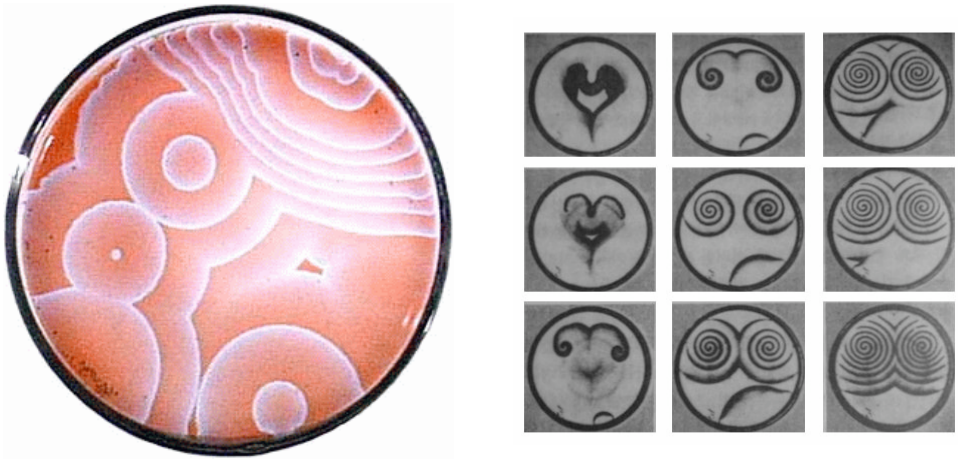

Figure 1.2: Left panel: A photograph of the Belousov-Zhabotinsky. Right panel: variety of patterns in the Belousov-Zhabotinsky reaction.

One of the first and most eminent contribution to the role of reaction-diffusion system in biology was made by Alan Turing [5]. He proved that a spatially homogeneous distribution of certain chemical substances, called *morphogens*, can become unstable due to the presence of diffusive coupling. This instability may lead to development of spatial structures and patterns, which include both standing and propagating waves. It was suggested that stationary waves in two dimensions can account for phyllotaxis (arrangement of leaves on the shoot of a plant) and can provide various stripe, circular and spot patterns of zebras, leopards, certain fishes and many other animals. In three spatial dimensions, the instability of a spherically symmetrical zygote can break the symmetry and lead to principally new forms of the growing organism. However, the stationary patterns predicted by Turing were experimentally observed in a chemical reaction only in 1990 [6]. The instability, which lead to the appearance of standing waves is now referred to as the *Turing instability*.

Another important example of non-linear phenomena is represented by calcium waves in living cells [7], which are believed to be one of the major signaling mechanisms. One distinguishes between four types of those: ultrafast, fast, slow and ultraslow calcium waves. The propagation of the fast calcium waves was found to be provided by the reaction-diffusion nature of the underlying processes. Again, a rich variety of dynamical behavior is reported, including the mentioned above spiral waves, which were found both in experiments and numerical simulations with the derived models. Recently, the role of

fluctuations in the calcium dynamics was demonstrated to be fundamental due to the relatively small number of interacting elements.

The propagation of neural activity was also found to be of reaction-diffusion type. Pulses of such activity in the axons of giant squids [8] were successfully modeled by a set of non-linear ordinary differential equations, which can be coupled diffusively in order to get a one-dimensional model of the axon. In this case, the equations describe the currents and potentials across the cell membrane rather then concentration of chemical species from the above examples. A simplification of the Hodgkin-Huxley model lead to the two-component FitzHugh-Nagumo system [9, 10], which is considered as the most generic model for an excitable medium and is capable to reproduce a plethora of non-linear wave phenomena.

Maybe the most important application of the theoretical studies of non-linear waves in excitable systems is the problem of ventricular fibrillation. This pathological malfunction of heart causes several hundred thousands deaths annualy in the USA only. In [11] it was proposed that ventricular fibrillation can be caused by multiple wave segments that propagate chaotically in the heart muscle. If the refractory period between two waves becomes shorter than the normal refractory period of healthy heart, the cells fail to respond. The initial model of the heart tissue was based on the cellular automata model, whereas in the meantime it is possible to study the problem using realistic reaction-diffusion heart models [12].

We would like to recall some recent theoretical and mathematical results on the wave propagation in reaction-diffusion systems. The most common tool to analyze the propagation of waves is the bifurcation theory for non-linear ordinary and partial differential equations. Considering one-dimensional systems, it is often possible to reduce the problem to the level of ordinary differential equation instead of solving the original PDE. The bifurcation theory for non-linear ODE (see [13] and numerous references within) insures that many wave phenomena in different systems can be classified in a relatively small number of known bifurcations. This often allows to make generic statements about the behavior of waves in dependence on the change of parameters of the system. We would like to mention a nice review on the theory of stability of travelling waves [14], which can be seen as the first reading suggestion for the recent results on the field.

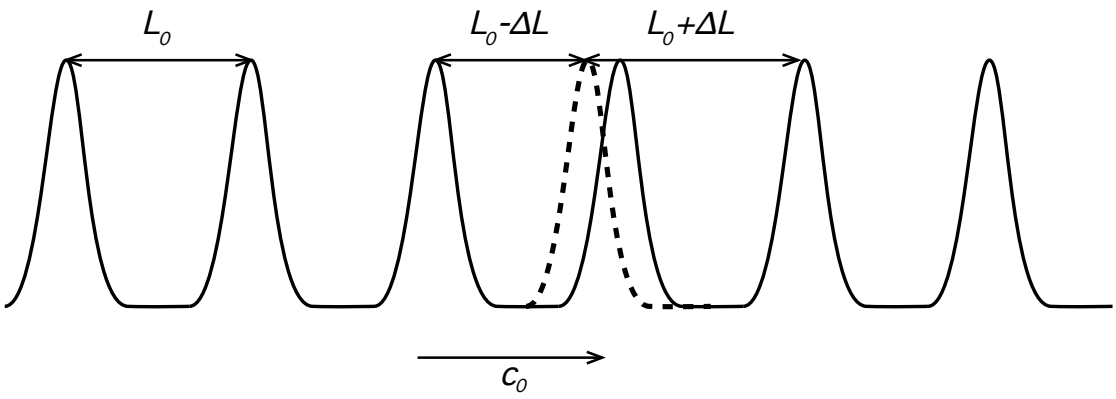

Figure 1.3: Kinematic approach to dispersion and pulse interaction in a pulse train, see text.

1.2 Statement of the problem

The central problem that the present Thesis deals with is the dynamics and stability of non-linear waves in excitable media.

Unlike classical waves (for instance, electromagnetic waves), non-linear waves can propagate either alone in form of solitary pulses or form pulse trains. In the latter case the velocity of pulses depends on the interpulse distance. In the case of spatially periodic pulse trains, all interpulse distances are equal and hence, typically, all pulses in the pulse train propagate at the same velocity. The so-called *(nonlinear) dispersion* relates the velocity of pulse train c with the interpulse distance L

$$c = c(L).$$

It is widely believed that the slope of the dispersion $\frac{d}{dL}c(L)$ determines the stability of the pulse train and the interaction between the pulses. Indeed, for the case of large interpulse distances $L \to \infty$, the interaction between the pulses is weak and mutual influence of pulses is reduced to small velocity corrections. The reason for this is that the pulses are strongly (actually, exponentially) localized in the space and can be thought of as particles, whose velocity depends only on the distance to the next one.

In order to illustrate this approach, which is often called kinematic approach [15], suppose for a moment that we have a pulse train of interpulse distance L_0 and velocity c_0. Suppose further that $\frac{d}{dL}c(L_0) > 0$. Now let us virtually shift one of the pulses in the pulse train by ΔL and look what happens in this case. The effective interpulse distance

in front of the shifted pulse increases $L_0 + \Delta L > L_0$. As a result, the velocity of the shifted pulse becomes larger, since $\frac{d}{dL}c(L_0) > 0$, which compensates the shift. So the perturbation in the form of shifting of individual pulses would decay with the time. It means in turn that a positive slope of the dispersion curve $c = c(L)$ corresponds to the stability of the pulse train with respect to the perturbation in a form of shifting of individual pulses.

The positive slope of dispersion implies also the repulsive interaction of two pulses under the assumption that the distance between two pulses is large. The first pulse in a pulse pair "sees" no pulse in front of it and hence propagates at the velocity of the solitary pulse. The second pulse is however always slower than the first one since there is always a finite distance to the first one. In this case one speaks about a repulsive interaction of pulses in a pulse pair.

The case of negative slope of the dispersion $\frac{d}{dL}c(L_0) < 0$ delivers a quite opposite result: the pulse train turns out to be unstable, since the shifted pulse becomes slower upon increase of the interpulse distance in front of it. Perturbations in the form of shifting of individual pulses do not decay. The periodicity of the pulse train tends to break up, whereas pairs of pulses are formed. Analogously, negative slope of the dispersion can lead to an attractive interaction between solitary pulses and to the formation of pulse pairs.

Suppose now that the slope of dispersion $c(L)$ changes the sign in dependence on L. This would mean that spatially periodic pulse trains can be either stable or unstable depending on the interpulse distance. The interaction between solitary pulses, either attractive or repulsive, would also depend on L.

The recent mathematical studies on the stability of pulse trains with large wavelengths [16, 17] rigorously prove the intuitive considerations above. The following important result was proven: the stability properties of a given pulse train can be unambiguously read off from the exponential tails of the corresponding solitary pulse. However, this result is applicable again *only* for large L.

The plethora of pulse interaction patterns was experimentally found in many physical, biological and chemical systems, see for example [18, 19, 20, 21, 22, 23, 24] (we will give more specific references in the following chapters). However, in many real experimental situations the interaction of pulses is not weak, in contrast the interaction can even be so strong that it can lead to merging of pulses or propagation failure. Thus

there is a clear need for the comprehensive study of pulse propagation, which can be conducted without the assumption on the large interpulse distance.

The aim of the Thesis is to describe the dynamics and stability of pulses and pulse trains in the domain of wavelengths where kinematic theory is not applicable and the interaction cannot be considered as weak. This means that we cannot reduce the problem of interaction to the "particle" level, i.e. we have to solve the existence and stability problems with respect to the whole underlying partial differential equation. We use the results of the large wavelength limit in order to check the numerous computational methods and compare our numerical results with the analytically known expressions for $L \to \infty$.

More specifically, the results of the thesis can be classified in two cases, depending on the decay properties of the solitary pulse. In the first case, the solitary pulse has an oscillating decay, which gives rise to complicated dynamics of both solitary and periodic waves. The oscillatory wake is provided by the complex-conjugate eigenvalues of the linearization in the rest state in the profile equation. We report on the bistable dispersion curve for periodic wave trains and discuss the stability of the corresponding waves. Moreover, we found that the aforementioned emergence of small amplitude oscillations occurs close to the transition between trigger and phase waves. We extensively describe the bifurcation scenario of this transition and present numerous results on their stability.

The second case is presented by pulses with monotonous decay, which propagate in an excitable medium subjected to non-local coupling. This type of coupling can be reformulated in terms of an additional reaction-diffusion equation, which is coupled to the original system. The presence of non-local coupling affects the decay properties of monotonous wake behind the pulse and makes possible the emergence of bound states (or pulse pairs). For this case, we show that the emergence of bound states is model-independent and is provided only by the exponentially decaying coupling kernel. We discuss the stability of the corresponding pulse trains and bound states in details.

1.3 Grasshopper's guide to the Thesis

This thesis consists of the introduction, four chapters and conclusion.

1. The first chapter is the Introduction.

2. The second chapter can be divided in two unequal parts. In the first part we will

give a brief introduction to reaction-diffusion systems. Excitable and oscillatory media will be considered in more detail. We will introduce the modified Oregonator model, which was originally derived to describe the light-sensitive Belousov-Zhabotinsky reaction. We will also show that the Oregonator model is capable to reproduce two main types of the local dynamics, namely, excitable and oscillatory, which allows us to use it for the study of different wave types. Then we will proceed to the coherent structures approach, which makes possible to reduce the problem from the level of partial differential equations to ordinary differential equations, that describe the profile of the wave. In particular, we will be interested in solitary waves and the accompanying periodic wave trains with large spatial period. Such waves correspond to the so-called homoclinic and periodic orbits with large period in the profile equation. With the known profile and velocity of the wave, we will turn to the question of its stability. The description of the stability theory for different wave types and boundary conditions completes the second chapter.

3. In the third chapter, we discuss the bistability of periodic wave trains due to anomalous oscillatory dispersion, which is distinguished by the presence of bistable domains. In such domains alternative stable pulse trains with the same wavelength and different velocities coexist. We present a detailed study of the stability of the coexisting pulse trains in the bistable domains. The phenomenon of bistability is found to be provided by the oscillatory recovery of excitations which causes small amplitude oscillations in the refractory tail of pulses. Crucial for the bistability is that the pulses in the trains are locked into one oscillation maximum in the tail of the preceding pulse in the train. It is found that such regime is typical for excitable media close to the transition to oscillatory local dynamics through a supercritical Hopf bifurcation, followed by a canard explosion of the limit cycle. This fact connects the phenomenon of bistability with the transition between trigger and phase waves.

4. In the fourth chapter, we will present new results on the transition between trigger and phase waves, which represent the "natural" waves for excitable and oscillatory kinetics, respectively. In many system the local dynamics can be switched between oscillatory and excitable with a single parameter. For example, the light-sensitive Belousov-Zhabotinsky reaction demonstrate oscillatory kinetics for low intensity of the applied light and excitable kinetics for high values of the light intensity. In

this section, we consider the Oregonator model as the representative example of the systems with both types of kinetics. Trigger and phase waves are thoroughly studied close to and in the transition region. It turns out that both types of waves are connected in the small-wavelength region and we can precisely define the point where the transition between them takes place. The central object of our analysis in this chapter is homoclinic orbits and accompanying periodic orbits close to a codimension-2 Shilnikov-Hopf bifurcation. The presence of small-amplitude oscillations in the wake of the pulse close to the Shilnikov-Hopf bifurcation is reflected in a wiggly dispersion curve. We support our analysis of the transition by the stability studies of both types of waves and numerical simulation of the destruction of the waves due to the switching of the parameter through the boundary.

5. The fifth chapter is devoted to the effect of non-local (or long-range) coupling on the propagation of solitary pulses and periodic wave trains in purely excitable media. This coupling represents long-range connections between the elements of the medium; the connection strength decays exponentially with the distance. Without coupling, pulses interact only repulsively and bound states with two or more pulses propagating at the same velocity are impossible. Upon switching on non-local coupling, pulses begin to interact attractively and form bound states. First we present numerical results on the emergence of bound states in the excitable Oregonator model for the photosensitive Belousov-Zhabotinsky reaction with non-local coupling. Then we show that the appearance of bound states is provided solely by the exponential decay of non-local coupling and thus can be found in a wide class of excitable systems, regardless of the particular kinetics. The theoretical explanation of the emergence of bound states is based on the bifurcation analysis of the profile equations that describe the spatial shape of pulses. The central object is a codimension-4 homoclinic orbit which exists for zero coupling strength. The emergence of bound states is described by the bifurcation to 2-homoclinic solutions from the codimension-4 homoclinic orbit upon switching on non-local coupling.

6. In the last section, we make the conclusions to the results of the work and suggest possible directions for further studies.

Chapter 2

Nonlinear waves in reaction-diffusion systems

2.1 Reaction-diffusion systems

As we have already mentioned in the introduction, the main motivation for the so-called *reaction-diffusion* systems came from the discovery of the oscillating Belousov-Zhabotinsky reaction in the fifties of the twentieth century. However, already in 1920 Lotka suggested that the following hypothetical chemical autocatalytic reactions

$$\begin{aligned} A + X &\to 2X, \\ X + Y &\to 2Y, \\ Y &\to P \end{aligned} \tag{2.1}$$

can lead to the emergence of temporal oscillations of the concentration of reagents X and Y [25]. Nevertheless, the oscillations in the system given by (2.1) are not *limit cycle* oscillation. In contrast, the oscillatory regime is sensitive to the initial conditions and starting the reaction from different concentrations of X and Y leads to different temporal evolutions of the reaction.

In the beginning of the seventies, another chemical reaction was proposed in Brussels

$$\begin{aligned} A &\to X, \\ B + X &\to Y + D, \\ 2X + Y &\to 3X, \\ X &\to E, \end{aligned} \tag{2.2}$$

which allowed for the limit cycle behavior [26, 27, 28]. This "Brusselator" reaction was shown to exhibit complex spatial and temporal structures in a good comparison to the experiments.

2.1.1 Oregonator model for BZ reaction

In 1972, Field with co-authors came up with a new and relatively simple explanation of the Belousov-Zhabotinsky (BZ) reaction, which is believed to include more than 20 intermediate steps [29, 25]. The main idea was to understand that there are two independent processes A and B that can occur in the solution, depending on the bromide ion concentration. Above a critical concentration, the process A dominates, otherwise the dominant process is B. Oscillations are possible due to the fact that the process A consumes the bromide ion and the process B produces it.

The Field-Körös-Noyes (FKN) mechanism of the Belousov-Zhabotinsky reaction is given by

$$\begin{aligned} A + Y &\rightleftharpoons X, \\ X + Y &\rightleftharpoons P, \\ B + X &\rightleftharpoons 2X + Z, \\ 2X &\rightleftharpoons Q, \\ Z &\rightleftharpoons fY. \end{aligned} \tag{2.3}$$

The double-arrows denote the reversibility of the reactions and f is the stoichiometric factor, which must be determined to provide a zero net production of X, Y and Z. Here, the identities are

$$\begin{aligned} X &\equiv HBrO_2, \\ Y &\equiv Br^-, \\ Z &\equiv Ce(IV), \\ A &\equiv B \equiv BrO_3^-. \end{aligned} \tag{2.4}$$

By the law of mass action (see Appendix) and appropriate rescaling of the variables, one obtains the following three equations for dimensionless variables $\alpha \propto X, \eta \propto Y$ and

$\rho \propto Z$:

$$\begin{aligned} \dot{\alpha} &= s(\eta - \eta\alpha + \alpha - q\alpha^2), \\ \dot{\eta} &= s^{-1}(-\eta - \eta\alpha + f\rho), \\ \dot{\rho} &= w(\alpha - \rho). \end{aligned} \tag{2.5}$$

The parameters s, w and q are determined from the rates of the reactions, see [29, 25].

Krug et al. introduced in [30] the modified Oregonator model, which describes the light sensitivity of the Belousov-Zhabotinsky reaction. For this purpose, the reaction scheme (2.3) was extended by a simple reaction, corresponding to the light-induced bromide flow

$$\xrightarrow{\Phi} Y,$$

which leads to the modified three-component Oregonator model, given by

$$\begin{aligned} \epsilon\dot{x} &= x(1-x) + y(q-x), \\ \epsilon'\dot{y} &= \phi + fz - y(q+x), \\ \dot{z} &= x - z. \end{aligned} \tag{2.6}$$

The parameter ϕ accounts for the light intensity. The following parameter values were suggested: $q = 2 \times 10^{-3}, f = 2.1, \epsilon = 0.05, \epsilon' = \epsilon/8$. With this set of parameters, it was found that for $\phi = 1.762 \times 10^{-3}$ the stable equilibrium in Eq. (2.6) undergoes a Hopf bifurcation, thus giving access to both excitable (monostable) and oscillatory reaction kinetics upon variation of the parameter ϕ near the bifurcation value.

Often, one can exploit the smallness of the parameter ϵ' and set the left-hand side of the second equation in Eq. (2.6) equal zero. In this case the model can be further reduced to the so-called two-component version of Oregonator, which reads

$$\begin{aligned} \dot{u} &= \frac{1}{\epsilon}\big[u - u^2 - (fv + \phi)\frac{u-q}{u+q}\big], \\ \dot{v} &= u - v. \end{aligned} \tag{2.7}$$

We would like to mention that Eq. (2.7) is qualitatively similar to the FitzHugh-Nagumo equation [9, 10], which describes the propagation of the action potential in the squid axons.

For spatially extended Belousov-Zhabotinsky reaction we must account for diffusion:

$$\begin{aligned} \partial_t u &= \frac{1}{\epsilon}\big[u - u^2 - (fv + \phi)\frac{u-q}{u+q}\big] + D\Delta u, \\ \partial_t v &= u - v. \end{aligned} \tag{2.8}$$

The u variable is supposed to diffuse, whereas the catalyst v is often immobilized in a gel matrix. Since there is only one diffusive variable, we can always rescale the space and set the diffusive coefficient $D = 1$. Eq. (2.8) represents a typical reaction-diffusion system, which can be generalized for the case of N species as

$$\partial_t u = f(u; p) + D\Delta u, \quad u \in R^N, \quad p \in R^P. \tag{2.9}$$

Here, $f(u; p)$ denotes the non-linear local dynamics (or, equivalently, *kinetics*), which can be controlled by P parameters p. The matrix $D = \mathrm{diag}(d_j), j = 1, \ldots, N$ with non-negative entries describes the local diffusive coupling between the elements of the medium.

2.1.2 Excitable and oscillatory Oregonator kinetics

The Oregonator kinetics

$$\begin{aligned} \dot{u} &= F(u, v) := \frac{1}{\epsilon}\big[u - u^2 - (fv + \phi)\frac{u - q}{u + q}\big], \\ \dot{v} &= G(u, v) := u - v \end{aligned} \tag{2.10}$$

belongs to the wide class of activator-inhibitor models with two well-separated time scales (ϵ is assumed to be small) and a typical "s"-shaped nullcline $F(u, v) = 0$. The Oregonator kinetics (2.10) has only one fixpoint, which can be either stable or unstable, which roughly corresponds to the excitable and oscillatory kinetics, respectively.

In what follows we discuss two types of the Oregonator kinetics (excitable and oscillatory) in more detail. We fix the following parameters values

$$\epsilon^{-1} = 20, \quad f = 2.1, \quad q = 0.002.$$

Excitable kinetics is distinguished by the stability of the fixed point, which is given by the intersection of both nullclines. The linear stability of the equilibrium implies that small perturbations decay. However, introducing a supra-threshold perturbation, it is possible to get a large-amplitude response from the excitable system.

A typical large-amplitude response is qualitatively depicted in Fig. 2.1 (a). There are four phases of the excitation excursion in the phase space of the excitable system:

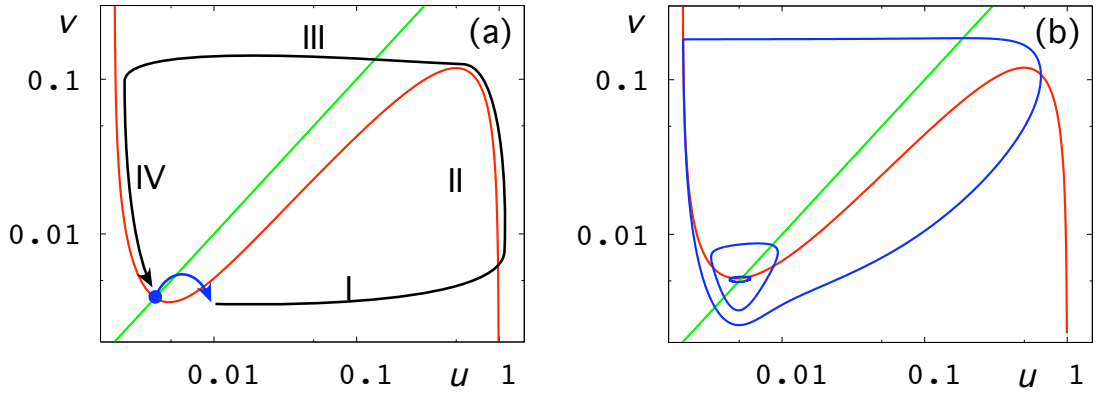

Figure 2.1: (a) Nullclines of an excitable system in logarithmic scale. The red (green) line represents the $F(u,v)=0$ ($G(u,v)=0$) nullcline, respectively. The blue arrow denotes a supra-threshold perturbation which is needed to trigger an excitation. The black curve qualitatively represents the excitation excursion. (b) Limit cycles in the Oregonator kinetics (blue lines). The red (green) line represents the $F(u,v)=0$ ($G(u,v)=0$) nullcline, respectively. Note that their intersection is very close to one of the extrema of the red $F(u,v)=0$ nullcline. This plot is in logarithmic scale in both u and v. The smallest limit cycle corresponds to $\phi = 1.0\times10^{-3}$, the largest to $\phi = 7.0\times10^{-4}$ and the middle to $\phi = 8.3\times10^{-4}$.

1. Usually, one needs to perturb the variable u about the middle branch of the nullcline $F(u, v) = 0$ in order to get an excitation. After the perturbation, the phase trajectory rapidly jumps to the right branch of the $F(u, v) = 0$ nullcline (part I in Fig. 2.1 (a)).

2. After that, the trajectory slowly moves along the nullcline up to its extremum (part II in Fig. 2.1 (a)).

3. At the maximum of the nullcline the trajectory jumps rapidly to another branch of the nullcline again (part III in Fig. 2.1 (a)).

4. Then the phase point slowly relaxes to the stable equilibrium (part IV in Fig. 2.1 (a)). It is impossible to trigger a new excitation before the system is sufficiently close to the equilibrium.

The separation between the fast parts (I and III) and slow parts (II and IV) of the excursion is provided by the small parameter ϵ.

Oscillatory kinetics The stable fixed point can undergo a supercritical Hopf bifurcation at some value of the parameter $\phi_{hb} = 1.04 \times 10^{-3}$. Under further decrease of ϕ the stable limit cycle passes through a so-called canard explosion at ϕ_c and its size rapidly grows up. In Fig. 2.1 (b) we present different limit cycles at different values of the parameter ϕ. A detailed theoretical analysis of the canard behavior and its relation to the excitability properties of the spatially extended system can be found in [31].

2.2 Profile equations

For some simple reaction-diffusion systems it is possible to analyze propagation of waves considering only the kinetics of the system. For example, in [32] the authors calculated the velocity of waves projecting the dynamics of the PDE on the phase space of a single excitable element. The main idea was to calculate the velocities of the front and back of the wave in dependence on the slow variable and find the conditions, under which both velocities are equal. However, under many circumstances we can not just "forget" about the diffusive coupling and treat the problem only from the viewpoint of the kinetics.

In what follows we present an approach which allows to reduce the reaction-diffusion system from PDE to an ODE, which describes the profile of the wave. The only as-

sumption that we need is that the wave propagates at a constant velocity and without changing its profile. We will obtain equations, in which the evolution variable is represented by the spatial coordinate, giving the profile as a function of space. Thus the stability of the solutions of the profile equation are irrelevant for the stability of the wave with respect to the full PDE.

2.2.1 Co-moving frame approach

Suppose that we have a reaction-diffusion equation with N species U and kinetics F

$$\partial_t U = F(U) + D\,\partial_{xx} U, \tag{2.11}$$

with a diffusion matrix $D = \mathrm{diag}(d_j), j = 1, \ldots, N$ with non-negative entries. In a moving frame $z = x - Ct$ with velocity C we have to transform

$$U(x,t) \to U(x - Ct, t) = U(z,t),$$

and Eq. (2.11) reads

$$\partial_t U = F(U) + C\,\partial_z U + D\,\partial_{zz} U. \tag{2.12}$$

We make now an assumption that will be very important for our whole considerations later or. We interested only in those solutions $U(z,t)$ to Eq. (2.12) that propagate with a certain velocity $C = c$ without changing their profile. It means that in Eq. (2.12) with $C = c$ they are stationary solutions, i.e. $\partial_t U = 0$. They thus obey the following ODE

$$F(U) + c\,U' + D\,U'' = 0, \tag{2.13}$$

where the prime denotes a derivative with respect to the moving coordinate z.

We obtained an ordinary differential equation (2.13) which governs the spatial profile of the solution $U(z)$. We cast this profile equation as a system of first-oder ODE. For those components U_i of U that diffuse we have

$$d_i U_i'' + c U_i' + F_i(U) = 0,$$

which leads to two first-order equations

$$\begin{aligned} U_i' &= V_i, \\ V_i' &= -d_i^{-1}(cV_i + F_i(U)). \end{aligned}$$

For those species U_i that do not diffuse ($d_i = 0$), the equation reads

$$U_i' = -c^{-1} F_i(U).$$

We obtain a set of $k, N \leq k \leq 2N$ ordinary differential equations of first order.

Often it is more advantageous to assume that all N species diffuse, but some of the diffusional constants d_j are vanishingly small. In this case the structure of the first-order ODE system is more regular, which simplifies analytical manipulations with the equations and implementation of numerical methods. For the sake of simplicity, we write the system of the profile equation as

$$u' = f(u; c), \quad u \in \mathbb{R}^{2N},$$

where $f(u; c)$ is accordingly adapted right hand-sides of the equations above. We emphasize that the dependence of the function $f(u; c)$ on the velocity c is essential: We have to tune the parameter of nonlinearity in order to obtain the correct solution. Physically that means that for a given reaction-diffusion system the wave typically propagates at a certain velocity c. Upon changing parameters of the reaction-diffusion system, for instance, the diffusion coefficients, the propagation velocity c changes as well. From the viewpoint of dynamical systems, the solutions of the profile equation are usually of codimension-1.

2.2.2 Some examples of travelling waves

Homogeneous states are the simplest class of the solutions to the profile equation. Their existence just follows from the fact that every equilibrium of the kinetics is an equilibrium in the profile equation (2.13) for every velocity c.

Periodic wave trains of wavelength L are represented by limit cycles of period L in the profile equation. Here, the dependence on the velocity c is essential. In fact, we have the following boundary-value problem

$$\begin{aligned} F(U) + c\,U' + D\,U'' = 0, \quad 0 < z < L, \\ U(L) = U(0), \end{aligned} \tag{2.14}$$

solutions of which depend, of course, on the velocity c, which plays the role of the parameter to be solved for in order to fulfill the boundary conditions. We can also

consider the first-order formulation, using the rescaled variable $\zeta = z/L$, we obtain then

$$\begin{aligned} &\partial_\zeta u = Lf(u;c), \quad u \in \mathbb{R}^{2N}, \quad 0 < \zeta < 1, \\ &u(1) = u(0) \end{aligned} \tag{2.15}$$

where the prime denotes a derivative with respect to ζ. Usually we expect that periodic wave trains come in families, depending on the wavelength L, we denote the corresponding dependence of the velocity on the wavelength

$$c = c(L)$$

as the *nonlinear dispersion relation* for spatially periodic wave trains. It turns out that the slope of the dispersion curve

$$\frac{d}{dL}c(L)$$

is of certain importance for their stability properties and interaction between waves in a wave train.

Solitary pulses and bound states are represented by homoclinic orbits in the profile equation. They converge to the same asymptotic value U_0 as $z \to \pm\infty$. They propagate at a certain velocity c, which is reflected by the fact that the homoclinic orbits are of codimension-1 in the profile equations.

Solitary pulses are accompanied by families of spatially periodic wave trains. The asymptotic profile of the solitary pulse plays a crucial role for the dispersion relation of the wave trains of large wavelength. We will discuss this in more detail in the next section.

Under certain conditions, solitary pulses can form so-called *bound states* with two or more pulses propagating at the same velocity. Such bound states are described by N-homoclinic orbits in the profile equations. There is a number of bifurcations which can produce N-homoclinic orbits, given the 1-homoclinic orbit exists; we will comment on this later on.

Fronts can be seen as a generalization of solitary pulses in the sense that they are spatial structures connecting two *different* asymptotic states for $z \to \pm\infty$. The asymptotic states can be either homogeneous states or periodic wave trains. For fronts the uniqueness of the propagation velocity is sometimes violated. For the same parameters of the kinetics there can coexist different fronts with different profiles and propagation velocities, see [33].

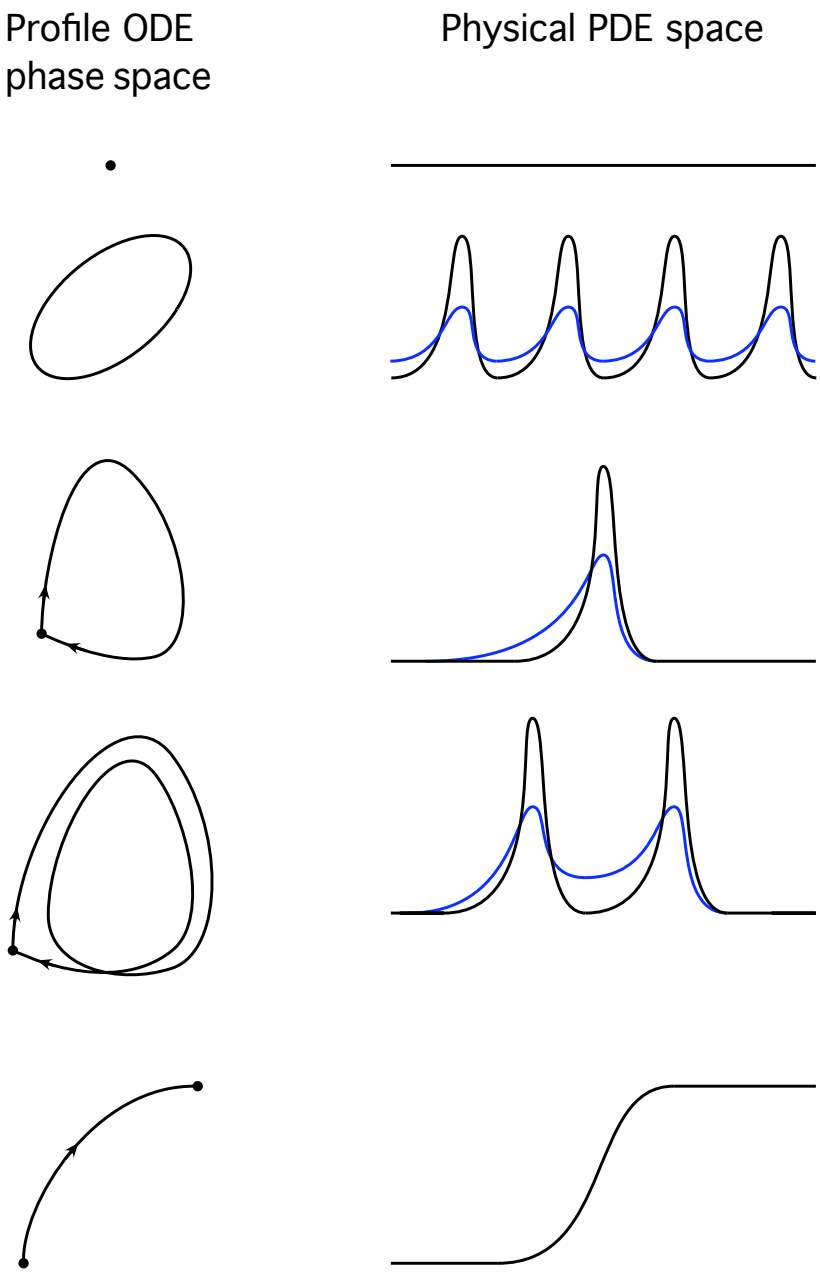

Figure 2.2: Representation of different travelling patterns in the phase space of the profile ODE.

2.3 Homoclinics and accompanying periodic orbits

In this section we consider special biasymptotic solutions to an ordinary differential equation

$$u' = f(u;p), \quad u \in \mathbb{R}^N, N \geq 2 \tag{2.16}$$

with a parameter p.

In what follows we use t as the evolution variable of Eq. (2.16) in order to be able to speak about the evolution in "forward" and "backward" time. In the equations that describe the profile of a wave solution in the reaction-diffusion system we use the co-moving coordinate z as the evolution variable.

For the sake of simplicity we assume that $f(0;p) = 0$ for all p, i.e. the equation has an equilibrium at zero. We will call the *stable manifold* W^s all solutions that converge to the equilibrium forwards in time (i.e. for $t \to \infty$) and the *unstable manifold* W^u all solutions that converge to the equilibrium backwards in time (i.e. for $t \to -\infty$).

We are interested in such solutions $q(t)$ to Eq. (2.16), which asymptotically approach the equilibrium in both forward and backward time

$$\lim_{t \to \pm\infty} q(t) = 0. \tag{2.17}$$

These solutions are called *homoclinic solutions*. Clearly, the homoclinic solutions belong to the intersection of the stable manifold W^s and the unstable manifold W^u of the equilibrium.

We consider homoclinic solutions to a hyperbolic equilibrium, it means that the dimensions of the stable and unstable manifolds sum up to the dimension of our phase space N. This means that the codimensions[1] of the stable and unstable manifolds also sum up to N. It is also known that the codimensions of two intersecting manifolds sum up (at most) to N, where N is exactly achieved only for transversal[2] intersections[3]. However, the intersection of the stable and unstable manifold is not transversal, since the

[1] We denote the difference between the dimension of the space N and the dimension of a given object (manifold or subspace) as its *codimension*, i.e. $\operatorname{codim} A = N - \dim A$.

[2] An intersection of two manifolds in $\mathbb{R}^N$ is called *transversal* if in every point of the intersection there exist N linearly independent vectors which are tangent to one of both manifolds.

[3] In $\mathbb{R}^2$, for instance, a line is of dimension 1 and of codimension 1. If the intersection of two lines is transversal than the codimension of the intersection (a point in this case) is $1+1 = 2$, for non-transversal intersection this does not hold. For example, two co-axial circles intersect only non-transversally, resulting in an intersection of dimension 1 and codimension 1.

bounded solution v to the linearized equation (see Eq. (2.18) below) is tangent to both stable and unstable manifold for every intersection point (i.e. belonging to the homoclinic orbit). It means that we can find only $N-1$ linearly independent vectors, which are tangent to one of both manifolds. The non-transversality of the intersection means that this intersection does not persist under parameter change, i.e. is *not structurally stable*. In the connection to travelling waves, we have always to tune the velocity c in order to obtain the corresponding homoclinic connection.

For the further study of homoclinic orbits the solutions of two linear equations are of certain importance. First, one assumes that there exists an unique solution to the linearized equation

$$v' = \mathcal{A}(t)v, \quad \text{where} \quad \mathcal{A}(t) = \partial_u f(q(t)), \tag{2.18}$$

given by $v = q'(t)$ (this can be seen taking a derivative with respect to t of Eq. (2.16)) and an unique solution to the adjoint variational equation

$$\psi' = -\mathcal{A}^*(t)\psi, \tag{2.19}$$

We can immediately see that the solution $\psi(t)$ to Eq. (2.19) is always perpendicular to the solution $v(t)$ of the variational equation Eq. (2.18). We consider

$$\begin{aligned} \frac{d}{dt}\langle v, \psi\rangle = & \\ &= \langle v', \psi\rangle + \langle v, \psi'\rangle = \\ &= \langle \mathcal{A}(t)v, \psi\rangle - \langle v, \mathcal{A}^*(t)\psi\rangle = \langle \mathcal{A}(t)v, \psi\rangle - \langle \mathcal{A}(t)v, \psi\rangle = \\ &= 0 \end{aligned} \tag{2.20}$$

together with

$$\langle v, \psi\rangle\big|_{\pm\infty} = 0$$

which leads to

$$\langle v, \psi\rangle = 0$$

for all t.

So the solution $\psi(t)$ of the adjoint equation is always perpendicular to the solution of the linearized equation (2.18). Moreover, one can show that $\psi(t)$ is perpendicular to the tangent spaces of both the stable and unstable manifolds of the equilibrium [13]. With the help of $\psi(t)$ one defines the *orientation* of the homoclinic orbit as

$$\mathcal{O}(q) = \lim_{t\to\infty} \operatorname{sign}\langle \psi(t), q(-t)\rangle \cdot \langle \psi(-t), q(t)\rangle, \tag{2.21}$$

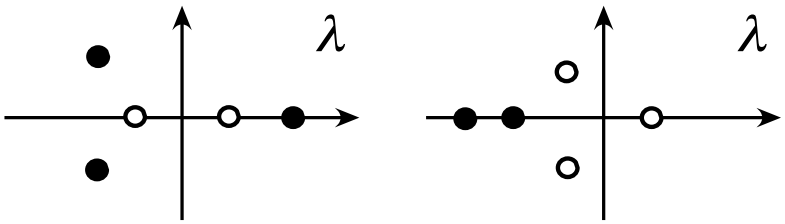

Figure 2.3: Left: Real leading eigenvalues. Right: leading stable eigenvalues are complex conjugate.

if this limit exists, see [34].

The asymptotic flow near the equilibrium is given by

$$v' = \mathcal{A}(0)v. \tag{2.22}$$

Since $f(u)$ is a real-valued function, the eigenvalues of the matrix $\mathcal{A}(t)$ are either real or complex-conjugate. Moreover, we assume that the equilibrium is hyberbolic, which means that $\mathrm{spec}(\mathcal{A}(0)) \cap i\mathbb{R} = \emptyset$. The closest to the imaginary axis eigenvalues (i.e. with smallest real parts) of the linearization in the equilibrium $\mathcal{A}(0)$ are called leading stable and leading unstable eigenvalues. The corresponding eigenvectors are called leading stable and unstable eigenvectors. For a codimension-1 homoclinic orbit the leading stable (unstable) eigenvector is tangent to the stable (unstable) manifold in the equilibrium, respectively.

We define also a *saddle quantity* σ of a saddle or saddle-focus as the sum of the real parts of the leading eigenvalues.

Two types of homoclinic solutions can be distinguished pretty artificially. The first one is represented by the so-called 1-homoclinics, with a single loop of the phase trajectory. The second class is the 2- and N-homoclinics, with the phase trajectory following the primary loop 2 or N times. In the context of pulses in excitable systems N-homoclinics describe bound states with N pulses, which propagate at the same velocity. Sometimes we will refer to both 2- and N-homoclinics as merely N-homoclinic solutions.

There is another classification of homoclinic orbits, depending on the type of the leading eigenvalues of $\mathcal{A}(0)$. For a general homoclinic orbit of codimension-1 the leading eigenvalues determine the asymptotical behavior for $t \to \pm\infty$. If the leading stable (unstable) eigenvalues are complex-conjugate, the homoclinic orbit approaches the equi-

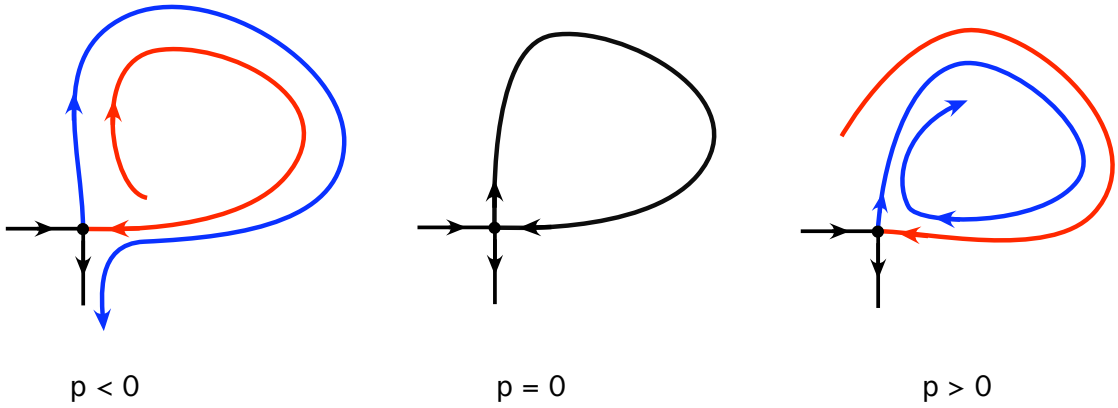

Figure 2.4: Unfolding of homoclinic bifurcation in $\mathbb{R}^2$ for saddle quantity $\sigma < 0$. Red curve denotes the stable manifold W^s of the equilibrium, blue curve denotes the unstable manifold W^u of the equilibrium.

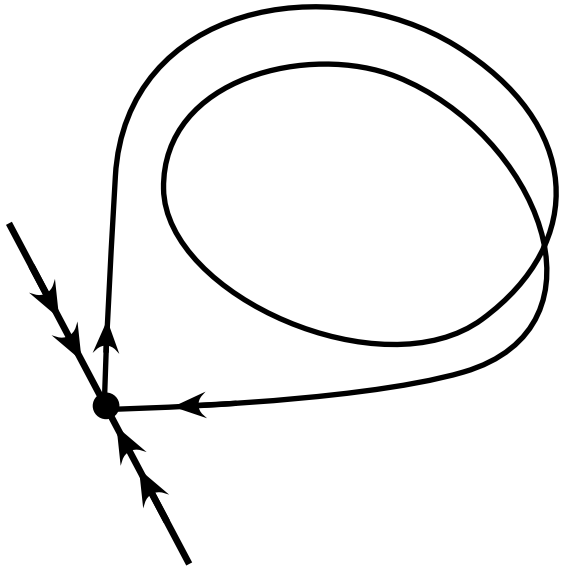

Figure 2.5: 2-homoclinic orbit.

librium in an oscillating manner for $t \to -\infty$ ($t \to +\infty$), respectively. It turns out that oscillating asymptotic behavior of a homoclinic orbit has a great impact on the properties of the homoclinics and possible bifurcations of it.

Homoclinic solutions are accompanied in the parameter space by periodic solutions. One of the most important theoretical results on the accompanying periodic solutions is that their period exponentially scales the distance to the homoclinic orbit in the parameter space. For the solitary pulses in reaction-diffusion systems it means the following: the velocity of a periodic wave train depends exponentially on its wavelength.

One can summarize the results on the accompanying periodic orbits:

1. For real leading eigenvalues there exist one limit cycle close to the primary homoclinic orbit independently on the saddle quantity σ.

2. For complex-conjugate eigenvalues there exist one limit cycles close to the primary homoclinic orbit for $\sigma < 0$ and infinitely many of them for $\sigma > 0$.

More specifically, the following relation between the bifurcation parameter p and period of limit cycle L

$$p = p_0 + \frac{1}{M}\Big[\langle\psi(-L), q(L)\rangle - \langle\psi(L), q(-L)\rangle\Big] \tag{2.23}$$

holds for large L. The homoclinic bifurcation is given by $p = p_0$. Here, $q(z)$ and $\psi(z)$ denote the homoclinic solution and the bounded solution to the adjoint problem, respectively. The constant M is a Melnikov integral, given by

$$M = -\int_{-\infty}^{\infty} \langle\psi(z), \partial_p f(q(z), p_0)\rangle\, dz \neq 0.$$

We note that, depending on the sign of σ one of the scalar products in (2.23) dominates over the other one, which allows to consider only one of them.

The found dependence of the period of limit cycles on a parameter close to a homoclinic orbit is important for the dispersion relation of periodic wave trains, which accompany the solitary pulse. In application to the profile equation, the relative velocity of the wavetrain c plays the role of the parameter p. The period of the limit cycles is the wavelength L of the spatially periodic wavetrain. The dependence of the wave train velocity c on L for large L reads then

$$c = c_0 + \frac{1}{M}\Big[\langle\psi(-L), q(L)\rangle - \langle\psi(L), q(-L)\rangle\Big], \tag{2.24}$$

where c_0 is the velocity of solitary pulse. For pulses, the sign of the saddle quantity σ determines whether the front or the back of the pulse decays slower. The sign of the scalar products can be estimated for large L, where $\psi(\pm L)$ and $q(\pm L)$ can be read off from the eigenvectors of the matrix $\mathcal{A}(0)$.

In the following subsections we will shortly review some well-known results on the homoclinic orbits for the case of real and complex-conjugate leading eigenvalues.

2.3.1 Real leading eigenvalues

For the sake of simplicity, we consider a homoclinic orbit to an equilibrium with real leading eigenvalues in a three-dimensional phase space, i.e. $N = 3$. The 3×3 matrix $\mathcal{A}(0)$ has three real eigenvalues $-\lambda_{ss} < -\lambda_s < 0 < \lambda_u$. However, for a codimension-1 homoclinic orbit, the dynamics is effectively only two-dimensional and sometimes we may consider Eq. (2.16) only in $\mathbb{R}^2$.

Let us recall three general assumptions on the homoclinics of codimension one [13]:

1. the leading eigenvalues are not in resonance $\lambda_u \neq \lambda_s$,
2. the solution $v(t)$ to the linearized problem Eq. (2.18) converges to zero along the leading eigenvectors of the linearization in the fixed point and
3. the same applies to the solution $\psi(t)$ of the adjoint problem Eq.(2.19).

The last assumption is sometimes called *the strong inclination property*, for homoclinic orbit in $\mathbb{R}^3$ it means that the two-dimensional stable manifold comes to the fixed point tangent to the strong stable direction (see Fig. 2.6 and Fig. 2.7). A homoclinic orbit of codimension-1 can be orientable or twisted, depending on the orientation of the strip of the two-dimensional manifold, which can be characterized by the orientation $\mathcal{O}(q)$, see Eq. (2.21). The stable manifold is topologically either a cylinder or a Möbius strip. The orientation of a homoclinic orbit can be changed upon one of the codimension-2 bifurcations.

Codimension-2 bifurcations

If one of the assumption on the codimension-1 homoclinic orbit fails, one speaks of a codimension-2 bifurcation. There are three kinds of those:

1. resonance homoclinic orbit, characterized by $\lambda_s = \lambda_u$,

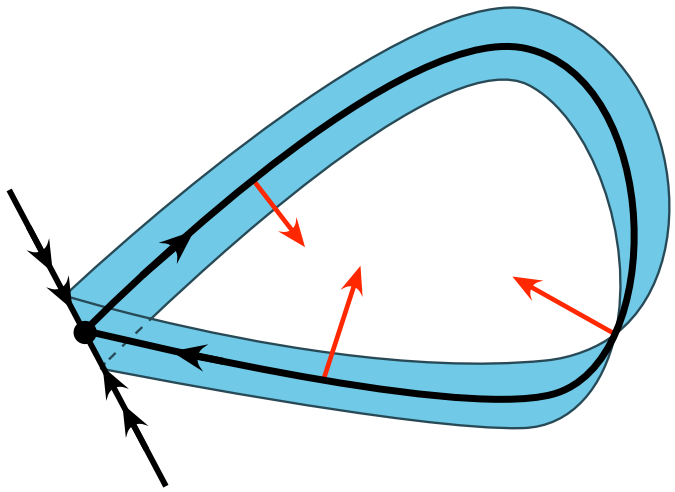

Figure 2.6: Orientable homoclinic orbit to a saddle. Red arrows denote the solution to the adjoint variational equation. Blue strip shows the two-dimensional stable manifold close to homoclinic orbit.

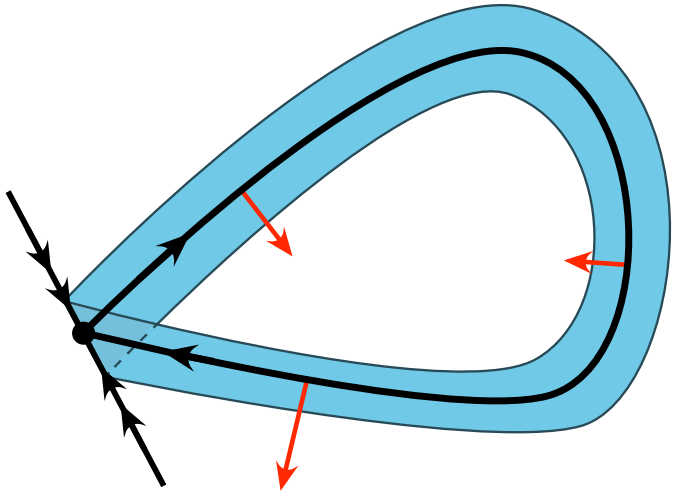

Figure 2.7: Twisted homoclinic orbit to a saddle. Red arrows denote the solution to the adjoint variational equation. Blue strip shows the two-dimensional stable manifold close to homoclinic orbit.

2. orbit flip, for which the solution of the linearized equation (2.18) approaches zero along a strongly (un)stable eigenvector and

3. inclination flip, for which the solution of the adjoint equation (2.19) approaches zero along a strongly (un)stable eigenvector.

We are interested in those bifurcations, since they can produce 2- and N-homoclinics (or, equivalently, *bound states* for pulses in reaction-diffusion system). The resonant bifurcation can produce only 2-homoclinics, the orbit flip and the inclination flip can both produce 2- and N-homoclinics, depending on the ratio between λ_{ss}, λ_s and λ_u (see Table I and Table II in [34]). A flip bifurcation, either orbit or inclination, corresponds to a switching of the solution of the linear equation through the strongly (un)stable subspace of $\mathcal{A}(0)$. We need an additional parameter μ in order to unfold a codimension-2 bifurcation of the homoclinic orbit.

Resonant homoclinic orbits were investigated in [35] and can already be found in $\mathbb{R}^2$.

There are two cases which have to be discussed separately.

1. If the original homoclinic orbit is orientable, the bifurcation involves emergence of a saddle-node bifurcation of limit cycles. For $\mu > 0$, limit cycles bifurcate from the original homoclinics for $p > 0$ and for $\mu < 0$ this occurs for $p < 0$.

2. For a twisted homoclinics, the resonance bifurcation involves a period doubling and bifurcation to a 2-homoclinic orbit. The period-doubling bifurcation stems from $(p, \mu) = (0, 0)$. The period of the bifurcating periodic orbit goes to infinity as $\mu \to 0$.

Homoclinic flips, namely, the orbit flip and the inclination flip are purely three-dimensional phenomena. They both are characterized by a change of the orientation of the strip of the (un)stable manifold close to the homoclinic orbit, see [36, 37, 38].

In a homoclinic flip bifurcation solutions of the linearized equation or adjoint variational equation flips through the strongly (un)stable eigenspace of $\mathcal{A}(0)$. In the orbit flip bifurcation the homoclinic orbit approaches the equilibrium along a strongly (un)stable eigenvector (see Fig. 2.8 and Fig. 2.9). In the inclination flip, the solution of the adjoint

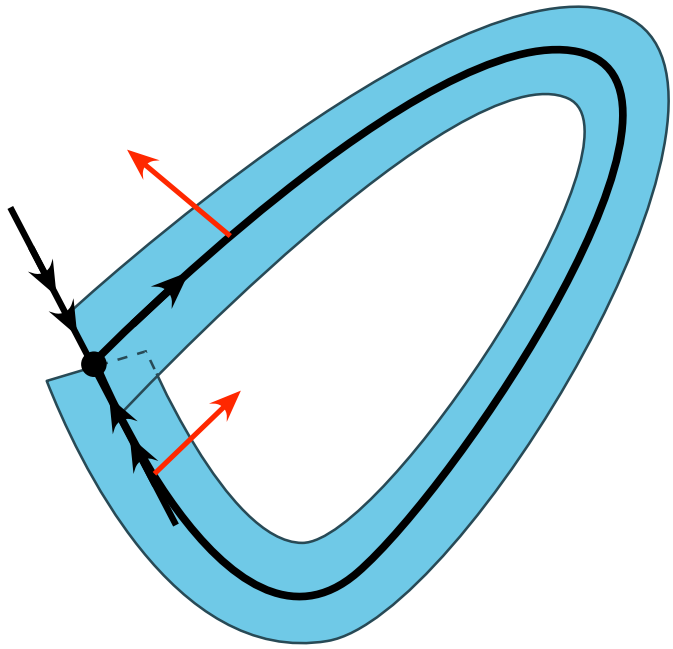

Figure 2.8: Codimension-2 orbit flip of homoclinic orbit. Red arrows indicate the solution to the adjoint equation $\psi(t)$.

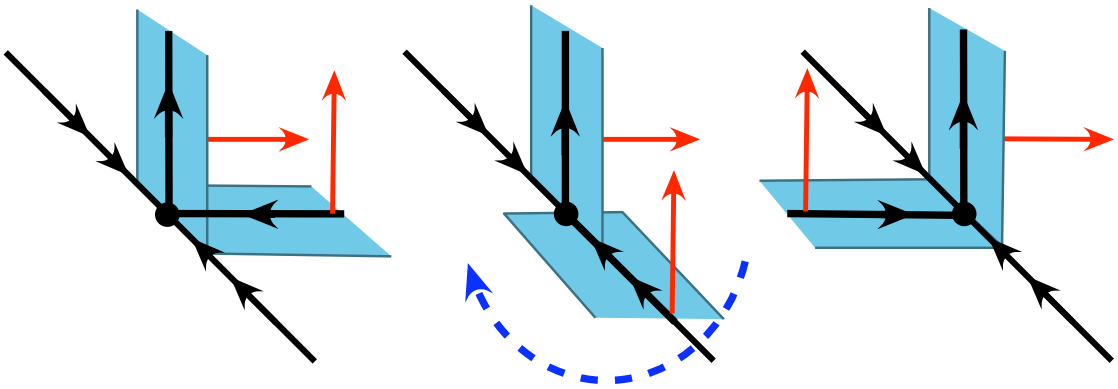

Figure 2.9: Details of the orbit flip bifurcation. Red arrows indicate the solution to the adjoint equation $\psi(t)$. Left: structure of stable manifold before bifurcation, center: structure of stable manifold in the bifurcation point, right: structure of stable manifold after the bifurcation.

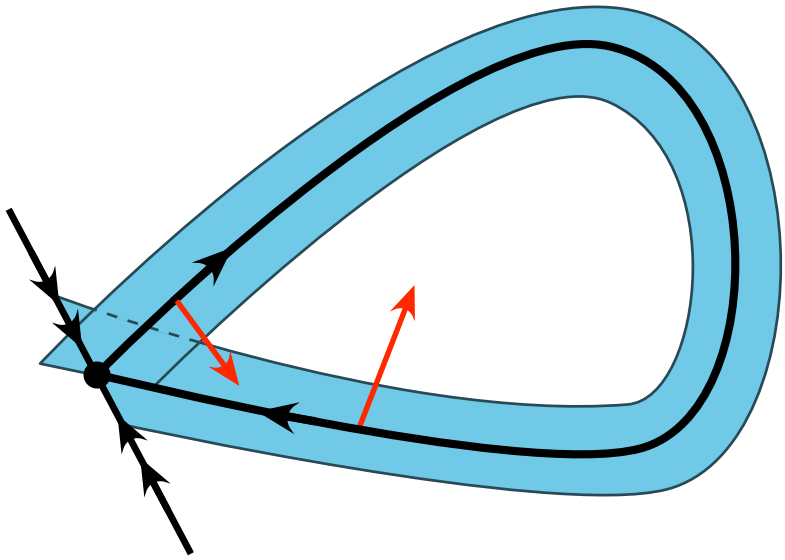

Figure 2.10: Codimension-2 inclination flip of homoclinic orbit. Red arrows indicate the solution to the adjoint equation $\psi(t)$.

variational equation (2.19 approaches zero along the strongly (un)stable eigenvector (see Fig. 2.10 and Fig. 2.11).

In dependence on the ratio between λ_{ss}, λ_s and λ_u, here are three cases to be considered separately

1. No extra bifurcations occur.

2. Bifurcation to 2-homoclinic orbit occurs together with appearance of a branch of period-doubling bifurcation for the accompanying limit cycles.

3. Bifurcation to N-homoclinics ($N \geq 3$) occurs. There also appear branches of n-periodic solutions and period-doubling bifurcations.

It is possible to detect all three bifurcations numerically with the help of the available numerical bifurcation analysis software AUTO [39]. For the resonant bifurcation we have to monitor the simple resonance condition on the leading eigenvalues of the matrix $\mathcal{A}(0)$, whereas the detection of the homoclinic flips is more involved and needs the computation of the solution to the adjoint variational equation.

Three discussed codimension-2 bifurcations of homoclinic orbits to a saddle with real leading eigenvalues seem to be the only mechanisms to produce N-homoclinics. This

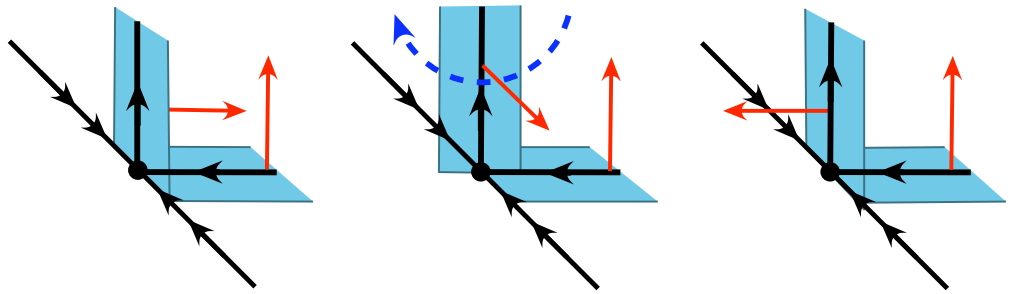

Figure 2.11: Details of the inclination flip bifurcation. Red arrows indicate the solution to the adjoint equation $\psi(t)$. Left: structure of stable manifold before bifurcation, center: structure of stable manifold in the bifurcation point, right: structure of stable manifold after the bifurcation.

fact simplifies the study of multiple pulse branching. If one has N-homoclinics solutions somewhere in the parameter space, one can continue the N-homoclinics solution to the point in the parameter space where it nearly coincides with the primary 1-homoclinics and expect that the 1-homoclinics undergoes one of the discussed codimension-2 bifurcations. In this sense, codimension-2 bifurcation act as organizing center for the appearance of N-homoclinics.

2.3.2 Complex-conjugate leading eigenvalues

The transition from saddle to saddle-focus can actually be seen as a fourth type of codimension-2 bifurcation of homoclinic orbits. Here we will consider a case with two stable complex-conjugate eigenvalues. Historically, the main results on the homoclinic orbit to saddle-foci were obtained by Shilnikov [40, 41, 42] (see also [43]), who proved, among others, the existence of an infinite number of periodic orbits close to the homoclinic one.

In Fig. 2.12 we can see an example of such homoclinic orbit in $\mathbb{R}^3$. The stable manifold is again two-demensional, and the unstable manifold is one-dimensional. The homoclinic orbit approaches the equilibrium in an oscillating manner in forward time. It was shown that at the point of transition to the saddle-focus, new branches of N-homoclinic solutions appear (see numerous references in [13], Chap. 6.3). So as soon as we have a 1-homoclinic orbit to a saddle-focus with complex-conjugate leading eigenvalues, there exist further homoclinic solutions with N-loops. Sometimes such N-homoclinics are

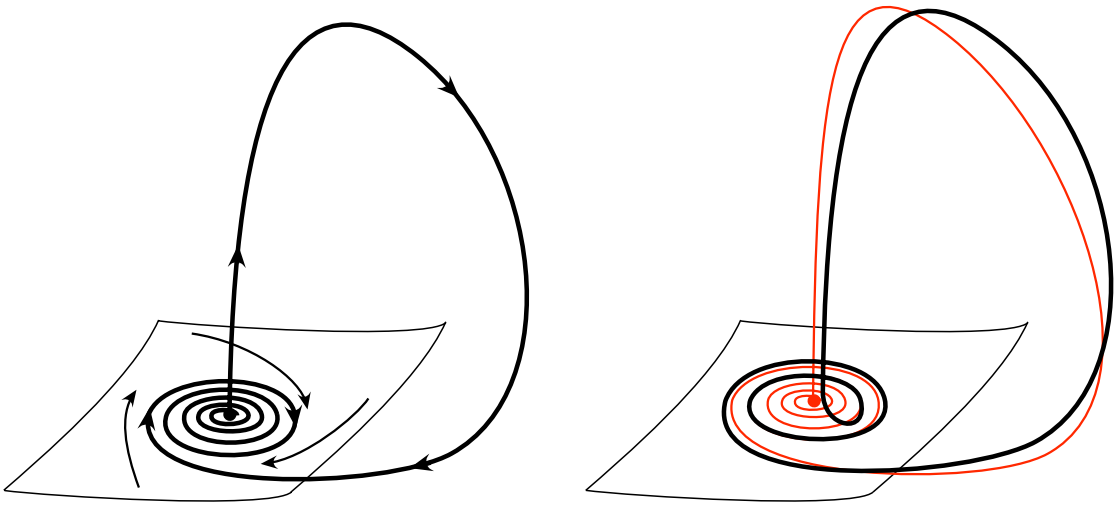

Figure 2.12: Left: Homoclinic orbit to a saddle-focus. Right: a periodic orbit (black) close to the primary homoclinic orbit (red).

referred to as subsidiary homoclinic orbits [44].

Homoclinic orbits to saddle-focus are as well accompanied by a family of periodic solutions. In the same way as for homoclinic orbits to a saddle, we can map an appropriate Poincaré section in itself close to the homoclinic orbit and study the fixed points of this map in dependence on the bifurcation parameter p. We refer to [44, 13] for the analysis of the map. Depending on the saddle quantity σ, we have two possibilities for the dependence of the period of the periodic solutions on p:

1. For saddle quantity $\sigma < 0$, the curve $p(T)$ for periodic orbits is monotonous.

2. For saddle quantity $\sigma > 0$, $p(T)$ is a wiggly curve, shown in Fig. 2.13. For $p = 0$ there exist infinitely many periodic orbits.

   Limit cycles that belong to different parts of the curve $p(T)$ have qualitatively different portraits. The first part of the curve $p(T)$ with positive slope is represented by the limit cycles, consisting of one large excursion near the primary homoclinic orbit and typically have only one maximum on the period. For every maximum on the $p(T)$ curve, the corresponding limit cycles make an additional small-amplitude winding around the equilibrium. The right panel in Fig. 2.12 shows a limit cycle with two windings around the equilibrium. The global shape of the homoclinic or-

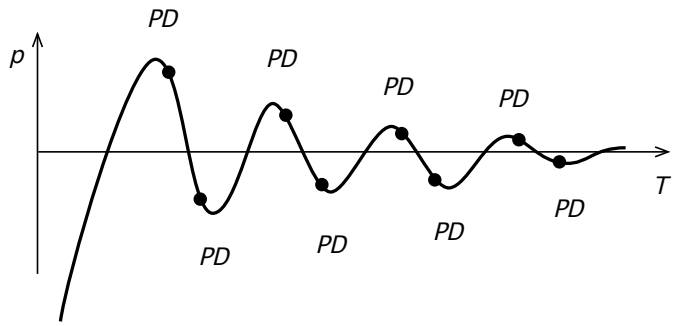

Figure 2.13: Dependence of the period of limit cycles on p for the case of homoclinic orbit to saddle-focus with saddle quantity $\sigma > 0$.

bit is nearly repeated by the periodic solution. Periodic orbits with large periods $T \to \infty$ have a growing number of windings around the equilibrium.

Close to each maximum of the curve $p(T)$ the limit cycle undergoes a period-doubling bifurcation. This bifurcation results in a new periodic orbit which also belongs to some other curve $p_2(T)$, which is also a wiggly curve. The secondary (or subsidiary) periodic orbits converge to 2-homoclinics for large T as well and also can undergo further period-doubling bifurcations close to the maxima of $p_2(T)$, giving raise to pretty reach dynamics.

Summarizing, in the parameter space near a 1-homoclinic orbit to a saddle-node with a saddle quantity $\sigma > 0$ (or equivalently $\delta < 1$) we find a complex structure, consisting of primary periodic orbits and subsidiary homoclinic and periodic orbits. It is possible to find any solution consisting of a given number of large and small oscillations. For the waves in reaction-diffusion systems it means that we can always construct a bound state with any given number of excitation pulses with small oscillations in between.

2.4 Stability of waves

For a comprehensive understanding of the wave dynamics a detailed stability analysis of the wave turns out to be essential. Moreover, as only stable travelling wave solutions can be observed experimentally, stability considerations are crucial for experimental verification of theoretical results.

To study the stability of the solutions to the reaction-diffusion system we use a straight-forward approach, linearizing the equation about the studied solution [14]. The elements of the spectrum of the obtained linear operator are the growth rates of small perturbations: instability of the solution is reflected by the presence of spectrum in the right complex half-plane.

In this section we will deal mainly with the stability of waves in reaction-diffusion equations posed on the whole real axis and on large domains with periodic boundary conditions. The stability of waves on bounded domains and the so-called *absolute stability* will be discussed only briefly.

2.4.1 Spectral approach

We suppose that we have found a solution to a reaction-diffusion system

$$\partial_t U = F(U) + D\partial_{xx} U, \quad U \in \mathbb{R}^N \tag{2.25}$$

in the form of a running wave $Q(z) = Q(x - ct)$ with constant shape and velocity c. As we have seen before, the function $Q(z)$ obeys the profile equation

$$DU'' + cU' + F(U) = 0, \tag{2.26}$$

that can be cast as a first-order system

$$u' = f(u; c), \quad u \in \mathbb{R}^{2N} \tag{2.27}$$

where prime denotes a derivative with respect to the co-moving coordinate z.

For a given solution $Q(z)$ of (2.26) we can formulate the corresponding linearized problem in the co-moving frame:

$$\partial_t W = F_U(Q(z))W + c\partial_z W + D\partial_{zz} W, \quad W \in \mathbb{C}^N \tag{2.28}$$

where F_U denotes the linearization of the function F. With a separation ansatz

$$W(t, z) = e^{\lambda t} V(z),$$

we obtain the following equation for λ and $V(z)$

$$\lambda V = F_U(Q(z))V + cV' + DV'', \quad V \in \mathbb{C}^N, \quad ' \stackrel{\text{def}}{=} \partial_z \tag{2.29}$$

or

$$\mathcal{L}V = \lambda V, \tag{2.30}$$

where the operator $\mathcal{L}$ is given by

$$\mathcal{L} = D\partial_{zz} + c\partial_z + F_U(Q(z)).$$

Again, we cast Eq. (2.29) as a first-order system

$$v' = A(z;\lambda)v, \quad v \in \mathbb{C}^{2N} \tag{2.31}$$

where

$$A(z;\lambda) = \tilde{A}(z) + \lambda B.$$

Matrices $\tilde{A}(z)$ and B are given by

$$\tilde{A}(z) = \begin{pmatrix} 0 & \mathrm{id} \\ -D^{-1}F_U(Q(z)) & -cD^{-1} \end{pmatrix}, \quad B = \begin{pmatrix} 0 & 0 \\ D^{-1} & 0 \end{pmatrix}. \tag{2.32}$$

The translation symmetry of the problem (2.25) provides that for non-constant $Q(z)$ Eq. (2.29) always has a bounded solution for $\lambda = 0$, which is given by $V(z) = Q'(z)$. We can easily check it by taking a derivative with respect to z of Eq. (2.26):

$$D(U')'' + c(U')' + F_U(Q)U' = 0 \cdot U'.$$

Definition of spectrum We consider the family of operators

$$\mathcal{T}(\lambda) \quad : \quad u \longmapsto \frac{du}{dz} - A(\cdot;\lambda)u \tag{2.33}$$

defined on the appropriate space [14]. λ acts as a parameter for the family.

We say that λ is in the spectrum Σ of $\mathcal{T}$ if $\mathcal{T}(\lambda)$ is not invertible, i.e. if the inverse operator does not exist or is not bounded. We say that $\lambda \in \Sigma$ is in the *point spectrum* Σ_{pt} of $\mathcal{T}$ or, alternatively, that $\lambda \in \Sigma$ is an *eigenvalue* of $\mathcal{T}$ if $\mathcal{T}(\lambda)$ is a Fredholm operator with index zero. The complement $\Sigma \setminus \Sigma_{\text{pt}} =: \Sigma_{\text{ess}}$ is called the *essential spectrum*. The complement of Σ in $\mathbb{C}$ is the resolvent set of $\mathcal{T}$ [14].

Below we give a short overview of the spectra of different wave types. For the sake of comparison, we qualitatively consider quantum mechanical problems for a particle in one spatial dimension with different types of potentials.

Homogeneous rest states $Q(z) = Q_0$. In this case the linearization has constant coefficients

$$v' = A(Q_0; \lambda)v = A_0(\lambda)v.$$

This equation has a bounded solutions on $\mathbb{R}$ if, and only if, the matrix $A_0(\lambda)$ is non-hyperbolic. λ is in the essential spectrum of $\mathcal{T}$ if, and only if,

$$d_0(\lambda, k) = \det[A_0(\lambda) - ik] = 0$$

has a solution $k \in \mathbb{R}$.

The function $d_0(\lambda, k)$ is referred to as the *linear dispersion relation*. The essential spectrum consists of curves $\lambda(k)$ in the complex plane.

We can define the *group velocity*

$$c_g = -\frac{d}{dk} \operatorname{Im} \lambda(k),$$

which represents the velocity of the wave packets centered near the wavenumber k in the linear equation $U_t = \mathcal{L}U$.

The point spectrum of homogeneous rest state is empty.

Traditionally, four types of instability of homogeneous rest state are distinguished. Supposed that at the onset of the instability there is a single k_{cr} with $\operatorname{Re} \lambda(k_{\text{cr}}) = 0$. Then we have the following cases:

1. $k_{\text{cr}} = 0, \quad \operatorname{Im} \lambda(k_{\text{cr}}) = 0$ corresponds to homogeneous saddle-node bifurcation.

2. $k_{\text{cr}} = 0, \quad \operatorname{Im} \lambda(k_{\text{cr}}) \neq 0$ corresponds to homogeneous Hopf bifurcation.

3. $k_{\text{cr}} \neq 0, \quad \operatorname{Im} \lambda(k_{\text{cr}}) = 0$ is referred to as *Turing* instability.

4. $k_{\text{cr}} \neq 0, \quad \operatorname{Im} \lambda(k_{\text{cr}}) \neq 0$ is referred to as *wave* instability. Sometimes terms like *Turing-Hopf* or *Turing-II* are used.

Quantum mechanical analogy: If we have a particle in a force-free space, every state of it is a free state. The energy levels form a continuous spectrum and every energy value is two-fold degenerated.

Periodic wave trains of period L. In this case the matrix $A(z;\lambda)$ is L-periodic, i.e.

$$A(z+L;\lambda) = A(z;\lambda)$$

for all z. The linearization around the wave train

$$v' = A(z;\lambda)v. \tag{2.34}$$

has periodic coefficients. By Floquet theory, the solutions of Eq. (2.34) have the following form

$$v = e^{\nu(\lambda)z} q_L(z;\lambda), \tag{2.35}$$

where $q_L(z+L;\lambda) = q_L(z;\lambda)$ is an L-periodic function. Casting the corresponding boundary-value problem for v, we obtain

$$\begin{aligned} v &= (\partial_u f(u(z);c) + \lambda B)\, v, \quad 0 < z < L, \\ v(L) &= e^{i\gamma} v(0). \end{aligned} \tag{2.36}$$

λ is in the essential spectrum of $\mathcal{T}$ if, and only if, Eq. (2.36) has a solution for some $\gamma \in \mathbb{R}$. $\lambda = 0$ is contained in the essential spectrum with the Goldstone mode given by $Q'(z)$. Near the origin, the spectrum $\lambda(\gamma)$ is approximated by

$$\lambda(\gamma) = -ic_g\gamma - d\gamma^2 + \mathcal{O}(\gamma^3),$$

where c_g denotes the group velocity. The sign of the constant d decides upon the stability, given the rest of the spectrum is contained in the left open half-plane. The Eckhaus instability is characterized by $d = 0$.

Spatially period wave trains usually live in families on the so-called dispersion curves $c(L)$. In the Appendix, we show that

$$\frac{d}{d\gamma} \operatorname{Im} \lambda(\gamma)\bigg|_{\gamma=0} = -c_g = \frac{d}{dL} c(L),$$

so the slope of the dispersion curve $c(L)$ coincides with the first coefficient of the expansion of spectrum at zero.

The point spectrum of a wave train is empty.

In the solid-state physiscs the representation given by Eq. (2.35) is known as Bloch-wave decomposition. For a particle in a periodic potential, the possible energy values form continuous bands.

Pulses on homogeneous background. In this case $Q(z)$ approaches a constant value as $z \to \pm\infty$, i.e.

$$\lim_{z\to\pm\infty} Q(z) = Q_0.$$

The matrix A has then also a limit value

$$\lim_{z\to\pm\infty} A(z;\lambda) = A_0(\lambda).$$

The essential spectrum of the pulse $Q(z)$ in this case is given by the essential spectrum of Q_0.

$Q'(z)$ is an eigenfunction of the linearization operator $\mathcal{L}$ to the eigenvalue $\lambda = 0$. There can also be some further eigenvalues in the point spectrum.

Quantum mechanical analogy: consider a particle in a localized potential. There are discrete energy levels, corresponding to the bound states and continuous energy spectrum of free states.

2.4.2 Stability of pulse trains with large wavelength

Solitary pulses in reaction-diffusion systems are known to be accompanied by spatially periodic pulse trains. Those pulse trains can be characterized by the dispersion relation, which expresses the dependence of the pulse train velocity c on its wavelength L. The aim of this subsection is to give a short overview of the theoretical results [16] on the stability of the periodic pulse trains with large L.

We suppose that we have a profile equation

$$u' = f(u, c), \tag{2.37}$$

which allows for a homoclinic solution $q(z)$ for $c = c_0$. This homoclinic solution represents the primary solitary pulse in the reaction-diffusion system. We assume that $f(0, c) = 0$ holds for all c and this equilibrium is hyperbolic for $c = c_0$.

Next, we cast the linearization around the pulse $q(z)$ as a system of first-order differential equations

$$v' = [\partial_u f(q(z), c_0) + \lambda B]v,$$

compare the previous sections. We assume that the only solution to the above equation for $\lambda = 0$ is given by $q'(z)$, so $\lambda = 0$ is an isolated eigenvalue. We assume the stability of the primary pulse $q(z)$, which means that the rest of the spectrum of the pulse is contained in the open left half-plane.

Furthermore, we assume that there exists a $2L$-periodic solution $p_L(z)$ to the profile equation (2.37) with c_L and $p_L(-L) = p_L(L)$. We are interested in large L, so the velocity of the $2L$-periodic pulse train c_L must be close to c_0. From the previous section, we know that λ is in the spectrum of $2L$-periodic pulse train $p_L(z)$ if, and only if, the boundary-value problem

$$\begin{aligned} u' &= [\partial_u f(p_L(z), c_L) + \lambda B]u, \qquad |z| < L \\ u(L) &= e^{i\gamma}\, u(-L) \end{aligned} \tag{2.38}$$

has a solution $u(z)$ for some real γ.

Gardner [45] proved that the essential spectrum of the primary solitary pulse is approximated by the essential spectrum of the $2L$-periodic solution $p_L(z)$. Moreover, for any $\lambda_* \in \Sigma_{\rm pt}(q)$ with multiplicity m and for every fixed spatial Floquet exponent $\gamma \in [0, 2\pi)$, Eq. (2.38) has precisely m solutions in a certain ϵ-neighborhood of λ_*. It means that we obtain circles (or closed curves) of essential spectra near every point of point spectrum of solitary pulse upon cloning the latter periodically in space with large enough interpulse distance.

The main result of [16] concerns the location of the circle of eigenvalues which arises from the eigenvalue $\lambda = 0$ of the pulse $q(z)$. We supposed that the pulse $q(z)$ is stable, so the location of this circle decides upon the stability of the $2L$-periodic solution $p_L(z)$. The expansion of $\lambda(\gamma)$ near $\lambda = 0$ is given by

$$\lambda = \frac{1}{M}\Big[(e^{i\gamma} - 1)\langle\psi(L), q'(-L)\rangle + (1 - e^{-i\gamma})\langle\psi(-L), q'(L)\rangle\Big] + R(\gamma, L) \tag{2.39}$$

with the rest term

$$R(\gamma, L) = (e^{i\gamma} - 1)\mathcal{O}(e^{-3\rho L}) + (1 - e^{-i\gamma})\mathcal{O}(e^{-3\rho L}),$$

where ρ is related to the magnitude of the eigenvalues of $\partial_u f(0, c_0)$.

The corresponding solutions of Eq. (2.38) are given by

$$u(z) = e^{ik\gamma} q'(z) + \mathcal{O}(e^{-\rho L}), \quad z \in [(2k-1)L, (2k+1)L], \quad k \in \mathbb{Z}.$$

Here, M is a Melnikov integral, given by

$$M = -\int\limits_{-\infty}^{\infty} \langle\psi(z), \partial_c f(q(z), c_0)\rangle\, dz = \int\limits_{-\infty}^{\infty} \langle\psi(z), Bq'(z)\rangle\, dz \neq 0.$$

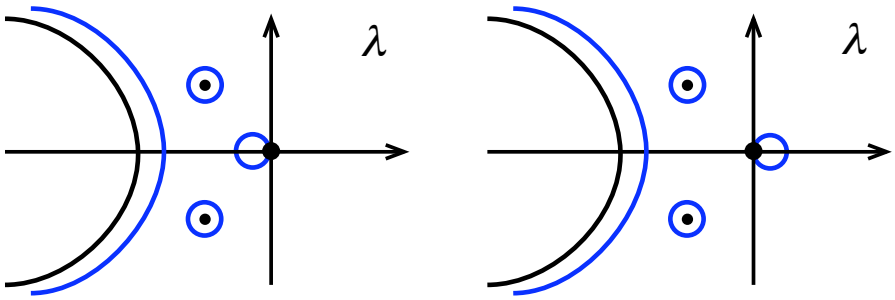

Figure 2.14: Spectrum of primary solitary pulse $q(z)$ is shown in black curves and dots. Spectra of $2L$- periodic solutions shown in blue lines. Left panel shows spectra of stable periodic solutions, right panel shows spectra of unstable periodic solutions. Note the location of the circle of critical eigenvalues near the origin.

Again, $\psi(z)$ denotes the solution of the adjoint variational equation

$$\psi' = -\partial_u f^*(q(z), c_0)\psi.$$

The sign of the curvature of the circle of critical eigenvalues

$$\frac{d^2}{d\gamma^2}\operatorname{Re}\gamma\Big|_{\gamma=0} = \frac{1}{M}\Big[(-\langle\psi(L), q'(-L)\rangle + \langle\psi(-L), q'(L)\rangle\Big]$$

shows whether the circle of critical eigenvalues lies in the right or in the left complex half-plane, i.e. whether the $2L$-periodic pulse train is stable or not. We refer to Fig. 2.14 for the structure of the spectra of periodic pulse trains close to the primary solitary pulse.

We can interpret the above results as follows. The expansion of $\lambda(\gamma)$ near the origin consists of the scalar products of the solutions to the adjoint equation $\psi(z)$ and the derivative of the pulse profile $q'(z)$ for large z. These are determined by the leading eigenvalue ν of the matrix $\partial_u f(0, c_0)$, which we assume to be real and, say, negative. Referring to [16], we obtain

$$q'(z) = e^{\nu z}v_0 + \mathcal{O}(e^{-(|\nu|+\delta)z}), \qquad q'(-z) = e^{\nu z}w_0 + \mathcal{O}(e^{-(|\nu|+\delta)z}),$$

for a some constant δ, where v_0 and w_0 are the corresponding eigenvectors of $\partial_u f(0, c_0)$ and $\partial_u f^*(0, c_0)$, respectively. We obtain then the expansion

$$\lambda = \frac{\langle v_0, w_0\rangle}{M}(1 - e^{-i\gamma})e^{2\nu L}.$$

The term

$$\langle \psi(z), q'(-z) \rangle$$

can be neglected, since it decays faster than $e^{-2\nu z}$ (recall our assumption on the leading eigenvalue ν). Finally, we obtain that the spatially periodic pulse trains are stable if $M\langle v_0, w_0 \rangle < 0$.

In the exactly same way we can obtain the expansion for a pair of complex-conjugate leading eigenvalues $\nu, \bar{\nu}$

$$\lambda = \frac{a}{M} \sin(2L \operatorname{Im} \nu + b)(1 - e^{-i\gamma}) e^{2L \operatorname{Re} \nu},$$

where a and b are real constants. The stability of the pulse trains which accompany a solitary pulse with oscillating wake changes periodically in dependence on L. The circle of critical eigenvalues flips over the imaginary axis on the period-doubling bifurcation of the limit cycles, belonging to the wiggly curve $c = c(L)$ (recall the section on the homoclinic orbits).

2.4.3 Numerical computation of spectra

We have to deal with two problems if we want to compute the stability of a given wave numerically. Firstly, we need an efficient and precise method of locating the spectrum and secondly we have to care about the boundary conditions since in numerical computations it is impossible to simulate wave dynamics on unbounded domains.

Below we shortly present the method of computing essential spectra of periodic wave trains. One can find a deeper insight in the method with a number of examples (including actual code) in [46].

Suppose that we have found a L-periodic wave train $Q(z)$. As we have seen already in the previous sections, λ is in the spectrum of the linearization about $Q(z)$ if, and only if, the boundary-value problem

$$\begin{aligned} v' &= f(v; c), \\ u' &= A(z; \lambda)u, \qquad 0 < z < L \\ u(L) &= e^{i\gamma + \eta} u(0) \end{aligned} \tag{2.40}$$

has a solution for $\eta = 0$ and some real γ. Note that we have also to solve for the profile of the wave, since the coefficients of the matrix $A(z; \lambda)$ depend on $Q(z)$. If we have a good starting solution to Eq. (2.40), we can continue it in $(\gamma, \lambda) \in \mathbb{R} \times \mathbb{C}$ and

obtain a curve of the essential spectrum $\lambda(\gamma)$. As the starting solution, we can use $\gamma = \eta = \lambda = 0, u(z) = Q'(z)$, which is always in the spectrum. Another possibility is to find an initial condition for the continuation of Eq. (2.40) by computing the eigenvalues and the corresponding eigenfunctions of the discretized operator $\mathcal{L}$.

The parameter η in Eq. (2.40) is normally set to zero, this is the condition for $\lambda \in \Sigma_{\text{ess}}$. However, with $\eta \neq 0$ it is possible to compute the spectrum on weighted spaces, which can be used to compute the direction of propagation of the possible unstable modes. Computations with $\eta \neq 0$ are also needed for the calculation of the absolute spectrum, which is discussed below; in this case we can tell apart between the absolute and convective instabilities of the travelling wave.

We would like to note that using the continuation techniques for computing spectra delivers very accurate results. The accuracy can be easily controlled and the computation of the relevant branches of the essential spectrum usually take no longer than several minutes. It is also possible to reach branches which can firstly be not connected to the branches with known starting solution, performing the continuation along the parameters of the non-linearity or in the dispersion plane (L, c).

It is also possible to use the continuation method to get an approximation of the point spectrum of solitary pulses. In this case, we can use the results on the stability of pulse trains with large spatial period that accompany the solitary pulse. Every λ in the point spectrum of the original pulse will be approached by a piece (typically, a circle) of the essential spectrum of the pulse train. The essential spectrum of the solitary pulse is approximated by the essential spectrum of the periodic pulse train.

The next paragraphs explain how to interpret the possible results of the calculation of the spectrum on bounded intervals. Here we have to distinguish between periodic and separated boundary conditions.

Periodic boundary conditions. Suppose we would like to estimate the spectrum Σ of a solitary pulse $Q(z)$. Σ consists of the point spectrum Σ_{pt} and the essential spectrum Σ_{ess}. With this purpose we consider a solution $Q_L(z)$ on large interval of length L with periodic boundary conditions. We denote by Σ_L^{per} the spectrum of $Q_L(z)$, this spectrum consists only of point spectrum. In [47] the following statements were proven:

- For every eigenvalue λ_* with multiplicity l in Σ_{pt}, there are precisely l elements in Σ_L^{per}, counted with multiplicity, close to λ_*, and these elements converge to λ_* as

$L \to \infty$. In other words, isolated eigenvalues of the pulse $Q(z)$ are approximated by elements in $\Sigma_L^{\rm per}$, counting multiplicity.

- Every $\lambda_* \in \Sigma_{\rm ess}$ is approached by infinitely many eigenvalues in $\Sigma_L^{\rm per}$ as $L \to \infty$.

So the spectrum $\Sigma_L^{\rm per}$ of the solution on the truncated domain with periodic boundary conditions converges to the spectrum Σ of the original pulse as $L \to \infty$.

Separated boundary conditions and absolute spectrum. In this case the stability of a travelling wave differs from that on the unbounded domain pretty dramatically.

We suppose that we have a travelling wave solution $Q(z)$ with two asymptotically states $Q_\pm(z)$, which can be either a constant or a periodic ones. The matrix $A(z;\lambda)$ of the linearized problem

$$u' = A(z;\lambda)u$$

has then also asymptotics given by $A_\pm(\lambda)$ for $z \to \pm\infty$. We assume that $A_\pm(\lambda)$ are both hyberbolic.

We denote by $\Sigma_L^{\rm sep}$ the spectrum of our solution on a large bounded domain of size L with separated boundary conditions. $\Sigma_L^{\rm sep}$ consists only of point spectrum. Below we will see that $\Sigma_L^{\rm sep}$ does not approach to Σ as $L \to \infty$, but to a quite different set that is called the absolute spectrum.

We need first to order the eigenvalues of $A_\pm(\lambda)$ according to their real parts

$$\operatorname{Re}\nu_1^\pm(\lambda) \geq \ldots \operatorname{Re}\nu_{n/2}^\pm(\lambda) \geq \operatorname{Re}\nu_{n/2+1}^\pm(\lambda) \geq \ldots \operatorname{Re}\nu_n^\pm(\lambda).$$

We define $\Sigma_{\rm abs}^+ = \{\lambda \in \mathbb{C}; \operatorname{Re}\nu_{n/2}^+(\lambda) = \operatorname{Re}\nu_{n/2+1}^+(\lambda)\}$ and $\Sigma_{\rm abs}^- = \{\lambda \in \mathbb{C}; \operatorname{Re}\nu_{n/2}^-(\lambda) = \operatorname{Re}\nu_{n/2+1}^-(\lambda)\}$. The *absolute spectrum* $\Sigma_{\rm abs}$ is the union of $\Sigma_{\rm abs}^+$ and $\Sigma_{\rm abs}^-$.

It can be shown that the point spectrum of a travelling wave approaches the so-called *pseudo-point spectrum* $\tilde\Sigma_{\rm pt}$ as $L \to \infty$.

The next result proven in [47] states that the spectrum $\Sigma_L^{\rm sep}$ does not approximate the spectrum $\Sigma = \Sigma_{\rm pt} \cup \Sigma_{\rm ess}$, but the set $\tilde\Sigma_{\rm pt} \cup \Sigma_{\rm abs}$:

- For every $\lambda_* \in \tilde\Sigma_{\rm pt}$ with multiplicity l, there are precisely l elements in $\Sigma_L^{\rm sep}$, counted with their multiplicity, close to λ_*, and these elements converge to λ_* as $L \to \infty$.

- Every $\lambda_* \in \Sigma_{\rm abs}$ is approached by infinitely many eigenvalues in $\Sigma_L^{\rm sep}$ as $L \to \infty$.

The nice thing about the absolute spectrum is that it depends only on the asymptotic states $Q_{\pm}(z)$ and can be computed with the help of the continuation techniques [46].

Sometimes it is possible to estimate the location of the absolute spectrum without computing it [48, 46, 49]:

- Typically, the absolute spectrum is to the left of the essential spectrum. This indicates that the convective instability develops prior to the absolute one. The essential spectrum can be already in the right half-plane, while the absolute spectrum in the left one.
- A closed piece of essential spectrum sometimes contains a piece of absolute spectrum in it.
- A point, where two curves of essential spectrum cross, belongs to the absolute spectrum.

We would like to refer to [50] for colorful results on the absolute spectrum of spiral waves.

Chapter 3

Bistable dispersion and coexisting wave trains

3.1 Overview of dispersion types

Travelling excitation pulses are one of the basic types of patterns in active media [2, 51]. They can form periodic wave trains that propagate through the medium with constant velocity and profile. An important characteristic of these pulse trains is the dispersion relation which expresses their velocity c as a function of their wavelength L. In the large-wavelength approximation, the form of the dispersion curve defines the type of interaction between the pulses in the train. Positive (negative) slope of the dispersion curve corresponds to repulsive (attractive) interaction.

So far three main types of dispersion curves are distinguished in reaction-diffusion systems [19]: (i) monotonic where $c(L)$ is a monotonously increasing function that asymptotically approaches a maximum value which equals the velocity of the solitary pulse c_0, (ii) nonmonotonic with a negative slope domain, corresponding to attraction between neighbouring pulses, and (iii) oscillatory with damped oscillations giving rise to alternating attractive and repulsive pulse interaction. The first case is called normal dispersion, while the last two possibilities are referred to as anomalous dispersion.

Theoretical analysis of oscillatory dispersion in excitable media has attracted much interest [52]. It was proven that a one-dimensional medium with this type of dispersion can provide infinitely many equally spaced wave trains with wavelengths ranging up to infinity moving with the same velocity. In a more general mathematical context, this is

another manifestation of the results on the periodic orbits near a homoclinics to a saddle-focus, which was discussed in the previous chapter. In two-dimensional media oscillatory dispersion can lead to coexisting non-planar fronts [53] and cause the coexistence of free spirals of different wavelengths [18].

Indications for anomalous dispersion have been found in natural systems, for example, in experiments on chemical waves that organize the early stages of aggregation in the life cycle of the cellular slime mould *Dictyostelium discoideum* [54] and in the reduction of NO with CO on Pt(100) surfaces [20].

The Belousov-Zhabotinsky (BZ) reaction [51, 4], which has been intensively studied as an easily controllable excitable medium, shows essentially normal dispersion [55]. This reaction involves the oxidation of an organic compound by bromate in acidic solution. Experimental results on anomalous dispersion with a negative slope part have been reported for a modified BZ system, in which the reaction is carried out with 1,4-cyclohexanedione in contrast to the classical case that employs malonic acid as the organic reactant [56].

In all referred above cases the dispersion curve is *single-valued*: for a given wavelength it defines an unique propagation velocity of stable pulse trains. This chapter reports on the oscillatory dispersion relation with a *multivalued* dependence of the propagation velocity on the wavelength. As a consequence, in one medium two alternative planar wave trains can exist having the same wavelength but different velocities. We analyze the stability of the coexisting pulse trains and compare the results with direct numerical simulations. Dominance of the faster pulse train over the slower one in head-on collision is illustrated by the shift of the annihilation position between the pulse trains.

3.2 Three-component Oregonator

In this chapter we use the modified three-variable Oregonator model for the photosensitive BZ reaction in one spatial dimension [30]

$$\begin{aligned} \partial_t u &= \epsilon^{-1}(u - u^2 - w(u-q)) + D_u \partial_x^2 u \\ \partial_t v &= u - v \\ \partial_t w &= \epsilon'^{-1}(fv + \phi - w(u+q)) + D_w \partial_x^2 w. \end{aligned} \tag{3.1}$$

Here u, v and w denote the dimensionless concentrations of bromous acid, the oxidized form of the photosensitive catalyst and bromide, respectively. The ratio of the

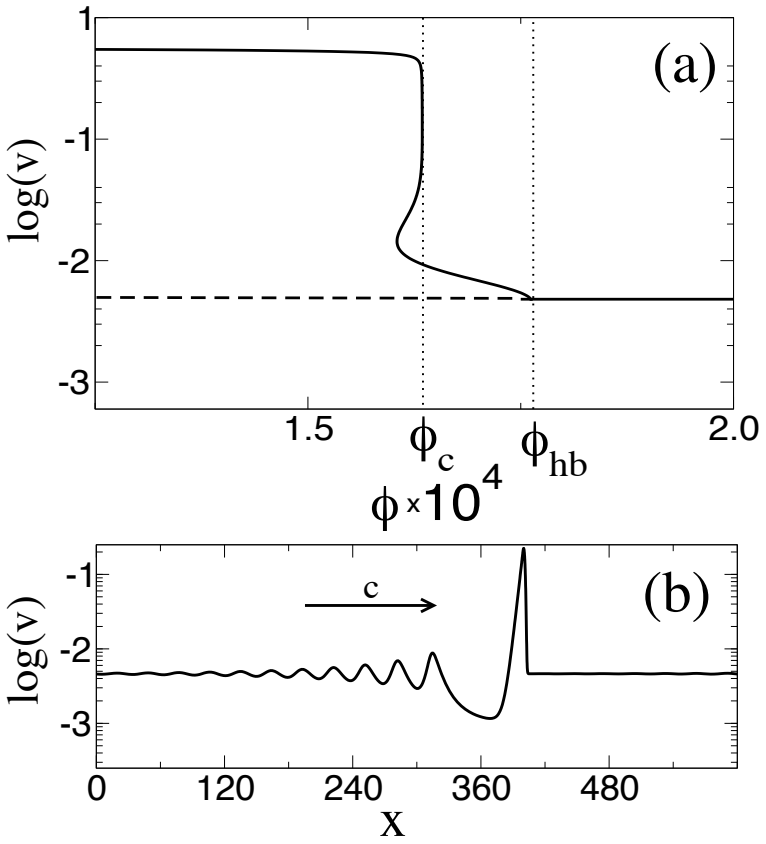

Figure 3.1: (a) Bifurcation diagram of the local dynamics described by eqs. (3.1). With the chosen parameter values for $\epsilon, \epsilon^{'}, f$ and q (compare text) a Hopf bifurcation occurs at $\phi_{hb} = 1.76 \times 10^{-4}$, for the canard point we find $\phi_c = 1.61 \times 10^{-4}$. Solid line shows the amplitude of oscillations around the unstable HSS (dashed line) below ϕ_{hb}. (b) Profile of the v variable of the stable solitary pulse propagating with velocity c to the right. Note the small amplitude oscillations in the refractory tail ($\phi = 2.0 \times 10^{-4}$).

diffusion coefficients for bromous acid and bromide $\delta = D_w/D_u$ can be estimated from the molecular weights of the two species yielding $\delta = 1.12$. Diffusion of v is omitted because in most experiments the catalyst is immobilized in a gel matrix. The time scales ϵ and $\epsilon^{'}$ follow from the recipe concentrations [30]. In this chapter, all parameters except ϕ are fixed at the following values $\epsilon = 0.09$, $\epsilon^{'} = \epsilon/8$, $f = 1.5$ and $q = 0.001$. The parameter ϕ is proportional to the intensity of applied illumination. It will be considered as the main bifurcation parameter which controls the local dynamics as well as the profile and the velocity of excitation pulses.

For the choosen parameters the system has only one homogeneous steady state, which undergoes a supercritical Hopf bifurcation at ϕ_{hb} (see Fig. 3.1(a)). With further decrease of ϕ the stable limit cycle born at ϕ_{hb} passes through a so-called canard explosion at ϕ_c and its size rapidly grows up.

We emphasize that the medium remains excitable in the parameter range $\phi_c < \phi < \phi_{hb}$. Triggered by a supra-threshold perturbation, a high-amplitude excitation relaxes to the tiny limit cycle around the unstable equilibrium.

Above the canard point ϕ_c the medium admits two solitary pulses: a fast stable one, presented in Fig. 3.1 (b), and a slow unstable pulse. The velocities of these pulses depend on ϕ, coinciding in a fold bifurcation point at some ϕ_{ext} (for our parameters choice $\phi_{ext} = 3.7\times10^{-3}$, not shown in the figure). Often ϕ_{ext} is referred to as extinction threshold because beyond this value the medium does not support pulse propagation. Below the canard point ϕ_c, solutions in the form of solitary running pulses do not exist and the system relaxes to homogeneous oscillations or phase waves. The amplitude of the stable fast pulse close to ϕ_c is approximately equal to the amplitude of the large limit cycle after the canard explosion. Below we will refer to the high-amplitude part of the pulse as to the "head" of the pulse, and to the oscillatory refractory zone behind the pulse head as to the "pulse tail".

Since the velocity of the solitary pulse is uniquely defined for given parameters, we can transform to a co-moving frame by setting $u(x,t)$, $v(x,t)$ and $w(x,t)$ to be functions of a single variable $z = x - ct$. The partial differential equations (3.1) can be reduced to a set of ordinary differential equations in a five-dimensional phase space spanned by $u(z)$, $v(z)$, $w(z)$ and their derivatives $u_z(z)$ and $w_z(z)$ with c (the velocity of the co-moving

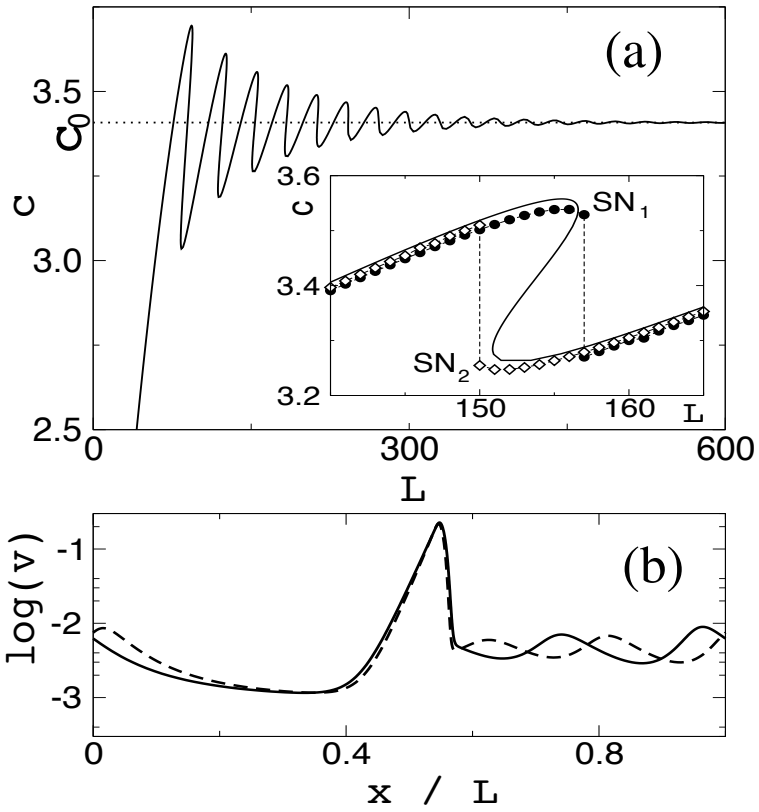

Figure 3.2: (a) Dispersion curve for pulse trains for $\phi = 2.0 \times 10^{-4} > \phi_{hb}$. The inset shows one enlarged part of the dispersion curve. Circles have been obtained from one-dimensional simulations of the underlying Oregonator model under slow increase of the integration domain size L, while diamonds correspond to slow decrease of L. (b) v profiles of one pulse in the train belonging to the upper (solid line) resp. lower (dashed line) stable branch in the inset of (a).

coordinate) as an extra parameter:

$$\begin{aligned} u' &= U, \\ v' &= -c^{-1}(u - v), \\ w' &= W, \\ U' &= -D_u^{-1}[cU + \epsilon^{-1}(u - u^2 - w(u - q))], \\ W' &= -D_w^{-1}[cW + \epsilon^{'-1}(fv + \phi - w(u + q))]. \end{aligned} \tag{3.2}$$

The solitary pulse corresponds to the homoclinic connection to the saddle-focus equilibrium in the co-moving frame ODE (3.2). The eigenvalues of the saddle-focus have non-zero imaginary parts which correspond to oscillations in the refractory tail of the solitary pulse. These tail oscillations are crucial for the oscillatory dispersion of the pulse trains.

An infinite pulse train of wavelength L is represented by a limit cycle of the same period L in the co-moving frame ODE. In the limit of infinitely large wavelength $L \to \infty$ the limit cycle touches the saddle-focus, forming the above mentioned homoclinic connection.

Continuation of the limit cycle with the help of the AUTO software [39] in the (c, L) parameter plane results in the dispersion relation for pulse trains plotted in Fig. 3.2(a). This is an oscillating function, approaching c_0 as L increases. The most important feature of this dispersion is the presence of a number of bistability domains.

Every such domain contains for a given wavelength L three different pulse train solutions, two stable and one unstable and is bounded by two fold points SN_1 and SN_2, at which one of the stable solutions collides with the unstable one (inset of Fig. 3.2(a)). The size of the overlapping domains becomes smaller for larger wavelengths L.

A closer inspection of pulse profiles on both stable branches of the dispersion relation reveals that the high-amplitude heads of the pulses in the pulse train are locked in one of the local maxima of the oscillations in the tail behind the preceding pulse. Every jump from the upper stable branch to the lower one causes the appearence of one more maximum between the successive pulses. On the leftmost branch of the dispersion curve there is non-oscillatory partial recovery between the successive pulses in the train, the next stable branch has one maximum between two neighboring pulses and so forth.

An example of two different coexisting pulse trains is shown in Fig. 3.2(b). Both trains have the same wavelength $L = 153$, but different profile and velocity. Pulses form-

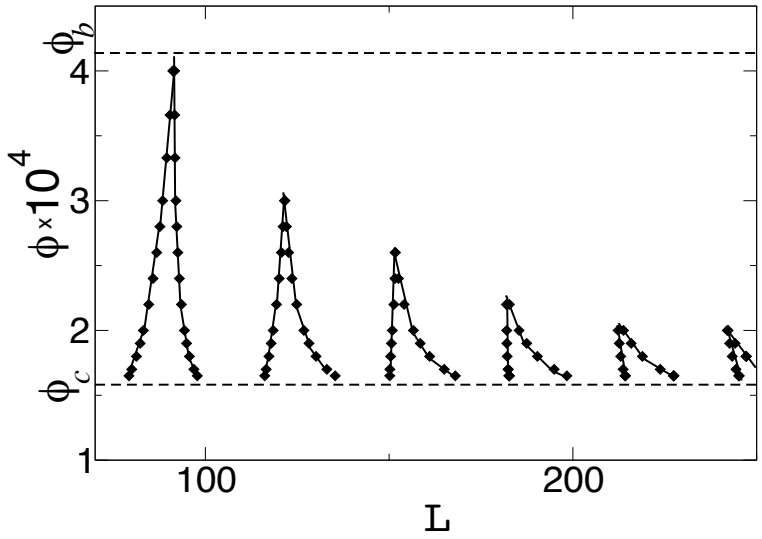

Figure 3.3: Boundaries of the bistability domains in the dispersion curve for different value of the excitability parameter ϕ. Bistability is observed in the interval $\phi_c < \phi < \phi_b = 4.18 \times 10^{-4}$ around the Hopf bifurcation of the homogeneous steady state.

ing the faster train (upper branch in the inset of Fig. 3.2(a)) have two tail oscillations between neighboring high-amplitude pulse heads (solid line in Fig. 3.2(b)). The dashed line with three local maxima of the variable v in the refractory tail represents the profile of the alternative pulse train, which corresponds to the lower branch with the slower velocity in Fig. 3.2(a).

In order to quantify the bistability phenomenon, we plotted the boundaries of the bistable domains versus the parameter ϕ in Fig. 3.3. These boundaries are the loci of codimension-1 fold points SN_1 and SN_2 that intersect at codimension-2 cusp-like points. Note the order of appearence of the bistability domains: the first one (at the smallest wavelengths) arises at the largest $\phi = \phi_b$ value, then the next one at larger wavelengths appears at a smaller ϕ value, and so on.

3.2.1 Point spectrum of pulses on a ring

To study the stability properties of the co-existing pulse trains, we solved the corresponding eigenvalue problem for the linearized operator around the pulse solution in the co-moving frame. For that purpose we first discretized pseudospectrally $N = 1, 2, 8$ periods of the pulse train in Fourier space using 256 modes for every period. This ap-

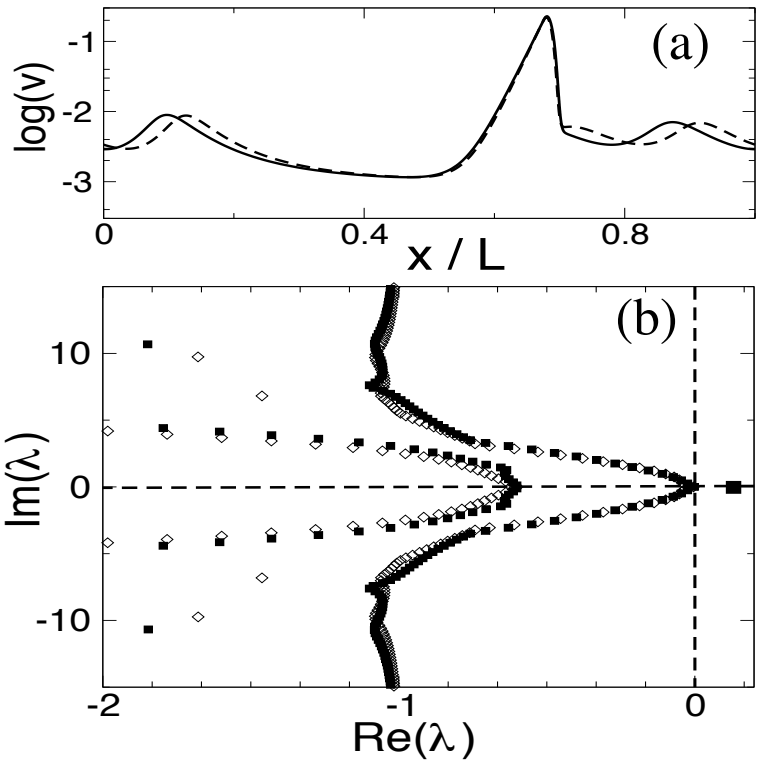

Figure 3.4: (a) Profiles of the stable (solid line) and the unstable (dashed line) pulse train for $L = 153$. Only one spatial period of the v variable is shown. (b) Leading parts of the eigenvalue spectra of the stable faster pulse train (empty diamonds) and the unstable pulse train (filled boxes), which is shown in (a).

proach was successfully used to study different pulse instabilities in reaction-diffusion systems and transition to turbulence [57, 58]. The choice of the periodic functions basis naturally corresponds to periodic boundary conditions. The point spectra of both stable and unstable pulse trains are plotted in Fig.3.4 (b). The instability of the pulses on the middle branch in the bistability domain is provided by N eigenvalues with positive real part. They cross through the imaginary axis in the bifurcation point close to SN_1 and SN_2. However, we could not resolve the underlying structure of these eigenvalues computing the eigenvalues of the discretized operator.

3.2.2 Essential spectrum

In order to get a better picture of the instabilities in the bistable domain, we calculated the essential spectrum of the wave trains using the continuation technique, as described in the previous chapter. The key idea here is to cast the eigenvalue problem in the form of the boundary-value problem

$$\begin{aligned} u' &= A(z;\lambda)\,u, \qquad 0 < z < L \\ u(L) &= e^{i2\pi\gamma}u(0), \end{aligned} \tag{3.3}$$

where the eigenvalue λ acts as a parameter. Note that we here renormalized the parameter γ so that for $\gamma = 0, 1, 2, 3, \ldots$ the eigenfunctions $u(z)$ are L-periodic in space. Starting with a known solution (for example, from the Goldstone mode), we can continue the solution of the linearized problem along the branches of the essential spectrum, which is parameterized by the wavenumber γ of the eigenfunction $u(z)$.

In Fig. 3.5 the qualitative scheme of the upper part of a bistable dispersion domain is shown. The corresponding spectra of the wave trains are presented in Fig. 3.6[1]. Note that here the dispersion curve and the location of the bifurcation points are presented only qualitatively, since in the real computation the corresponding values of L are distinguished only in the seventh decimal place.

Far away from the extrema of the dispersion curve we find a single spectral curve, going through the origin of the complex λ plane, see plot (a). Between (b) and (c), the co-called circle of critical eigenvalues nucleates from the rest of the essential spectrum. The circle of critical eigenvalues can be thought of as a blow-up of the Goldstone mode of the solitary pulse [16]. So the whole spectrum of the trigger wave breaks up into two pieces: the spectrum of the background state and the circle, originating from the Goldstone mode of the primary solitary pulse. Given the background state is stable, the stability of the wave train is thus determined by the location of the circle of critical eigenvalues.

In the point (d) the wave train becomes unstable through a long-wavelength instability, which is characterized by the condition

$$\frac{d^2}{d\gamma^2}\mathrm{Re}\,(\lambda)\bigg|_{\gamma=0} = 0.$$

[1]For the sake of simplicity, we will omit the whole references to both figures Fig. 3.5 and Fig. 3.6 in the following paragraphs and will only refer to the spectra by calling the legend letter like (a) or (k).

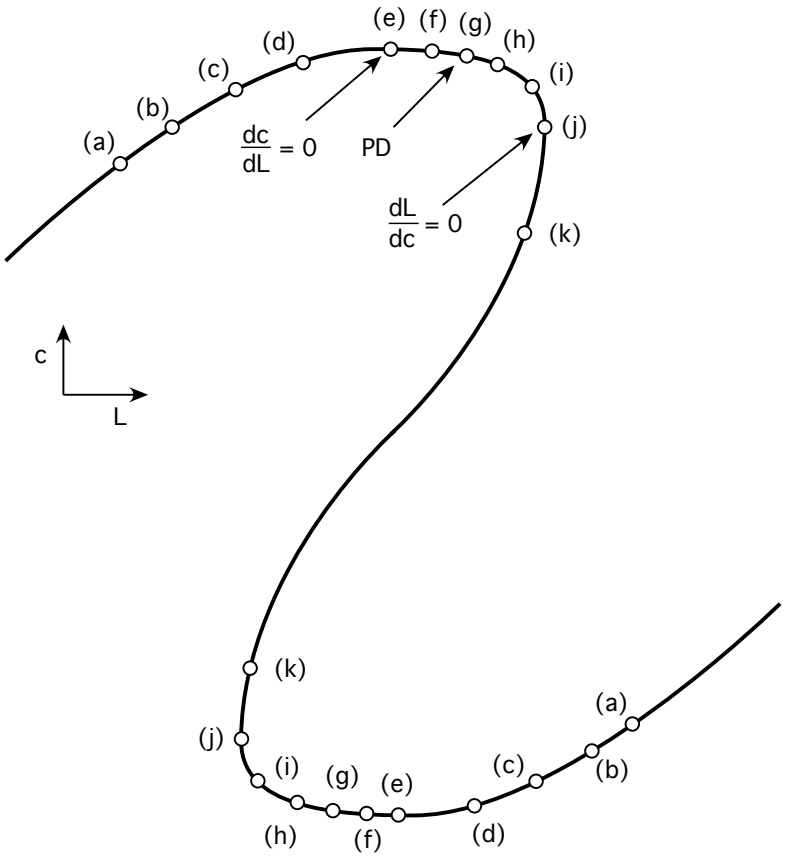

Figure 3.5: A qualitative drawing of a part of the bistable dispersion relation. Labels from (a) through (k) correspond to the spectra in Fig. 3.6.

As we see from spectrum (d), the first unstable eigenvalues are those close to $\lambda = 0$.

Moving further along the dispersion curve, we arrive at the extremum point (e), which is given by

$$\frac{d}{dL}c(L) = 0.$$

As shown in Appendix, the above condition implies

$$\frac{d}{d\gamma}\mathrm{Im}\,(\lambda)\Big|_{\gamma=0} = 0$$

as well. This means in turn that the spectrum has a cusp in the origin. Moving further on, the circle of critical eigenvalues becomes two-fold, as demonstrated in (f); after that we arrive at the period-doubling bifurcation of the periodic solution, describing the wave

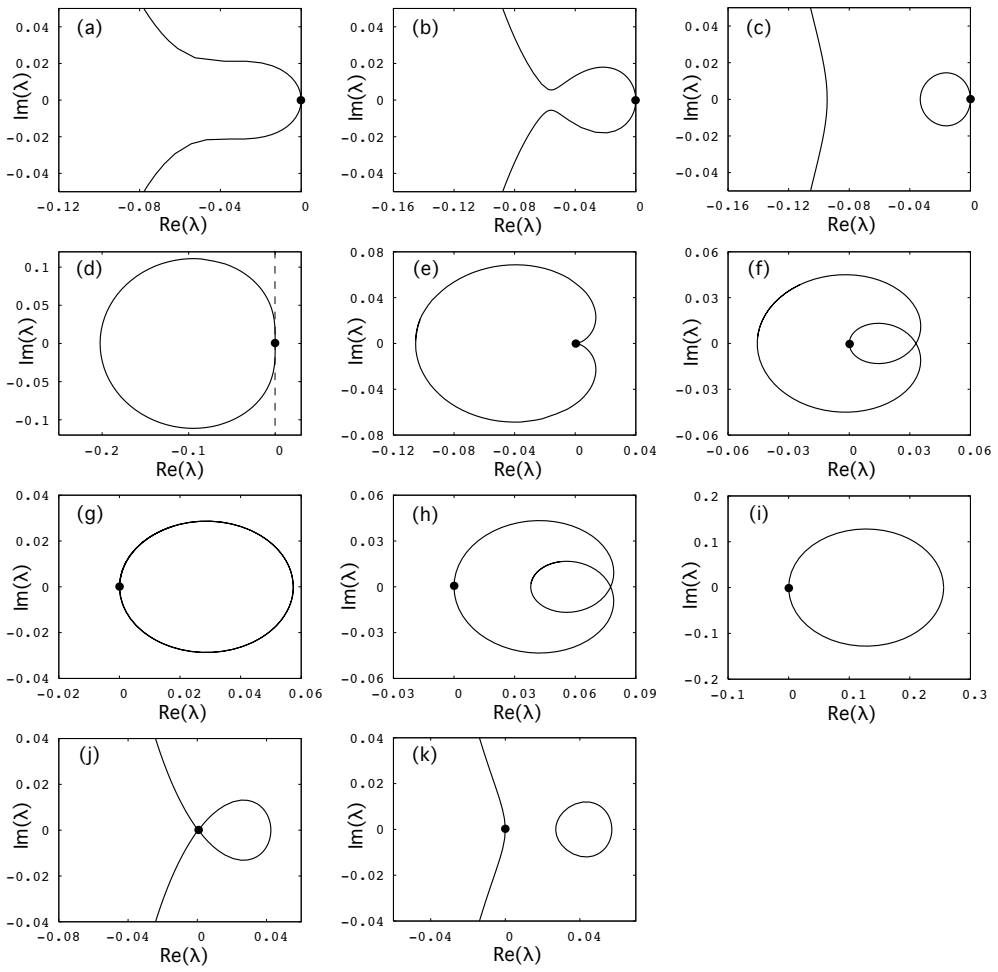

Figure 3.6: Spectra of wave trains, see Fig. 3.5 for legend.

train (see spectrum (g)). For the spectrum, it means

$$\lambda(i\gamma)\Big|_{\gamma=0.5} = 0,$$

so the corresponding eigenfunction is $2L$-periodic. This is the first instability which can be seen considering two pulses on a ring in contrast to the previous instabilities, which need more than two wavelengths of the wave train to be observed.

Going along the dispersion curve to the points (h) and (i), the spectrum unfolds to a single circle again. In the point (j) the rest part of the essential spectrum touches the origin, forming a single loop with the circle of the critical eigenvalues. After that, the

circle detaches from the origin, see (k).

Moving on further, we observe the reversed scenario: the detached circle of critical eigenvalues moves back to the origin, attaches to zero, flips back to the left half-plane and unites with another spectral curve. Up to the specific locations of the bifurcation points this instability scheme is qualitatively the same for all overlapping regions of the wiggly dispersion curve.

The instability between points (d) and (j) differs from that of the middle branch between two points (j). The first one can be observed only considering two or more equidistant pulses on a ring. The unstable eigenfunction has a period larger than L. The instability between two points (j) of the middle part of the bistable region can already be seen with one pulse on a ring of length L, since there exist an unstable eigenfunction of period L.

We would like to note that the sign of the slope of the dispersion nearly coincides in our case with the curvature of the spectrum at the origin. Points (d) and (e) are found to be very close to each other, so the circle of the critical eigenvalues flips through the imaginary axis near the extremum of the dispersion curve. For the parts of the dispersion with positive slope we nearly always find positive curvature of the spectrum, but there may exist another branch of the spectrum in the right complex half-plane (see the case with the detached circle of critical eigenvalues).

3.2.3 Extrema of the dispersion curve

It is possible to show that $\lambda = 0$ has an algebraic multiplicity two at the extrema of dispersion curve. We would like first to comment on the points (e). They are given by

$$\frac{d}{dL}c(L) = 0. \tag{3.4}$$

We recall the profile equation written as a first order system

$$u' = f(u; c(L)).$$

We assume that there exist a family of wave trains, parameterized by the wavelength L. For the profile u we substitute then $u = u(z; L)$. Upon rescaling the spatial coordinate $z \to z/L$, we obtain for the profile equation

$$\frac{u'}{L} = f(u(z; L); c(L)).$$

We take the first derivative of the above equation with respect to L:

$$\frac{u'_L(z;L)}{L} - \frac{u'(z;L)}{L^2} = f_u(u(z;L);c(L))\, u_L(z;L) + f_c(u(z;L);c(L))\underbrace{c_L}_{=0}, \tag{3.5}$$

which leads to

$$\big[\frac{1}{L}\partial_z - f_u(u(z;L);c(L))\big]\, u_L = \frac{1}{L^2}u'(z;L).$$

With Eq. (3.4) we obtain finally

$$\mathcal{T}(0)\, u_L(z;L) = \frac{1}{L^2}u'(z;L), \tag{3.6}$$

where the family of operators $\mathcal{T}(\lambda)$ is defined as

$$\mathcal{T}(\lambda) \quad : \quad v \longmapsto \frac{1}{L}\partial_z v - A(\cdot;\lambda)v + \frac{i\gamma}{L}v, \quad A = f_u(u(z;L);c(L)) + \lambda B, \tag{3.7}$$

(see also the second chapter and the first Appendix).

We recall that $u'(z;L)$ belongs to the null-space of the operator $\mathcal{T}(0)$. Eq. (3.6) means that the operator $\mathcal{T}(0)$ has a generalized eigenfunction, given by $\partial_L u(z;L)$. So the eigenvalue $\lambda = 0$ has an algebraic multiplicity equal two in the points on the dispersion curve where (3.4) holds.

A similar consideration is applicable for the points (j), where

$$\frac{dL}{dc} = 0. \tag{3.8}$$

Here, we use the second-order formulation of the profile equation

$$D\frac{1}{L^2}U'' + c\frac{1}{L}U' + F(U) = 0, \tag{3.9}$$

which we can derive with respect to the velocity c, obtaining with $\frac{dL}{dc} = 0$

$$D\frac{1}{L^2}U''_c + c\frac{1}{L}U'_c + F_U\, U_c = -\frac{1}{L}U', \tag{3.10}$$

which we write with the help of the operator

$$\mathcal{L} := \frac{D}{L^2}\partial_{zz} + \frac{c}{L}\partial_z + F_U \tag{3.11}$$

as

$$\mathcal{L}\, U_c = -\frac{1}{L}U'. \tag{3.12}$$

Again, we recall that U' is in the null-space of $\mathcal{L}$, the previous equation then means that U_c is a generalized eigenfunction to $\mathcal{L}$ in the points on the dispersion curve with $\frac{dL}{dc} = 0$. It means that the algebraic multiplicity of $\lambda = 0$ is here equal two.

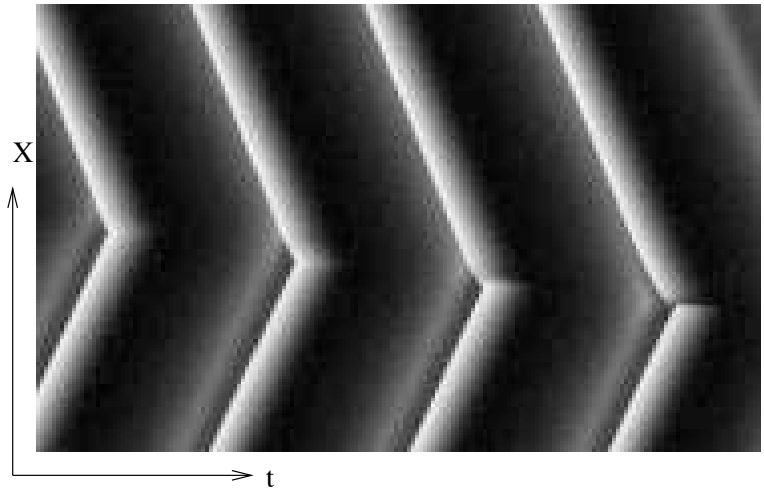

Figure 3.7: Space-time plot of annihilating pulse trains that have the same wavelength but different velocities. The logarithm of the v variable is coded in grey-scale with light (dark) colours corresponding to high (low) values, respectively. The collision position drifts towards the slower pulse train.

3.2.4 Numerical simulations

To complement the stability analysis, we performed direct simulations of the full PDE system. For this purpose, we integrated Eq. (3.1) with periodic boundary conditions in a one-dimensional spatial domain of size L. Results obtained as L is slowly increased (decreased) are plotted in the inset of Fig. 3.2(a) as circles (diamonds). As we choose the initial conditions on the upper branch of the dispersion curve and slowly increase the size of the domain, the system follows this branch until the point SN_1 and rapidly jumps to the lower stable branch. Moving now in the opposite direction by decreasing L, the lower branch remains stable up to the SN_2 point, where the system jumps back to the upper branch. Thus, in accordance with the results obtained within the co-moving frame ODE approach we find coexistence of fast and slow pulse trains. The phenomenon of bistability manifests itself in hysteresis-like transitions between alternative stable pulse trains.

The difference in the propagation velocities leads to the domination of the faster pulse train over the slower one in head-on collision. As shown in Fig. 3.7, due to different propagation velocities of the colliding pulse trains the annihilation point shifts with the time towards the slower pulse train. From the viewpoint of [33], the line of the head-on

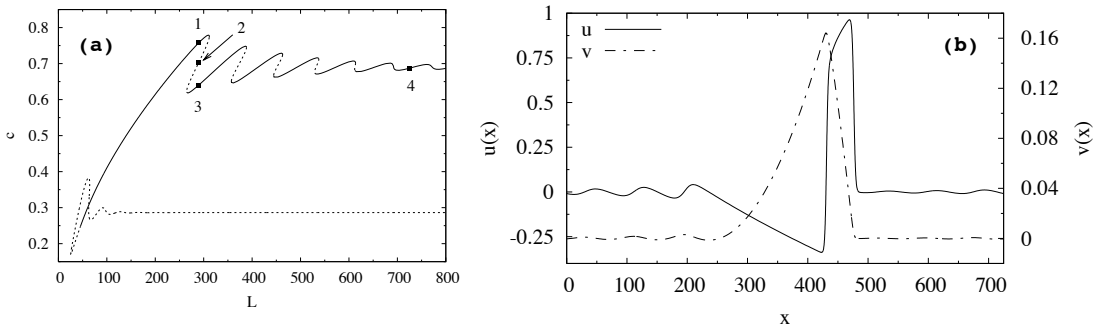

Figure 3.8: (a) Dispersion of periodic wave trains in FitzHugh-Nagumo model. Labels $1, 2$ and 3 denote coexisting wave trains. (b) Profile of wave train, denoted by 4 in (a).

collision of two wave trains represents a sink defect.

3.3 Bistability of dispersion in FitzHugh-Nagumo model

Georg Röder [59, 60] computed the dispersion curves for periodic pulse trains in the FitzHugh-Nagumo [9, 10] model, which is given by

$$\begin{aligned} \partial_t u &= -u(u-1)(u-a) - v + \partial_x^2 u, \\ \partial_t v &= \epsilon(u - bv). \end{aligned} \tag{3.13}$$

An exemplar dispersion relation displaying domains of bistability is shown in Fig. 3.8 (a) and u and v profiles of a long-wavelength pulse train are shown in Fig. 3.8 (b). Again, we see domains of bistability, where two pulse trains of the same wavelength and with different propagation speeds coexist. The spatial profile of the pulse displays oscillations in the refractory period.

3.4 Summary

To summarize, we provide evidence for oscillatory dispersion of planar pulse trains characterized by the bistability of propagation speed at a fixed wavelength. We thus add a new type to the observed cases of dispersion curves in excitable media. To our knowledge, with the exception of a model for intracellular Ca^{2+} dynamics discussed by Falcke *et al.* [61] even non-oscillatory dispersion curves with two coexisting stable branches have

not been discussed before. In the cited work one of the stable branches is stable over the almost entire wavelength range. The coexistence of two stable wave trains propagating with different velocity has not been discussed in that paper.

Although our calculations are carried out only for the Oregonator and FitzHugh-Nagumo models, we expect that other models of excitable media can obey bistable dispersion relations in a parameter range close to the transition from locally excitable to oscillatory behavior. Accordingly, coexisting stable pulse trains should be characteristic for a variety of physical, chemical and biological excitable media.

Possibly, the presented results can modify the existing view on alternative types of spiral wave with different wavelengths in two-dimensional excitable media [18], since a spiral wave far from its core can be modeled by a one-dimensional pulse train.

Chapter 4

Transition between trigger and phase waves

4.1 Introduction and Motivation

Both trigger and phase waves belong to the basic types of the patterns in active media and can arise in many physical, chemical and biological systems [2, 51]. Trigger waves are typical for excitable media [32], where an element of such medium can produce a burst of activity, triggered by a supra-threshold perturbation, produced by the diffusional flow from its neighborhood. After the activity burst, the element of the excitable medium slowly relaxes to the typically stable rest state. The velocity of such waves depends strongly on the diffusion. Trigger waves can propagate either alone or form trigger wave trains. Spatially periodic trigger wave trains can be characterized by a dispersion curve, which describes the dependence of the wave train velocity c on its wavelength L. [1]

Phase waves are merely phase-shifted oscillations of the bulk of the medium, they exist if the kinetics of the underlying reaction-diffusion system is oscillatory. The propagation velocity of phase waves is reciprocal to the initially introduced phase gradient, resulting in linear dispersion curve. The diffusion does not significantly affect their velocity. The dynamics of phase waves can be well understood in generic models like amplitude equations [62, 3]. In the parameter plane including the wavenumber k and the time scale ratio ϵ there are well-known regions of existence and stability of such waves.

[1] In the following we reserve the term "trigger waves" for both solitary and spatially periodic structures.

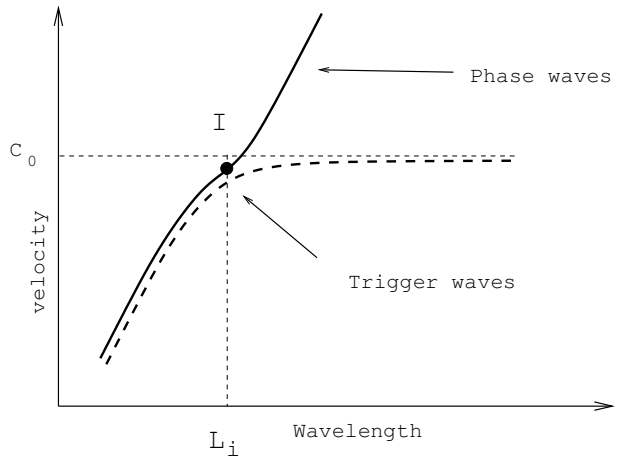

Figure 4.1: Dispersion curves of phase waves (solid line) and dispersion of trigger waves (dashed line). They nearly coincide up to some wavelength L_i. The velocity of trigger waves has limit c_0 - the velocity of solitary pulse. I denotes the inflection point.

The stability boundaries are the Eckhaus boundary [63] and the so-called zigzag boundary [64]. Phase waves in real systems like the BZ-reaction are often considered to be produced by an inhomogeneity, which introduces a phase gradient in stable homogeneous bulk oscillations [65].

One of the first theoretical studies on the transition between trigger and phase waves in a model of the Zhabotinsky reaction was presented in [66]. In the case of oscillatory kinetics trigger waves can coexist with phase waves. If the velocity of the phase wave is smaller than the velocity of the coexisting trigger wave, the former can initiate a new trigger wave. A stricter distinction between phase and trigger wave trains, based on the shape of their dispersion curves was proposed in [67]. First, it was demonstrated that up to a certain wavelength phase and trigger waves have roughly the same dispersion (inflection point I in Fig. 4.1). Then, depending on the type of the wave, under further increase of wavelength the velocity of the wave can either grow infinitely – this corresponds to the phase waves, or saturate, approaching the limit c_0. In the latter case the wave is of trigger type and c_0 is the velocity of the solitary pulse.

In the same time many qualitatively different types of dispersion curves for trigger waves were found [19], which can be classified into: (*i*) monotonous, (*ii*) non-monotonic with a negative slope domain and (*iii*) oscillatory, which gives rise to alternating attrac-

tive and repulsive pulse interaction.

The more interesting case, namely oscillatory dispersion, is shown to be provided by the oscillatory decay of excitation behind a solitary pulse. It often occurs close to a supercritical Hopf bifurcation in the kinetics of the reaction-diffusion system. Due to the oscillation in the pulse tail, one can construct infinitely many equally spaced wave trains with wavelengths ranging up to infinity moving with the same velocity [52, 18]. The resulting wave train changes its stability depending on the interpulse distance periodically [18, 16]. Experimental evidence for oscillatory dispersion was reported as well, for example, in gas discharge experiments [24]. The interaction between the oscillatory tail and the head of the successive pulses can be so strong that it leads to locking-type phenomena, described theoretically in [68, 69, 70], see also previous chapter. Such locking results in the coexistence of two stable pulse trains with the same wavelength, but different propagation velocities.

There are many examples that in the same reaction-diffusion system both kinds of waves can exist at different parameters values [71], but the question of the transition between those wave types remains to our knowledge open. Moreover, waves at the boundary between phase and trigger dynamics are rich in instabilities, which can lead to new patterns like trace- and backfiring [72]. The purpose of the present chapter is to *capture the bifurcation scenario of the transition* between two types of waves in specific details, including the stability of waves in the transition region. The analysis of travelling waves is reduced to the study of their profiles and velocities in the so-called travelling wave ODE (profile ODE) assuming that the propagation velocity of the waves is constant.

First, we describe the origin of trigger and phase waves. Spatially periodic trigger wave trains are constructed of infinitely many periodic replications of the primary solitary pulse. In the phase space of the travelling wave ODE the limit cycles, representing these wave trains, exist close to the homoclinic solution, which describes the solitary pulse. The profile of phase waves is represented by periodic solutions that stem from a Hopf bifurcation of the homogeneous rest state of the PDE. In the limit of large wavelengths, trigger wave trains converge to solitary pulses with finite velocity. The profile of phase waves of large wavelengths approximates the limit cycle in the kinetics of the reaction-diffusion system under infinite increase of the propagation velocity. However, the large-wavelength limit is not always accessible in experiments (for example, spiral

waves usually send out short-wavelength wave trains), that is why we are interested in the connection between trigger and phase waves in the short-wavelength region.

Upon varying the control parameter from the regime of trigger waves to the regime of phase waves, we first observe twisted trigger wave dispersion, which is essentially provided by the oscillatory decay behind the solitary pulse. After the Hopf bifurcation in the appropriate co-moving frame, a branch of phase waves appears. At the critical point the dispersion curve of phase waves collides with the dispersion curve of trigger waves in the region of small wavelengths. The curve of the dispersion of the trigger waves collapses in a series of saddle-node bifurcations. The only dispersion curve, which persists in the "wavelength - velocity" parameter plane, is the dispersion of phase waves.

In order to get a thorough insight in the studied transition, we discuss in detail the stability properties of both types of waves close to the transition threshold. We elaborate the stability of the phase waves close to the transition region as well and show that phase waves first appear as unstable small-amplitude pattern and then stabilize, reaching large amplitude. We support our studies of the conversion between trigger and phase waves by one-dimensional simulations, which can be thought of as the first starting point for experimental proof of our results.

4.2 Model and methods

4.2.1 Model

In this chapter, as a representative model displaying for appropriately chosen parameter values both oscillatory as well as excitable kinetics, we consider the two-component Oregonator model modified to describe the photosensitive version of the BZ reaction [30]. In this reaction trigger and phase waves have been extensively studied for a long time [51]. The equations for the dimensionless concentration of bromous acid u, and the oxidized form of the catalyst v, read

$$\begin{aligned} \partial_t u &= \frac{1}{\epsilon}\big[u - u^2 - (fv + \phi)\frac{u-q}{u+q}\big] + \partial_x^2 u, \\ \partial_t v &= u - v. \end{aligned} \tag{4.1}$$

Diffusion of v is omitted because in most experiments the catalyst is immobilized in a gel matrix. The time scale ratio ϵ follows from the recipe concentrations [30]. In this

chapter, all parameters except ϕ are fixed at the following values $\epsilon = 0.05$, $f = 2.1$ and $q = 0.002$. The parameter ϕ is proportional to the intensity of applied illumination. It will be considered as the main bifurcation parameter which controls the local dynamics as well as the profile and the velocity of different wave solutions, playing the role of the "excitability" parameter in the system.

As already mentioned in the previous chapters, the Oregonator kinetics

$$\begin{aligned} \dot{u} &= \frac{1}{\epsilon}\big[u - u^2 - (fv + \phi)\frac{u - q}{u + q}\big] =: F(u, v), \\ \dot{v} &= u - v =: G(u, v) \end{aligned} \tag{4.2}$$

belongs to the wide class of activator-inhibitor models with two well-separated time scales (ϵ is assumed to be small) and a typical "s"-shaped nullcline $F(u, v) = 0$ (see Fig. 4.2 (b) and (c) for a sketch of nullclines $F(u, v) = 0$ and $G(u, v) = 0$). With the chosen parameters the Oregonator kinetics (4.2) has only one fixpoint, which undergoes a supercritical Hopf bifurcation at ϕ_{hb} (see Fig. 4.2). It is convenient to use ϕ_{hb} as a reference point for other bifurcations, say, for the stability threshold of solitary pulses. Under further decrease of ϕ the stable limit cycle born at ϕ_{hb} passes through a so-called canard explosion at ϕ_c and its size rapidly grows up. Detailed analysis of such bursting behavior and its relation to the excitability properties of the spatially extended system was presented in [31].

4.2.2 Methods

Again, we use the co-moving frame approach, considering only travelling waves with constant speed and profile. For the two-component Oregonator PDE the profile equations read

$$\begin{aligned} u'' + cu' + \frac{1}{\epsilon}\big[u - u^2 - (fv + \phi)\frac{u - q}{u + q}\big] &= 0, \\ cv' + u - v &= 0, \end{aligned} \tag{4.3}$$

where the prime denotes a derivative with respect to the co-moving coordinate and c denotes the velocity of the co-moving frame. We solve Eq. (4.3) for homoclinic connections and periodic solutions of period L which describe the solitary pulses and spatially periodic wave trains, respectively.

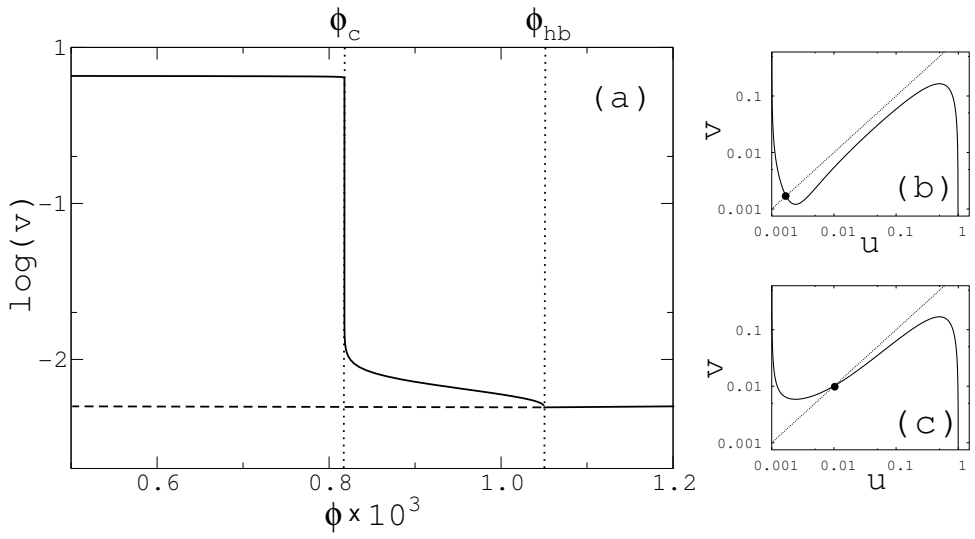

Figure 4.2: (a) Bifurcation diagram of the kinetics described by eqs. (4.2). Hopf bifurcation occurs at $\phi_{hb} = 1.04 \times 10^{-3}$. For the canard point we find $\phi_c = 0.81 \times 10^{-3}$. (b) Nullclines of the kinetics (4.2) above the Hopf bifurcation. (c) The same as (b) but below the ϕ_{hb}-point.

The linearization of Eq. (4.1) in the co-moving coordinate reads

$$\begin{aligned} \lambda u &= F_u u + F_v v + c u' + u'', \\ \lambda v &= u - v + c v', \quad u, v, \lambda \in \mathbb{C}. \end{aligned} \tag{4.4}$$

In order to get the stability properties of a given wave train, we equip the above system with the following boundary conditions:

$$(u, u', v)(L) = e^{2\pi(\eta + i\gamma)}(u, u', v)(0), \quad \eta, \gamma \in \mathbb{R}. \tag{4.5}$$

We say that λ is in the spectrum of the wave train if Eqs. (4.4), (4.5) have a bounded solution for $\eta = 0$.

In order to calculate the point spectrum of solitary pulses we approximate them by periodic solutions with large wavelength L. Every point eigenvalue of the solitary pulse is then approximated by a closed curve of the essential spectrum. The size of the curve goes exponentially to zero as $L \to \infty$, see second chapter.

4.3 Trigger Waves

As mentioned above, trigger waves are slow diffusion-dependent propagating structures. They can appear either as solitary pulses or form spatially periodic trigger wave trains. The dispersion curve and the stability properties of the latter are strongly determined by the type of decay behind the corresponding solitary pulse [73, 74, 45]. Under decrease of parameter ϕ (increase of excitability), three qualitatively different types of solitary pulses and dispersion curves of the accompanying wave trains are found.

4.3.1 Solitary pulses

The reaction-diffusion system (4.1) supports propagation of solitary excitation pulses in the parameter region $\phi > \phi_c$. We obtain the dependence of the pulse velocity on ϕ performing continuation of the corresponding homoclinic solution of Eq. (4.3) in the (ϕ, c) parameter plane (Fig. 4.3 (a)). For a given ϕ value there simultaneously exist two pulses, one stable and one unstable. They collide in a saddle-node bifurcation SN at $\phi = \phi_{SN}$ parameter value (for comparison, see analytical results on FitzHugh-Nagumo model in [75]). The present work focuses on the stable pulses belonging to the upper branch.

This branch is divided by point F (Fig. 4.3 (a)). At this point the equilibrium in the travelling wave ODE (4.3) undergoes a saddle to saddle-focus transition and the homoclinic trajectory approaches the equilibrium in an oscillating manner. The equilibrium has for $\phi_H < \phi < \phi_F$ one unstable one-dimensional manifold (for the pulses, propagating to the left, as shown by Fig. 4.3), which describes the front of the pulse. The stable two-dimensional manifold with the corresponding complex-conjugated eigenvalues describes the decay behind the pulse (Fig. 4.3, compare panels (c) and (d)). For the pulses that propagate in the opposite direction with velocity $-c_0$, the fixpoint has contrariwise two unstable complex-conjugated eigenvalues that render the oscillatory tail of the pulse, and one stable eigenvalue, which is responsible for the front of the pulse.

With further decrease of ϕ parameter the equilibrium of the profile equations undergoes a Hopf bifurcation (point H in Fig. 4.3) at $\phi_H = 9.0 \times 10^{-4}$, and the pair of complex-conjugated eigenvalues crosses the imaginary axis, moving from the right to the left complex half-plane. The pulse solution below this bifurcation corresponds to a heteroclinic connection between the equilibrium and the small-amplitude limit cycle,

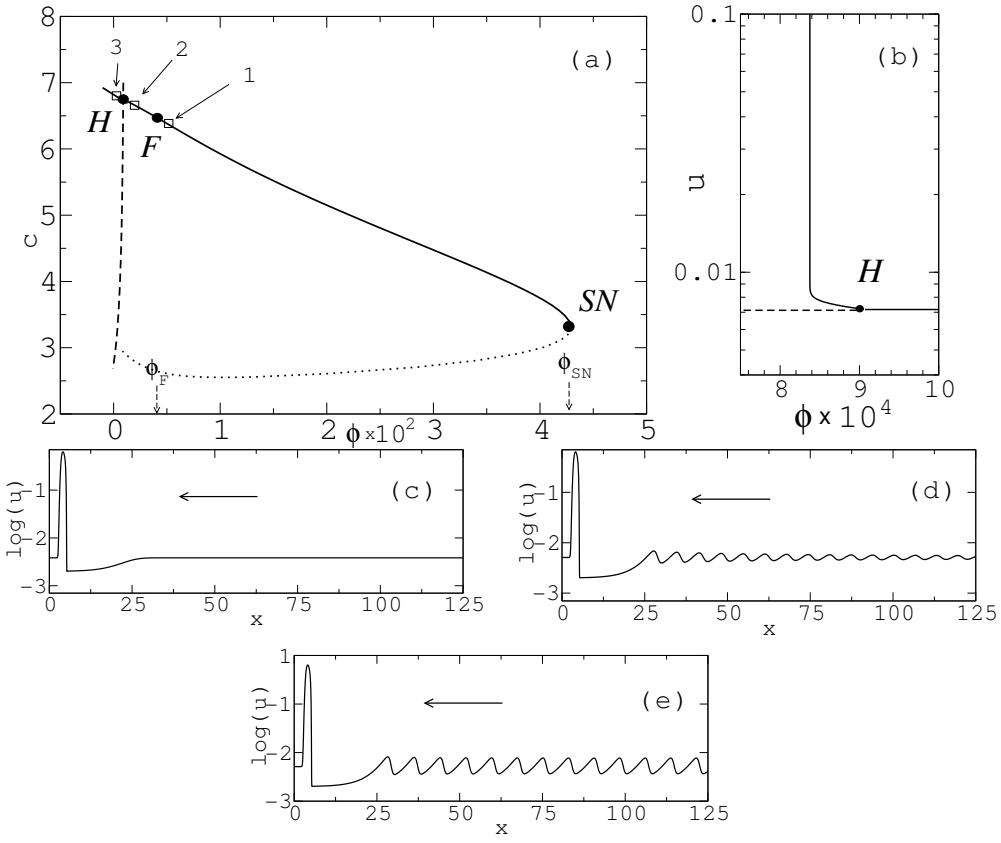

Figure 4.3: (a) Velocity of solitary pulse vs. parameter ϕ. SN denotes the saddle-node bifurcation (extinction threshold), F denotes the transition from saddle to saddle-focus and H corresponds to the Hopf bifurcation of the equilibrium. The solid line corresponds to stable pulses, the dotted - to unstable. The dashed line denotes the locus of the Hopf bifurcation of the equilibrium in the travelling wave ODE. The extinction threshold is given by $\phi_{SN} = 4.29\times10^{-2}$, point F - by $\phi_F = 4.1\times10^{-3}$ and H point by $\phi_H = 9.0\times10^{-4}$. Labels $1, 2$ and 3 mark the location of the pulses in panels (c)-(e). (b) Unfolding of the Hopf bifurcation in the travelling wave ODE for a given value of c with a rapid canard-type growth of the amplitude of the new-born limit cycle. The Hopf bifurcation for the given velocity c occurs at $\phi_H = 9.03\times10^{-4}$, and the canard explosion at $\phi_c = 8.38\times10^{-4}$. (c) Stable pulse profile for $\phi_F < \phi = 4.2\times10^{-3} < \phi_{SN}$. (d) Stable pulse profile for $\phi_H < \phi = 9.5\times10^{-4} < \phi_F$. (e) Pulse with undamped oscillatory tail for $\phi = 8.5\times10^{-4} < \phi_H$.

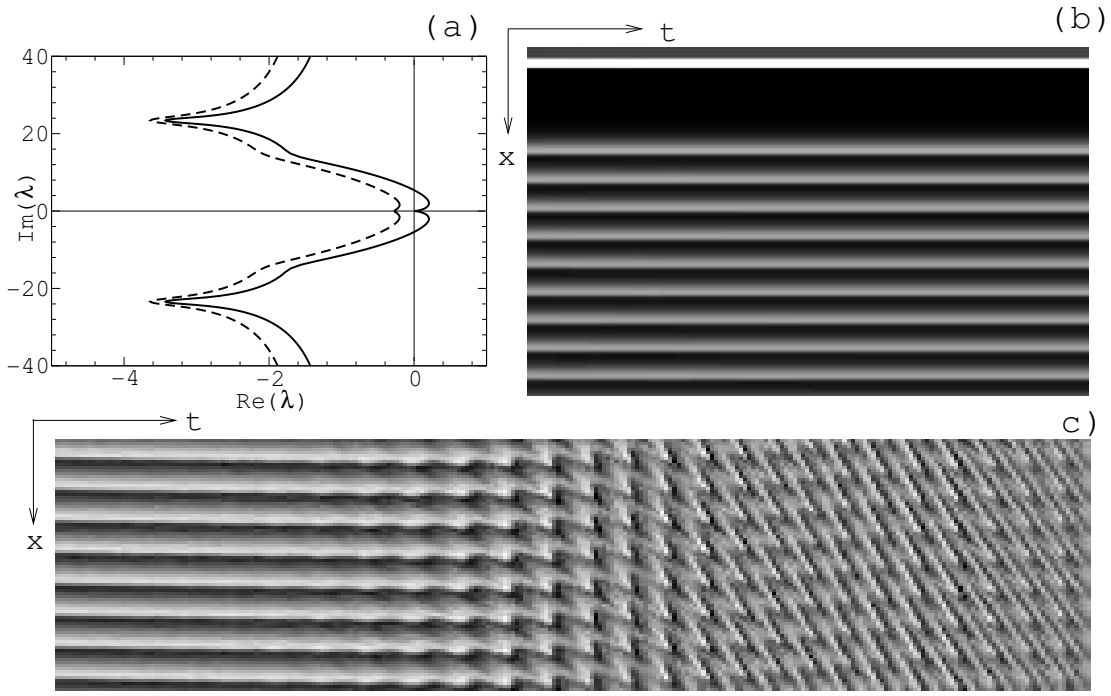

Figure 4.4: (a) Solid line shows the leading part of the essential spectrum of the small-amplitude wave train behind the pulse head. Dashed line shows the spectrum in the weighted space with weight $\eta = 5.26 \times 10^{-1}$. (b) Space-time plot of a running solitary pulse in the co-moving frame. The logarithm of the u variable is coded in gray-scale with light (dark) colors corresponding to high (low) values, respectively. The simulations were made with Dirichlet boundary conditions in the front of the pulse and Neumann boundaries behind it. (c) Space-time plot of simulations of the periodic wave train, the color coding is renormalized to the actual maximal and minimal values of the variable. Periodic boundary conditions are applied.

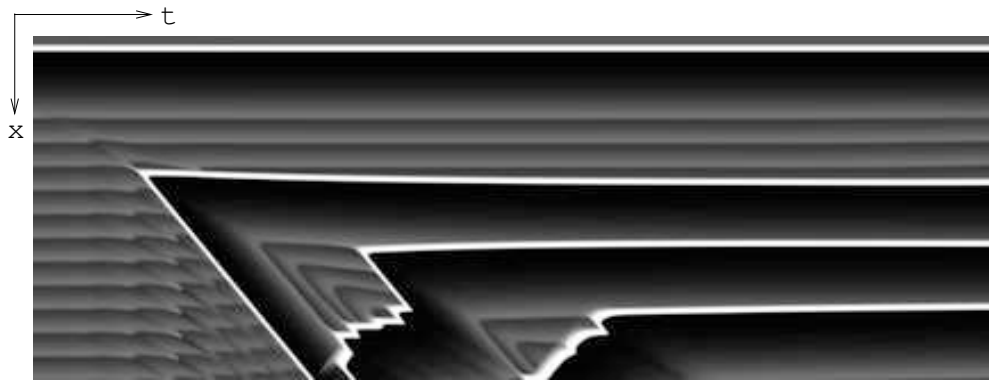

Figure 4.5: Appearance of high-amplitude pulse heads behind the primary pulse ($\phi = 8.405 \times 10^{-4}$). Dirichlet boundary conditions and co-moving coordinate system.

which is born in the bifurcation point (Fig. 4.3(e)). This bifurcation is of very special meaning for the pulses in the reaction-diffusion system: it describes the appearance of undamped tail oscillations behind the pulse. From the mathematical point of view, this is a codimension-2 Shilnikov-Hopf bifurcation [76].

Now we turn to the stability properties of the solitary pulses. Pulses belonging to the faster branch, are found to be stable for $\phi_{hb} < \phi < \phi_{SN}$. We checked this fact by simulating the time evolution of the corresponding profiles. The essential spectrum of the solitary pulse is contained in the left half-plane, since the homogeneous background is stable for $\phi > \phi_{hb}$. The isolated eigenvalues were checked numerically by direct computation of the eigenvalues of the discretized linear operator.

Next, we discuss the pulses below the H point with the undamped oscillations in the tail. Numerical simulations reveal that they are stable on bounded domains due to the convective nature of the instability of the periodic wave train behind the pulse head (Fig. 4.4(b), see also section "Phase Waves"). The essential spectrum of the small-amplitude wave train is shown on Fig. 4.4(a). The instability is of a long-wavelength type, since $\frac{d^2}{d\gamma^2}\mathrm{Re}(\lambda) > 0$ (see Eq. (4.5)) near the origin. Moreover, the instability is only convective, because we can shift the spectrum completely in the left half-plane, introducing an exponential weight $\eta \neq 0$ (see Eq. (4.5)). Simulations of the small-amplitude wave train with periodic boundaries uncovers the essential instability (Fig. 4.4(c)).

Under further decrease of parameter ϕ we see the phenomenon, which is often referred

to as trace- and backfiring [72]. A pair of the high-amplitude pulse heads emerges behind the primary pulse (Fig. 4.5). After a certain transient time, the whole domain behind the pulse is occupied by the high-amplitude wave train. This stationary pattern can be thought of as a heteroclinic connection between the equilibrium and a periodic orbit, representing the wave train, triggered by the running pulse. We would like to note that the discussed appearance of the new high-amplitude pulse heads seems also to be of the canard-like nature, because small changes in the parameter values lead to a significant transformation of the solution.

4.3.2 Trigger wave trains

Now we would like to construct periodic wave trains of pulses with identical profiles. The interaction and stability of such wave trains will be determined mostly by the decay behind the corresponding solitary pulse, which was discussed in the previous subsection.

In Fig. 4.6 we compare the type of the dispersion relation with the corresponding type of the decay behind the associated solitary pulses (Fig. 4.3). Low excitability of the system, which causes the tail of the solitary pulse to relax to the background state monotonously, results in a monotonous dispersion relation for the associated wave trains. After the transition from saddle to saddle-focus, marked as the F-point in Fig. 4.3 (a), below which a solitary pulse displays damped tail oscillations, the dispersion curve becomes non-monotonous, combining parts with negative and positive slope.

The corresponding periodic orbits include a high-amplitude part and small-amplitude windings, whose number grows for large periods L. This picture is general for periodic orbits near a homoclinic connection of the Shilnikov type [40, 41]. The interaction between the pulses in such a wave train, either attractive or repulsive, depends on the interpulse distance. Note also that there can coexist infinitely many wave trains with the *same velocity*, but of *different wavelengths*.

Crossing the line of the Hopf bifurcation under decrease of ϕ, we observe a qualitatively new type of dispersion curve (Fig. 4.6 (c)). From the dynamical systems viewpoint, for $L \to \infty$ we have a codimension-zero situation with two homoclinic trajectories to a limit cycle, accompanied by a set of periodic orbits. These periodic orbits form a wiggly curve with fold points, accumulating at homoclinic tangencies [76, 77]. The small-amplitude windings of the limit cycles are very close to the small periodic orbit, which was born in the Hopf bifurcation. Another important feature of this dispersion is

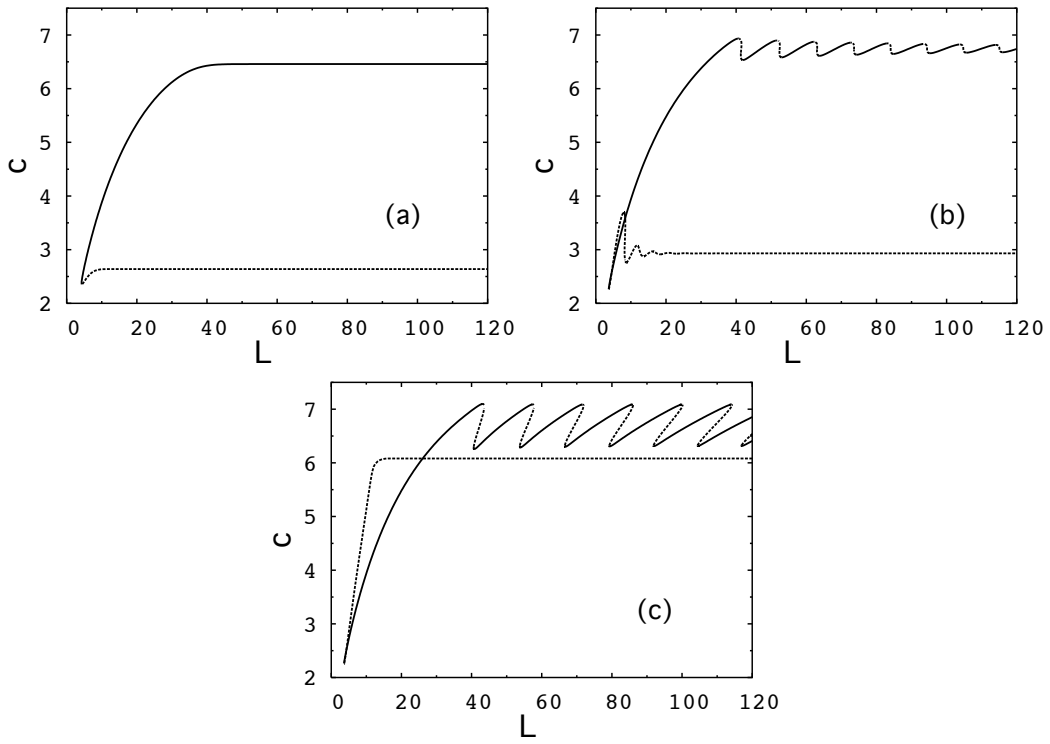

Figure 4.6: Different dispersion curves of trigger wave trains as parameter ϕ is decreased (increasing excitability). Solid lines show stable solutions, dashed lines show unstable solutions. (a) Just above the F point, $\phi = 4.2\times10^{-3}$. Solitary pulse has monotonously decaying tail, compare with Fig. 4.3 (c). (b) Between the Hopf bifurcation and the F point, $\phi = 9.5\times10^{-4}$. Solitary pulse has decaying oscillatory tail, compare with Fig. 4.3 (d). (c) Below the Hopf bifurcation $\phi = 8.5\times10^{-4}$. Solitary pulse has non-damped oscillatory tail, compare with Fig. 4.3 (e).

the presence of domains of bistability. Every such section contains three coexisting wave train solutions, two of them are stable and separated by an unstable one.

The phenomenon of the bistability of wave trains was first reported in [70] (see also the previous chapter). However, in the case of the three-component Oregonator model, the phenomenon of coexistence occurs above the Hopf bifurcation and, as a consequence, the size of the bistability domains decreases with L. In the present case the bistability domains become larger with increasing L. Considering the stability of the wave trains belonging to the domains of bistability, we found for the two-component Oregonator qualitatively the same results as reported in the previous chapter. Here, we omit the details on the stability of periodic wave trains which belong to the domains of bistability.

The last part of this section on trigger waves we would like to address to their instabilities, caused by an increase of the excitability of the system (decrease of ϕ). Let us take a look at the dependence of the velocity of a particular trigger wave train of wavelengths $L = 48$ on parameter ϕ (see Fig. 4.7). We chose this wavelength, because the corresponding wave train belongs to the middle of the stable branch of the dispersion curve and is not subjected to the instability, which is related to the circle of critical eigenvalues and negative slope of the dispersion curve. In point U the wave train becomes unstable, this instability is of long-wavelength type, as it can be seen from Fig. 4.7 (b). Numerical simulations (Fig. 4.7 (c)) reveal that the wave head tends to solder with the minor maximum in front of it, effectively increasing the propagation velocity of the whole wave train. After a long transient process (not shown in Fig. 4.7(c)), we obtain a new wave train without secondary maxima between the successive pulse heads, propagating at a larger velocity (see section below).

In point SN in Fig. 4.7 (a) two limit cycles, one from the upper part of the dispersion curve and one from the lower unstable part, collide upon decrease of ϕ. Globally this leads to the disappearance of the whole dispersion curve of trigger waves for smaller values of the parameter ϕ. This fact will be important for the transition from trigger waves to phase waves, see the corresponding section below.

4.4 Phase Waves

Phase waves are simpler objects than trigger wave trains in the sense that their form and properties do not depend on the wavelength as dramatically.

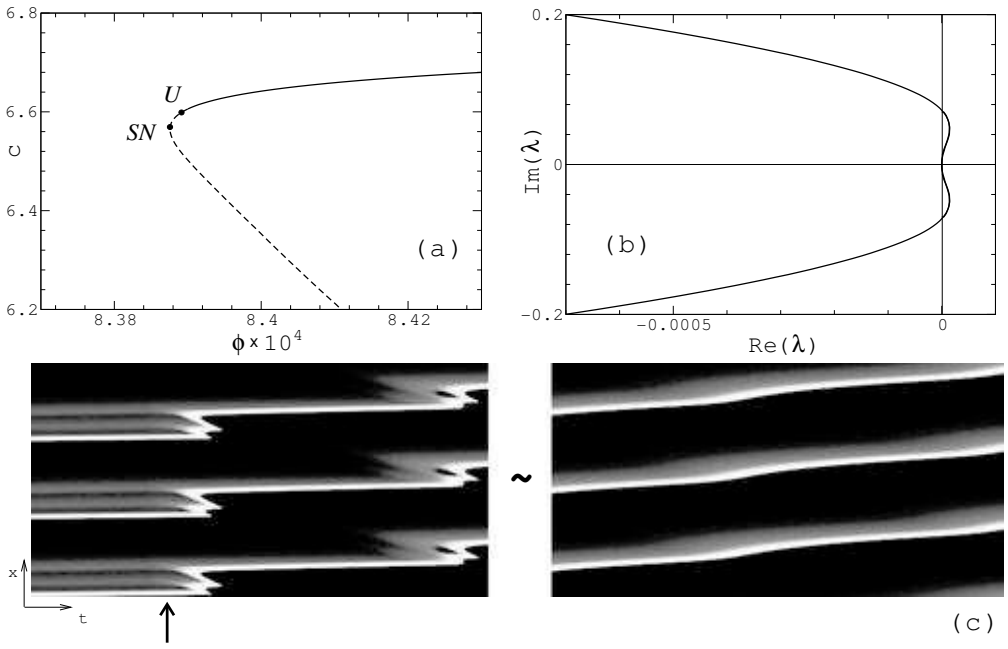

Figure 4.7: (a) Bifurcation diagram for a particular trigger wave train, showing the instability point U and the point of the collision with the twin wave train, belonging to the slower unstable dispersion branch. (b) Leading part of the eigenvalue spectrum of trigger wave train between U and SN points. (c) Space-time plot of a numerical simulation displaying the destruction of a trigger wave train. The parameter ϕ was initially set to $\phi = 8.4\times10^{-4}$ and than changed to the value $\phi = 8.0\times10^{-4}$. The arrow shows the parameter adjustment. The long transition process between the first and the last parts of the plot is cut out.

If $u(z)$ is a periodic solution of the profile equation

$$Du'' + cu' + f(u) = 0, \quad ' := \partial_z$$

then, introducing a new variable $\xi = cz$, we obtain

$$f(u) + \partial_\xi u + c^{-2} D\, \partial_\xi^2 u = 0.$$

In the limit of fast waves, $c \to \infty$, the diffusive term can be neglected ($c^{-2} \to 0$), and we end up with

$$\partial_z u = -c^{-1} f(u). \tag{4.6}$$

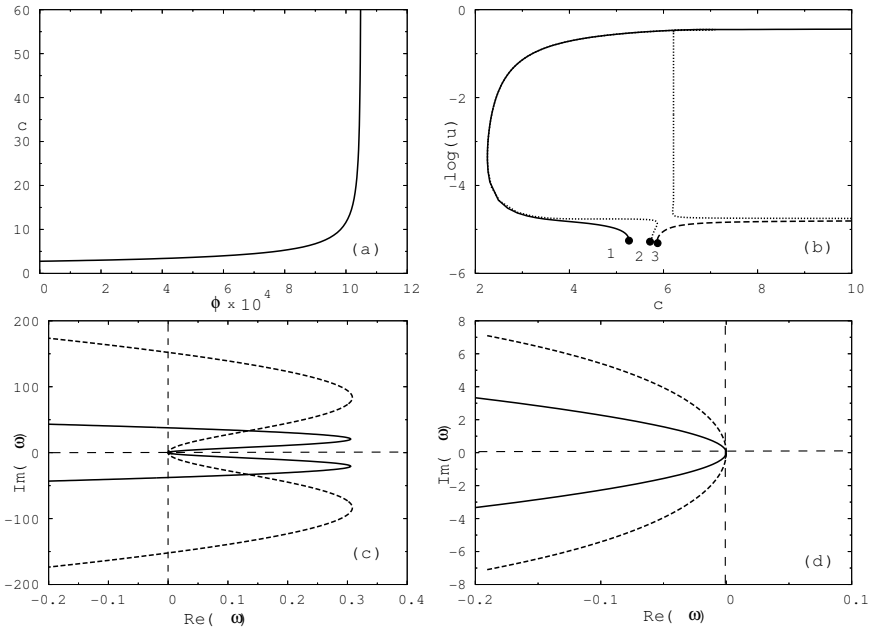

Figure 4.8: (a) Locus of the Hopf bifurcation in the (ϕ, c) parameter plane. (b) Three different scenarios of unfolding of the limit cycles from the Hopf bifurcation. Solid line, originating from point 1: $\phi = 8.0 \times 10^{-4}$. Dotted line, originating from point 2: $\phi = 8.41 \times 10^{-4}$. Dashed line, originating from point 3: $\phi = 8.5 \times 10^{-4}$. (c) Spectra of the small amplitude phase waves at $\phi = 8.5 \times 10^{-4}$: solid (dashed) line corresponds to wavelength $L = 50$ ($L = 200$). (d) Spectra of the large amplitude phase waves at $\phi = 8.0 \times 10^{-4}$: solid (dashed) line corresponds to wavelength $L = 50$ ($L = 100$).

We read off from Eq. (4.6) that the profile of the periodic solution $u(z)$ is given by the corresponding periodic orbit in the kinetics of the system with reversed variable z. For the periodic solution $u(z)$ of Eq. (4.6), parameter c scales its period, providing the observed linear dispersion relation $c = \alpha L, \alpha = \text{const}$, of phase waves for large c. Homogeneous bulk oscillations can be thought of as a degenerated example of phase waves propagating at infinite velocity.

Starting with initial values (ϕ_{hb}, ∞), which correspond to the appearance of homogeneous oscillations (Hopf bifurcation in the kinetics), continuation of the locus of the Hopf bifurcation in the (ϕ, c) parameter plane gives the curve depicted in Fig.4.8 (a). In order to get different dispersion curves of phase waves, we unfold the bifurcation in the

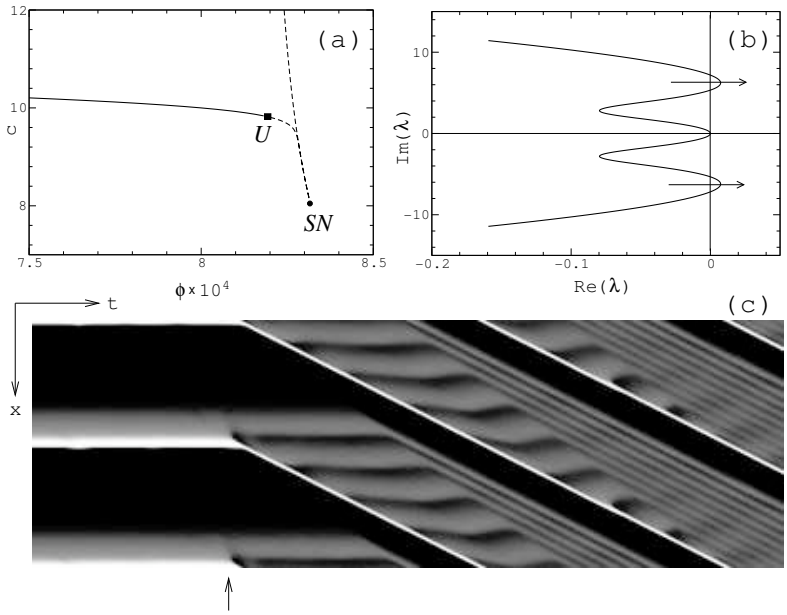

Figure 4.9: (a) Dependence of the propagation velocity of a phase wave train on the ϕ parameter. The U point denotes the instability of the wave train, the corresponding ϕ value is $\phi_U = 8.22 \times 10^{-4}$. The SN points denotes a saddle-node bifurcation of the corresponding limit cycles in the travelling wave ODE. (b) Part of the essential spectrum of the unstable phase wave train slightly above the U point, $\phi = 8.23 \times 10^{-4}$ (c) Space-time plot of phase wave train in the co-moving frame, subjected to parameter jump from $\phi = 8.0 \times 10^{-4}$ to $\phi = 8.5 \times 10^{-4}$. Logarithmic grayscale coding and co-moving frame coordinates as in the figures above. The vertical arrow shows the moment of the parameter switching.

(c, L) parameter plane for different values of ϕ (Fig.4.8 (b)).

There are two qualitatively different scenarios of unfolding of the phase waves from the Hopf bifurcation. The result of the first one is the appearance of large-amplitude phase waves. This scenario occurs for smaller values of ϕ, see the solid line in Fig.4.8(b). The velocity of the wave together and its wavelength both go to infinity, while the profile remains the same. If we unfold the bifurcation at a larger value of parameter ϕ, a large-amplitude wave doesn't emerge, see Fig.4.8(b), the long-dashed line. The profile of the wave again converges to the limit cycle of the kinetics as the velocity and the wavelength go to infinity. There is also some intermediate scenario, in which the wave first achieves

the full amplitude, but then becomes smaller again (Fig.4.8(b), short-dashed line).

We found that the small-amplitude phase waves are unstable in the whole wavelength range up to infinity (Fig.4.8(c)). Changing the wavelength and the velocity of the wave scales the spectrum of it in respect to the imaginary axis. The large-amplitude phase waves are found to be stable in the whole wavelength range with the same scaling property of their spectrum (Fig.4.8(d)).

Now we would like to describe the instabilities of the phase waves under variation of parameter ϕ. As we can see from the bifurcation diagram and the essential spectrum of the wave (Fig. 4.9 (a) and (b)), the phase wave train becomes linearly unstable. This instability occurs at a finite wavelength. Numerical simulations (Fig. 4.9 (b)) show that the instability of the phase waves leads to the appearance of a number of secondary maxima between two successive high-amplitude wave parts. The wave tries to "localize" itself, tending to form a trigger wave train, which propagates at a slower velocity.

It is worthwhile to compare the destruction of phase waves under increase of ϕ and the break-up of trigger waves while the parameter ϕ is decreased. Both Fig. 4.7 (c) and Fig. 4.9 (c) look very similar under reversion of time. Whereas the high-amplitude heads of the trigger waves tends to merge with the next maximum, the high-amplitude part of the phase wave train breaks down, sprouting a new small-amplitude maximum in front of it.

4.5 Collision of dispersion curves

It turns out that this transition can be captured in the dispersion plane, where trigger and phase waves are clearly distinguishable by the shape of their dispersion curve.

Fig. 4.10 (a) shows the initial situation before the transition: the line, which unfolds from the Hopf bifurcation, is the branch of phase waves, and the branch of trigger waves is presented by the comb-like dispersion (Fig. 4.10 (a)). Adjusting to $\phi = 8.41\times10^{-4}$ (Fig. 4.10 (b)), the dispersion of phase waves collides with the lower branch of the dispersion of trigger waves. Looking at the resulting joint curve we note that the dispersion that descends from the Hopf bifurcation goes now along the skeleton of the trigger wave dispersion towards large L, nearly repeating its shape. After that the curve turns back in point C and goes again towards infinity along the linear part of the dispersion. At $\phi = 8.2\times10^{-4}$ (Fig. 4.10 (c)) we observe a simple dispersion, originating from the Hopf bifurcation, with a linear part, which goes towards infinity without winding around the

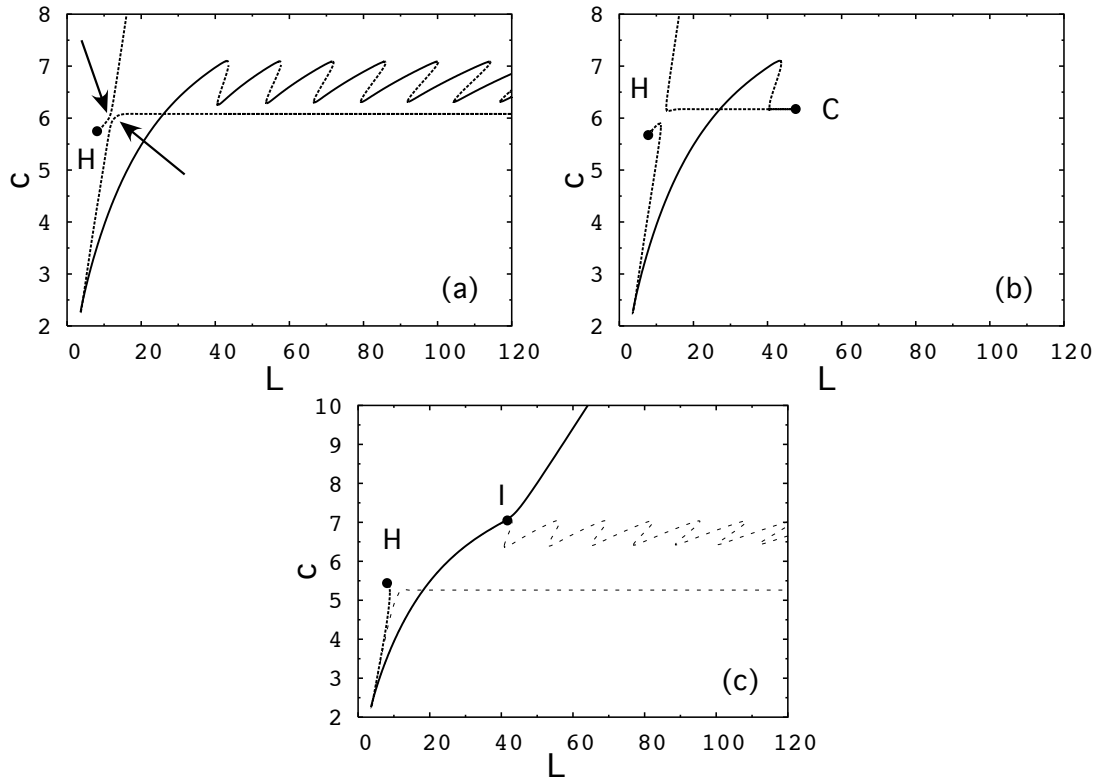

Figure 4.10: (a) Dispersion relation for trigger and phase waves for $\phi = 8.42 \times 10^{-4}$. The dotted curve, originating from point H represents phase waves. The curve with the comb-like upper branch is the dispersion relation of trigger waves. The arrows show the location of the up-coming transcritical collision between both curves. (b) Both dispersions, just after the transcritical collision, $\phi = 8.41 \times 10^{-4}$. C denotes the turning point, see text. (c) Dispersion relation of phase waves at an even lower value $\phi = 8.0 \times 10^{-4}$. The thin dashed gray line shows the dispersion of trigger waves at a different ϕ value for sake of comparison. I denotes the inflection point, see text.

"skeleton" structure of the trigger wave dispersion.

Concerning the position of the turning point C, we make the following observations. If ϕ is slightly smaller than the critical value $\phi_{tr} = 8.418 \times 10^{-4}$, the point C is located at large values of L. Upon further decrease of ϕ , point C shifts to the left and disappears. At $\phi = 8.2 \times 10^{-4}$ the dispersion curve leaves the skeleton in the I point, as described by Fig. 4.10 (c). Point C is closely related to the disappearance of the trigger waves, since it gives the section of the line of fold bifurcations of trigger waves (in three-dimensional parameter space (c, L, ϕ)) with parameter plane (c, L) . The section of the fold bifurcation line with plane (ϕ, c) is given by point SN in Fig. 4.7 (a).

We can define the parameter value ϕ_{tr}, at which the collision between dispersion curves of phase and trigger waves takes place, as the boundary, which delimits the regimes of phase and trigger waves. Above ϕ_{tr} there coexist stable trigger waves and unstable small-amplitude phase waves. Below the boundary the only waves that exist are phase waves. The value ϕ_{tr} is bracketed by the Hopf bifurcation ϕ_{hb} and the canard explosion ϕ_c of the limit cycle in the kinetics of the reaction-diffusion system.

4.6 Discussion and Outlook

In this chapter we reveal fine details of the transition between phase waves and triggers waves in a general two-component reaction-diffusion system with a cubic nonlinearity and well-separated time scales. The kinetics of the system can be controlled between excitable and oscillatory dynamics with a single parameter. Trigger waves and phase waves are "natural" spatial solutions for those two types of the kinetics.

The scheme of the transition between trigger and phase waves includes: (*i*) emergence of oscillations behind the solitary pulse, first damped. These cause damped oscillations in the dispersion relation of trigger wave trains. (*ii*) introduction of phase waves via the Hopf bifurcation in the travelling wave ODE, first at infinite velocity (bifurcation in the kinetics), then continuously in the co-moving frames with the appropriate velocity. The oscillations in the decay behind the solitary pulse and in the dispersion of trigger wave trains become undamped. (*iii*) The collision of the phase wave dispersion with the dispersion of trigger waves. (*iv*) Successive disappearance of trigger waves of large periods in a series of saddle-node bifurcations. Similar results on the studied transition were obtained for FitzHugh-Nagumo and Barkley models [59], which suggests that the observed scenario is generic for the whole class of active media, possessing in dependence

on a parameter both excitable (with one fixpoint) and oscillatory kinetics.

Being guided by the observation above, we find that the following classification between trigger and waves can be extremely useful. Phase waves are described by the periodic solutions of the travelling wave ODE, which descend from the Hopf bifurcation of the equilibrium. Trigger wave trains are described by periodic solutions, which exist close to the homoclinic orbit, that renders the shape of the appropriate solitary pulse. The origin of trigger and phase waves is reflected in the peculiarities in their dispersion curves, making the analysis of the dispersion curves a very suitable tool in the presented study.

We present results of the linear stability analysis of phase and trigger waves belonging to the colliding dispersion curves. For phase waves, we find that small-amplitude phase waves are unstable in the whole range of wavelengths and the full-developed, high-amplitude phase waves are stable.

We strongly believe that the experimental verification of the reported scenario of the transition between phase and trigger waves should be the next step on the field. One of the main objectives of the experimental proof is the existence of the small-amplitude phase waves, which play quite a deciding role in our study and which are experimentally not yet found to the best of our knowledge. However, the experimental evidences of trace- and backfiring can be thought of as hints for the existence of these small-amplitude oscillations.

Chapter 5

Creating bound states by means of non-local coupling

5.1 Introduction

Propagation of pulses in excitable media is an important phenomenon in physical, chemical and biological systems, including chemical reactions, signal propagation in neuronal tissue, brain activity and calcium waves in living cells [3]. Typically such pulses can propagate due to local diffusive coupling between the excitable elements of the medium. The interaction between two pulses that propagate in the same direction is usually repulsive, which means that the second pulse in a pulse pair runs more slowly than the first one [2].

However, pulses in reaction-diffusion systems do not always interact only repulsively, but can form so-called bound states with two or more pulses that propagate at the same velocity. Such bound states were found in chemical reaction-diffusion systems experimentally [20, 23, 22, 21]. A kinematic approach was introduced in [15, 78], where the existence of bound states was closely related to the anomalous dispersion of periodic pulse trains.

The main motivation for the consideration of non-local coupling comes from neuroscience – it was shown that neurons communicate by means of long-range interactions [79, 80]. Non-local coupling plays an important role in certain electrochemical reactions [81, 82] as well. Recent theoretical findings include the improvement of synchronization of coupled oscillators [83], the emergence of completely new dynamical regimes (the

so-called chimera states) [84], spiral waves with randomized core [85], chemical turbulence induced by non-local coupling [86], and many others. Nicola et al. reported a codimension-2 Turing-wave bifurcation and a region of bistability between Turing and wave patterns resulting from inhibitory non-local coupling [87, 88]. Spiral patterns on a stationary background have been observed recently in experiments with the Belousov-Zhabotinsky reaction under influence of non-local coupling with short-range activation and long-range inhibition [89]. For the Oregonator model of the Belousov-Zhabotinsky reaction it has been shown that non-local coupling can induce Turing and wave instabilities of the homogeneous steady state. While a long-range activation was found to induce travelling waves, long-range inhibition leads to stationary Turing patterns [90]. While most of the results on the impact of non-local coupling obtained so far are related to the instabilities of the homogeneously steady state, in this chapter we focus on the effect of non-local coupling on the interaction of propagating excitation pulses.

The main result of the present chapter is the following. Suppose that we have a reaction-diffusion system that supports propagation of solitary pulses of excitation, which interact repulsively through their monotonic refractory tails. Introducing non-local coupling in the form of a convolution of the pulse profile with an exponentially decaying kernel results in the attractive interaction of pulses and the emergence of bound states. Regardless of the particular excitable kinetics, bound states bifurcate from the primary solitary pulse at non-local coupling strength $\mu = 0$. More specifically, we show that the solitary pulse for $\mu = 0$ is represented by a homoclinic orbit of codimension-4, which is unfolded upon setting $\mu \neq 0$. In this description, bound states are represented by 2-homoclinic orbits which bifurcate at $\mu = 0$ from the primary one, corresponding to the solitary pulse. We illustrate our analysis by numerical calculations with a model for the light-sensitive Belousov-Zhabotinsky reaction [51].

From the mathematical viewpoint, the stability theory of multi-bump pulses (bound states of pulses) and weak interaction of pulses are developed in [17] and thoroughly reviewed in a more general context in [14]. The mathematical background for the bifurcation and the existence of bound states is provided by the theory of codimension-2 bifurcations of homoclinic orbits in $\mathbb{R}^N, N \geq 3$, see [13]. For a review and analytical description of codimension-2 homoclinic orbits in a simple toy model see [34] and references therein. We refer also to [91, 92] for codimension-3 resonant flip bifurcations.

This chapter is organized as follows. First, we present our numerical observations on

bound states in the Oregonator model with non-local coupling and give a simple model-specific explanation how these bound states come into play due to non-local coupling. Then we consider an abstract reaction-diffusion equation with non-local coupling and show that the emergence of bound states occurs independently on the specific kinetics of the model. In our considerations we will need some essential results on the codimension-2 bifurcations of homoclinic orbits, which will be discussed briefly in Section 5.3.2.

5.2 Results with Oregonator model

5.2.1 Emergence of bound states

We consider first solitary pulses in the Oregonator model for the excitable light-sensitive Belousov-Zhabotinsky reaction [30]

$$\begin{aligned} \partial_t u &= \epsilon^{-1}\big[u - u^2 - (fv + \phi)\frac{u-q}{u+q}\big] + \partial_{xx} u, \\ \partial_t v &= u - v, \end{aligned} \tag{5.1}$$

subjected to a non-local coupling through the field $\phi(x)$ of characteristic coupling range $\sigma^{-1} \gg 1$ and strength μ

$$\phi(x) = \phi_0 + \mu \int_{-\infty}^{\infty} e^{-\sigma|y|}[v(x+y) - v(x)]dy. \tag{5.2}$$

The activator variable u is proportional to the concentration of bromous acid and the inhibitor v represents the oxidized form of the catalyst. In this section, we fix the parameters values as follows: $\epsilon^{-1} = 20, f = 2.1, q = 0.002, \phi_0 = 0.008, \sigma = 0.1$. This choice of the parameters corresponds to excitable local dynamics of Eq. (5.1).

With the above set of parameters and $\mu = 0$, Eq. (5.1) supports propagation of stable solitary pulses of excitation, see Fig. 5.1 (a). The parameter ϕ_0 describes an additional light-induced inhibitor production and setting it to larger values makes the pulses of excitation propagate slower (Fig. 5.1(b)), which will be an important fact for our considerations later on. From this viewpoint, $\mu > 0$ corresponds to an inhibitory non-local coupling, while choosing $\mu < 0$ makes non-local coupling (5.2) be of an activatory type.

Without non-local coupling (i.e. for $\mu = 0$), pulses in Eq. (5.1) interact only repulsively, which can be seen from the positive slope of the dispersion curve for pulse trains

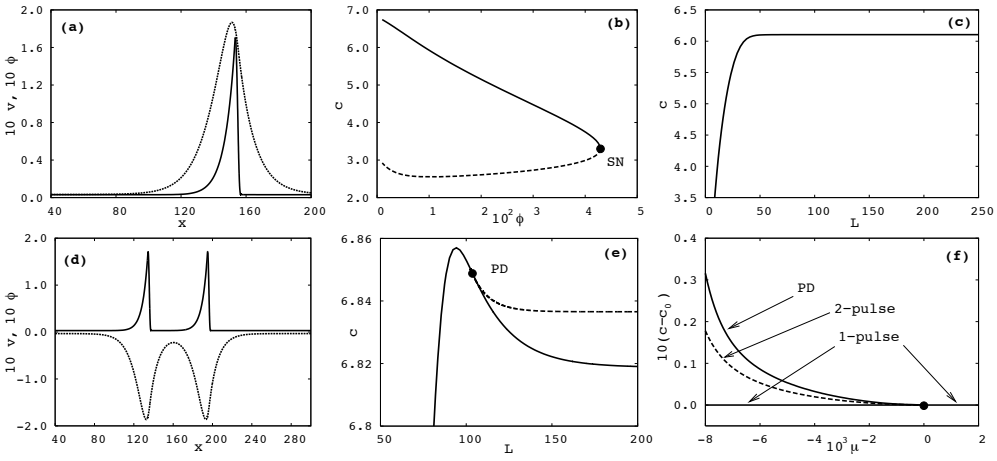

Figure 5.1: (a) Profile of a solitary pulse in Eq. (5.1) for $\mu = 0$, where rescaled variable $v(x)$ is shown by the solid line and the rescaled value of the integral in Eq. (5.2) is shown by the dashed line. (b) Dependence of the velocity of a solitary pulse c on the parameter ϕ_0. Solid (dashed) line represents stable (unstable) solitary pulses, respectively. (c) Dispersion curve of spatially periodic pulse trains for $\mu = 0$ showing the velocity of pulse train c versus the interpulse distance L. (d) Profile of a bound state for $\mu = -8.0 \times 10^{-3}$, solid and dashed line show rescaled $v(x)$ and rescaled $\phi(x)$, respectively. (e) Dispersion curve for $\mu = -8.0 \times 10^{-3}$. Point PD indicates period doubling, see text. Dashed line displays the dispersion curve for pulse trains with doubled interpulse distance. (f) Relative velocity of two-pulse solutions (dashed line) and that of the pulse trains that undergo the period-doubling bifurcations PD (solid line) in comparison with the velocity of solitary pulse c_0 versus the non-local coupling strength μ.

with large interpulse distances (Fig. 5.1 (c)). Upon switching on the coupling strength to the value $\mu = -8.0 \times 10^{-3}$, we observe that pulses do not interact repulsively anymore, but can in contrast form bound states with two pulses propagating at the same velocity (Fig. 5.1 (d)). Our numerical computations show that the emerged bound state is linearly stable, see next subsection. The dispersion curve for spatially periodic pulse trains for $\mu = -8.0 \times 10^{-3}$ displays an overshoot followed by a domain with a negative slope (Fig. 5.1 (e)). Near the maximum of the dispersion curve we find a period-doubling bifurcation that corresponds to the emergence of non-equidistant pulse trains.

Plotting the relative velocity of the double-pulse solution (i.e. compared to the velocity of the solitary pulse c_0 for the same value of μ) and that of the period-doubling

bifurcation versus the coupling strength μ, we see that the two-pulse solutions and the period-doubling bifurcation stem exactly from the point $\mu = 0$ (Fig. 5.1(f)). The interpulse distance of the pulse trains that undergo the period-doubling bifurcation PD approaches infinity for $\mu \to 0$ (not shown in figures).

Using the fact that the field $\phi(x)$ acts as a second inhibitor in Eq. (5.1), we can give a heuristic explanation for the emergence of bound states. For $\sigma^{-1} \gg 1$, the profile of $\phi(x)$ is much broader in comparison with $u(x)$ und $v(x)$, and the interaction of pulses within a bound state is dominated by the interaction of the second pulse with the ϕ-wake of the first pulse. If $\mu > 0$, the values of $\phi(x)$ are larger than ϕ_0, and the ϕ-wake of the first pulse slows down the second one, making bound states impossible. In the case of $\mu < 0$, the profile of $\phi(x)$ behind the first pulse approaches ϕ_0 from below, which effectively makes the second pulse propagate faster until it abuts against the stronger inhibitory tail of the variable $v(x)$. We stress that for every negative $\mu \to 0$ there exist a bound state, since for large interpulse distance the attracting interaction with longer tail of ϕ always dominates the repulsive interaction with the faster decaying inhibitory v-tail.

Summarizing the results with the Oregonator model, we conclude that bound states emerge due to the interplay between long-range attraction through the non-local coupling and short-range repulsion, provided by the inhibitory wake of the variable v behind the pulse.

5.2.2 Stability of bound states in Oregonator

We computed the linear stability of bound states, in which we linearized the reaction-diffusion system Eq. (5.1) with the non-local coupling, given by Eq. (5.2). The elements λ of the spectrum of the resulting linear operator represent the growth rates of a small perturbation around the original wave. A possible instability is reflected by the presence of eigenvalues with positive real parts. In what follows we shortly describe the method of computing the spectrum of a given travelling wave.

As shown in the next section, we can cast the Oregonator equations with non-local coupling in the form of the following reaction-diffusion equation

$$T\,\partial_t u = F(u) + D\,\partial_{xx} u, \quad u \in \mathbb{R}^3. \tag{5.3}$$

where D is a diagonal diffusion matrix with non-negative elements and $F(u)$ incorpo-

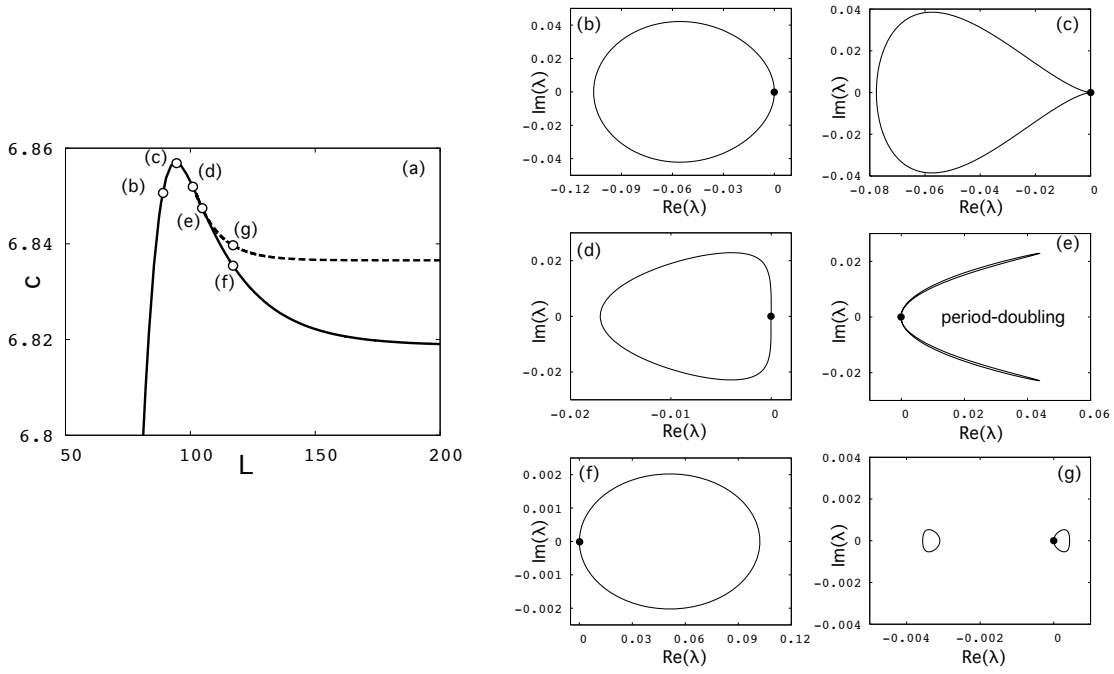

Figure 5.2: Stability of bound states for $\mu = -8.0 \times 10^{-3}$. (a) Dispersion curve of periodic pulse trains, displaying an overshoot. Velocity of L-periodic ($2L$-periodic) wave trains is shown by the solid (dashed) line, respectively. Empty dots $(b) - (g)$ denote the points for which the essential spectrum was computed. (b)-(g) The corresponding essential spectra.

rates the nonlinear Oregonator kinetics and the non-local coupling terms. The matrix T accounts for the fact that the equation for the non-local field (5.11) has no time dependence, i.e. we set $T = \mathrm{diag}(1, 1, 0)$.

In the frame $z = x - ct$ which moves with the velocity c we obtain from Eq. (5.3)

$$T\,\partial_t u = F(u) + cT\partial_z u + D\,\partial_{zz} u. \tag{5.4}$$

The profile $u(z)$ of travelling waves with constant velocity and shape is thus governed by the following ODE

$$D\,u'' + cTu' + F(u) = 0, \tag{5.5}$$

where the prime denotes a derivative with respect to the co-moving coordinate $z = x - ct$.

We consider first the stability of periodic pulse trains $u_L(z) = u_L(z + L)$. The

eigenvalue problem is then given by the following system

$$\begin{aligned} \lambda T w &= \partial_u F(u_L(z)) w + c T w' + D\, w'', \quad w \in \mathbb{C}^3, \\ (w, w')(L) &= e^{i2\pi\gamma}(w, w')(0). \end{aligned} \tag{5.6}$$

We say that λ is in the spectrum of the wave train $u_L(z)$, if Eq. (5.6) has a bounded solution for some $\gamma \in \mathbb{R}$ [47, 14, 73]. In order to obtain the spectrum of a given wave train, we solve the boundary-value problem (5.6) using the continuation software AUTO [39, 46]. The spectrum comes up in curves $\lambda = \lambda(i\gamma)$ in the complex plane. Note that $\lambda = 0$ with the eigenfunction given by $w(z) = u_L'(z)$ (the so-called Goldstone mode) is always in the spectrum due to the translation symmetry of the problem.

For $L \to \infty$ the spectrum of periodic wave trains exponentially converges to the spectrum of solitary pulses [47]. For wave trains of large spatial period, there is a circle of critical eigenvalues attached to the origin, which can be thought of as a blow-up of the isolated Goldstone eigenvalue of the solitary pulse [16]. Given the solitary pulse is stable, the location of this circle of critical eigenvalues (either in the left or right complex half-plane) describes the stability and interaction of pulses in wave trains with large wavelengths.

We calculated the leading parts of the spectrum of wave trains belonging to the different parts of the dispersion curve with an overshoot, see Fig. 5.2. The wave trains on the part of dispersion with positive slope $dc/dL > 0$ are found to be stable (Fig. 5.2(b)). As predicted by the theory [14], at the extremum of the dispersion curve $dc/dL = 0$ we obtain spectrum with

$$\frac{d}{d(i\gamma)}\mathrm{Im}(\lambda)\bigg|_{\lambda=0} = 0,$$

compare Fig. 5.2(c). Moving along the dispersion curve further, we observe a long-wavelength instability of wave trains, which is characterized by

$$\frac{d^2}{d(i\gamma)^2}\mathrm{Re}(\lambda)\bigg|_{\lambda=0} = 0,$$

see Fig. 5.2(d). In Fig. 5.2(e) we present the spectrum of a periodic wave train which undergoes the period-doubling bifurcation. We read from the spectrum that $\lambda = 0$ is two-fold degenerated, for the second eigenfunction we find $\gamma = 0.5$, which means that this eigenfunction has period $2L$. Exactly at this point, the branch of wave trains of doubled wavelength emerges from the primary dispersion curve.

Both L-periodic and $2L$-periodic wave trains are found to be unstable on unbounded domains for wavelengths larger then the wavelength of the period-doubling bifurcation, see Fig. 5.2(f) and (g), where the circle of critical eigenvalues belongs to the right half-plane. The instability of periodic wave trains reflects the attractive interaction between the pulses within a train, which causes a breakup of periodic structure and formation of pulse pairs. However, as $L \to \infty$ the critical circle of eigenvalues shrinks to the Goldstone eigenvalue $\lambda = 0$, and solitary pulses and bound states are thus stable.

For $2L$-periodic wave trains we found another part of spectrum in the left half-plane (Fig. 5.2(g)), which shrinks to a point eigenvalue for $L \to \infty$, i.e. for a solitary bound state. This point eigenvalue of the bound state can be thought of as the eigenvalue of the *weak interaction* between two pulses in the bound state [17]. In general, however, the interaction eigenvalue can belong to the right half-plane, making the bound state unstable. We refer to Section 5.3.6 for a more general discussion of the stability of bound states.

5.3 General description of the case $\mu = 0$

The aim of this section is to show that the emergence of bound states that are induced by non-local coupling is model-independent. We show that a solitary pulse undergoes a certain bifurcation at $\mu = 0$ and that this bifurcation produces bound states regardless of the specific underlying kinetics of the reaction-diffusion system.

5.3.1 Profile equations with non-local coupling

We consider a reaction-diffusion system in one spatial dimension with N species and kinetics f

$$\partial_t u = f(u, \phi(x)) + D\partial_{xx} u, \quad u \in \mathbb{R}^N \tag{5.7}$$

with a diffusion matrix $D = \mathrm{diag}(d_j), j = 1, \ldots, N$. The field $\phi(x)$ represents non-local coupling given by

$$\phi(x) = \phi_0 + \mu \int_{-\infty}^{\infty} e^{-\sigma|y|}[u_i(x+y) - u_i(x)]dy, \tag{5.8}$$

where we take the i-th species of u to construct $\phi(x)$. Again, the value σ^{-1} is considered to be large.

First, we derive the equation for the coupling field $\phi(x)$, which is given by

$$\phi(x) = \phi_0 + \mu \int_{-\infty}^{\infty} e^{-\sigma|y|}[u_i(x+y) - u_i(x)]dy, \tag{5.9}$$

where $u_i(x)$ is the i-the species of the original reaction-diffusion equation. We rewrite the coupling field in the form

$$\begin{aligned}\phi(x) &= \phi_0 + \mu \int_{-\infty}^{\infty} e^{-\sigma|y|}u_i(x+y)dy - \mu \int_{-\infty}^{\infty} e^{-\sigma|y|}u_i(x)dy \\ &= \phi_0 + 2\mu\left[\sigma X(x) - \frac{u_i(x)}{\sigma}\right].\end{aligned} \tag{5.10}$$

Using the Fourier transform

$$\int_{-\infty}^{\infty} e^{-\sigma|y|}e^{-iky}dy = \frac{2\sigma}{\sigma^2 + k^2},$$

it is not hard to see that the function $X(x)$ obeys the following linear differential equation

$$X_{xx} = \sigma^2 X - u_i. \tag{5.11}$$

Solutions to Eq. (5.7) in the form of $u(z) = u(x - ct)$ in the co-moving coordinate z are thus governed by the following profile equations

$$\begin{aligned}u'' + cu' + f(u, \phi(u_i, X; \mu)) = 0, \\ X'' - \sigma^2 X + u_i = 0,\end{aligned}$$

where the prime denotes a derivative with respect to z. X and ϕ are related through

$$\phi(u_i, X; \mu) = \phi_0 + 2\mu\left[\sigma X(x) - \frac{u_i(x)}{\sigma}\right].$$

We cast the profile equation as a first-order system

$$\begin{aligned}U' &= F(U, \Phi(U, Z; \mu); c), \qquad U \in \mathbb{R}^{2N} \\ Z' &= AZ - BU \qquad Z \in \mathbb{R}^2,\end{aligned} \tag{5.12}$$

where

$$A = \begin{pmatrix} 0 & 1 \\ \sigma^2 & 0 \end{pmatrix}.$$

Functions $\Phi(U, Z; \mu)$ and $F(U, \Phi(U, X; \mu); c)$ are obtained from given $\phi(u, X; \mu)$ and $f(u, \phi(u, X; \mu))$ in a straight-forward way. The matrix B accounts for the coupling between the appropriate components of U and Z. Non-local coupling effectively extends the phase space of the profile equation in a linear way by two dimensions. The asymptotic flow in the Z-subspace is given by the simple equation

$$Z'_{\pm} = \pm\sigma Z_{\pm}, \tag{5.13}$$

where $Z_{\pm}$ are the eigenvectors of the matrix A.

In our following analysis we consider the case $\mu = 0$. We assume that without non-local coupling the reaction-diffusion system supports propagation of stable solitary pulses. This means that there exist a homoclinic solution $(U^0, Z^0)(z)$ to the profile equation

$$\begin{aligned} U' &= F(U, \phi_0; c) \\ Z' &= AZ - BU. \end{aligned} \tag{5.14}$$

with some $c = c_0$. Then the linearization of Eq. (5.14) around $(U^0, Z^0)(z)$

$$v' = \mathcal{A}(z)v, \quad v \in \mathbb{C}^{2N+2}, \tag{5.15}$$

has a bounded solution given by $v(z) = \partial_z(U^0, Z^0)(z)$. The adjoint linearized problem

$$\psi' = -\mathcal{A}^*(z)\psi, \quad \psi \in \mathbb{C}^{2N+2}. \tag{5.16}$$

has a bounded solution as well [14]. The solution of the adjoint variational equation is perpendicular to the tangent spaces of the stable and unstable manifolds of the equilibrium, which is used in order to define the orientation of the homoclinic orbit later on.

The Jacobian matrix of Eq.(5.12) in the fixed point for $\mu = 0$ is given by

$$\mathcal{A}(0) = \begin{pmatrix} \partial_U F(0, \phi_0; c) & 0 \\ -B & A \end{pmatrix}. \tag{5.17}$$

The eigenvalues of $\mathcal{A}(0)$ are exactly those of the matrices $\partial_U F(0, \phi_0; c)$ and A. The leading eigenvalues of $\mathcal{A}(0)$ (those with smallest real parts) are then $\pm\sigma$ (see inset in Fig.5.4) and the corresponding leading eigenvectors are given by $(\underbrace{0, \ldots, 0}_{2N}, 1, \pm\sigma)^T$. Note that in the case $\mu = 0$ the leading eigenvectors are always perpendicular to the U-subspace, this corresponds to the fact that the profile of $u(x)$ is not affected by the variable $\phi(x)$ for $\mu = 0$.

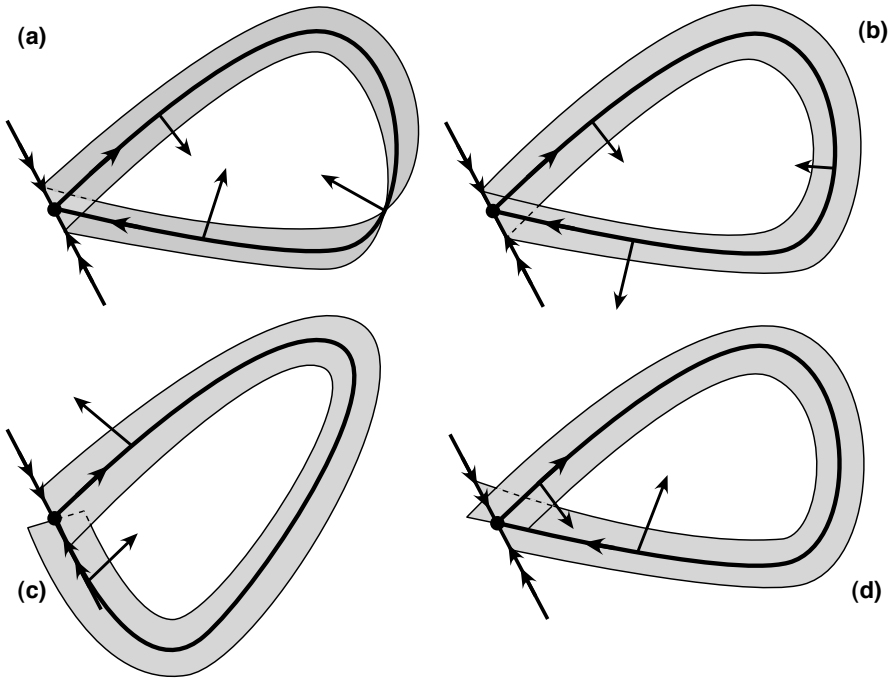

Figure 5.3: Sketches of homoclinic orbits. Filled circles denote the equilibrium. Leading directions are shown by single arrows, strong stable direction is shown by doubled arrows. Arrows perpendicular to the homoclinics indicate the solution to the adjoint variational equation. The gray strip shows the stable manifold of the fixed point close to the homoclinic orbit. (a) Generic codimension-1 orientable homoclinic orbit. (b) Generic codimension-1 twisted homoclinic orbit. (c) Codimension-2 orbit flip of homoclinic orbit. (d) Codimension-2 inclination flip of homoclinic orbit.

5.3.2 Codimension-2 bifurcations of homoclinic orbits

Now let us recall three general assumptions on the homoclinics of codimension one to a saddle equilibrium with real eigenvalues $-\lambda_{ss} < -\lambda_s < 0 < \lambda_u$ [13]:

1. the leading eigenvalues are not in resonance $\lambda_u \neq \lambda_s$,

2. the solution $v(z)$ to the linearized problem Eq. (5.15) converges to zero along the leading eigenvectors of the linearization in the fixed point and

3. the same applies to the solution $\psi(z)$ of the adjoint problem Eq.(5.16).

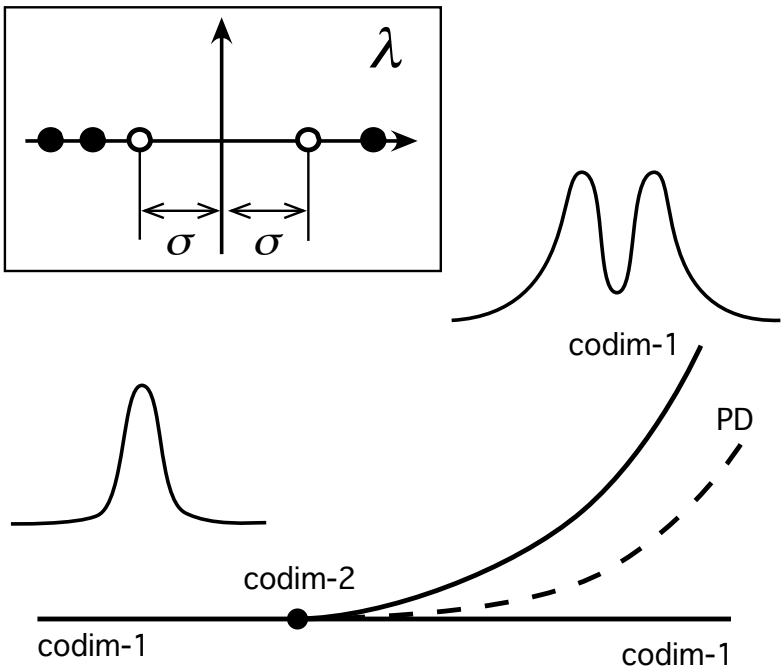

Figure 5.4: A codimension-2 bifurcation of a homoclinic orbit, the emergence of a 2-homoclinic orbit (solid line) and a period-doubling bifurcation PD (dashed line). Inset: Empty circles denote the eigenvalues of the matrix A, full circles show the eigenvalues of $\partial_U F(0, \phi_0; c)$.

The last assumption is sometimes called *the strong inclination property*, for homoclinics in $\mathbb{R}^3$ it means that the two-dimensional stable manifold comes in backward time tangent to the strong stable direction of the fixed point (see Fig. 5.3). A homoclinic orbit of codimension-1 can be orientable or twisted, depending on the orientation of the strip of the two-dimensional manifold, see Fig. 5.3 (a) and (b). One defines the *orientation* $\mathcal{O}$ of a given homoclinic orbit with the help of the solution $\psi(z)$ to the adjoint variational equation (5.16) as

$$\mathcal{O} = \lim_{z\to\infty} \operatorname{sign}\langle\psi(z), v(-z)\rangle \cdot \langle\psi(-z), v(z)\rangle, \tag{5.18}$$

where $v(z)$ denotes the solution to the linearized equation (5.15).

If one of the above assumptions is violated, one speaks of codimension-2 bifurcations of homoclinic orbits [13]. These are, in the order of the assumptions above:

1. resonance homoclinic orbit,

2. orbit flip and

3. inclination flip.

The resonance bifurcation can produce 2-homoclinics and both flip bifurcations can produce 2- and N-homoclinics. A branch of period-doubling bifurcation emerges from the bifurcation point as well (see Fig. 5.3 (c,d) and Fig. 5.4 for a qualitative picture of a codimension-2 bifurcation and the emergence of 2-homoclinics). In orbit (inclination) flip bifurcation, the vector $v(z)$ ($\psi(z)$) for $z \to \pm\infty$ switches through the strongly stable eigenspace of $\mathcal{A}(0)$, respectively. Both flip bifurcations correspond to the change of the sign of the scalar products that contribute to the orientation $\mathcal{O}$ and can be detected as zeroes of the orientation.

In our analysis of the effect of non-local coupling on the pulse dynamics we are particularly interested in the inclination flip. Let us recall the details of the inclination flip bifurcation of a homoclinic orbit in $\mathbb{R}^3$ to a saddle with one-dimensional unstable and two-dimensional stable manifold (see Fig. 5.5 (a)). Before and after the bifurcation the solution of the adjoint variation equation approaches zero along the leading eigenvector, as mentioned above. The two-dimensional stable manifold approaches the saddle point in backward time tangent to the strongly stable eigenvector. In the bifurcation point the solution of the adjoint equation picks the non-leading eigenvector of the linearization in the equilibrium for $z \to -\infty$. The two-dimensional stable manifold approaches the equilibrium in the backward time tangent to the weakly stable eigenvector.

5.3.3 Resonance and Inclination flips for $\mu = 0$

We can immediately see that non-local coupling for $\mu = 0$ breaks the first assumption, since the leading eigenvalues $\pm\sigma$ of the linearization (5.17) are obviously in resonance.

The second assumption about the asymptotics of the homoclinic orbit holds. It physically means that the non-local field decays in space much slower than the u-profile of the pulse.

The strong inclination property is violated at $\mu = 0$ with respect to both stable and unstable manifolds. It means that the homoclinic orbit that describes a solitary pulse in the absence of non-local coupling undergoes two inclination flip bifurcations if considered in the phase space extended by the coupling variable Z in Eq. (5.14). Let us consider the adjoint variational equation (5.16) together with Eq. (5.17) for $\mu = 0$

$$\begin{pmatrix} U \\ Z \end{pmatrix}' = - \begin{pmatrix} \partial_U F^*(U(z), \phi_0; c) & -B^* \\ 0 & A^* \end{pmatrix} \begin{pmatrix} U \\ Z \end{pmatrix}. \tag{5.19}$$

We see that the Z-subsystem is completely decoupled from the U-part. The equation for Z' is simply given by

$$Z' = -A^* Z, \quad A^* = \begin{pmatrix} 0 & \sigma^2 \\ 1 & 0 \end{pmatrix}, \tag{5.20}$$

and the variable U has no influence on the flow of Z, which is the counterpart of the fact that in the linearized equation (5.15) the U subsystem is not affected by Z.

We seek for a solution $(U, Z)(z)$ to Eq. (5.19), which vanishes for large z, i.e. $(U, Z) \to 0$ as $z \to \pm\infty$. For a codimension-1 homoclinic orbit, we expect that this solution approaches zero along the leading eigenvectors of $-\mathcal{A}^*(0)$, given by $(0, \ldots, 0, 1, \pm\sigma)^T$. However, the only bounded solution to Eq. (5.20) for $z \to \pm\infty$ is given by $Z = 0$, which means that the solution $(U, Z)(z)$ to Eq. (5.19) must pick the non-leading eigenvectors of $\mathcal{A}(0)$, given by $(U^\pm, 0, 0)^T$, in order to converge to zero for $z \to \pm\infty$. Here, $U^\pm$ represent the leading eigenvectors of the matrix $\partial_U F^*(U(z), \phi_0; c)$.

Finally we write

$$\psi(z) = \begin{pmatrix} U^\pm \\ 0 \\ 0 \end{pmatrix} e^{\mp\sigma z}, \quad \text{for} \quad z \to \pm\infty$$

for the solution $\psi(z)$ of the adjoint problem and

$$v(z) = \begin{pmatrix} 0 \\ 1 \\ \pm\sigma \end{pmatrix} e^{\mp\sigma z}, \quad \text{for} \quad z \to \pm\infty$$

for the solution $v(z)$ of the linearized problem, given by Eq. (5.15). Substituting the above expressions for $v(z)$ and $\psi(z)$ in Eq. (5.18)

$$\mathcal{O} = \lim_{z\to\infty} \operatorname{sign}\langle\psi(z), v(-z)\rangle \cdot \langle\psi(-z), v(z)\rangle,$$

we immediately see that both scalar products vanish, rendering two inclination flips with respect to the stable and the unstable manifolds.

5.3.4 Geometrical interpretation

We simplify the problem, exploring the extension of the profile equation only by one stable direction Y:

$$\begin{aligned} U' &= F(U, \phi_0; c) \\ Y' &= -\sigma Y - BU. \end{aligned} \tag{5.21}$$

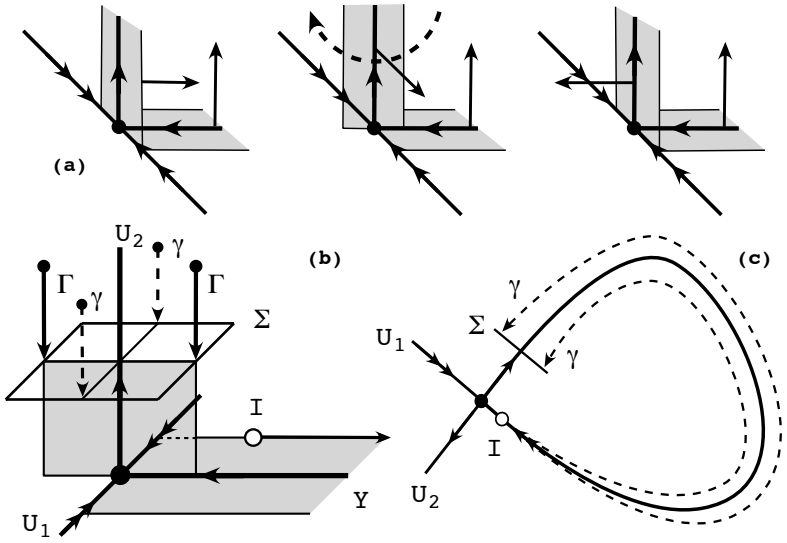

Figure 5.5: (a) Details of inclination flip bifurcation. Left panel: stable 2D manifold of the fixed point before the bifurcation. Middle panel: stable 2D manifold in the bifurcation point, note that the solution to the adjoint equation is directed along the strongly stable direction. Right panel: the same 2D stable manifold after the bifurcation. (b) Illustration of the inclination flip in the extended system (5.21). Empty dot I shows the initial condition in the stable manifold for the integrating in backward time, Σ shows the Poincaré section, γ denotes the unfeasible hypothetic trajectories that start in the phase point I, and Γ denotes the feasible trajectories, see text. (c) Projection of the homoclinic orbit in Eq. (5.21) on the U-subspace. I, Σ and γ have the same meaning as in (b)

We are interested in the behavior of the stable manifold of the equilibrium of Eq. (5.21) in backward time.

We emphasize once again that we work with non-local coupling switched off, i.e. $\mu = 0$, and assume that there exists a homoclinic orbit in the U-subsystem of Eq. (5.21). This implies that in the extended system there exists a homoclinic orbit as well, and the homoclinic orbit in the extended system approaches the equilibrium along the Y direction, since the Y axis is the leading stable eigenvector to the leading eigenvalue $-\sigma$ of the Jacobian of Eq. (5.21).

We refer to Fig. 5.5 (b) for the geometry of the eigendirections and the stable manifold in the system. Our idea is to compare the full phase space of the extended

system with its projection on the U variables, where the actual dynamics takes place. The U-subspace of Eq.(5.21) is decomposed in the leading unstable direction U_2 and the strongly stable eigendirection U_1. The leading stable eigendirection is Y.

We choose a Poincaré section Σ across the leading unstable eigenvector close to the equilibrium. Next, we put an initial condition (marked by I in Fig. 5.5 (b)) close to the homoclinic orbit in the two-dimensional stable manifold, and follow it in backward time along the homoclinic orbit. An important question is how this trajectory returns to the previously chosen Poincaré section. For a generic codimension-1 homoclinic orbit, the trajectory from our initial condition returns along one of the dashed lines with the arrows marked by γ in Fig. 5.5 (b). In the projection on the U plane it would mean, however, that the trajectory does not remain on the homoclinic orbit, which is impossible because the starting point belongs to the homoclinic orbit in the U-subspace, which in turn is an invariant trajectory (see Fig. 5.5(c) for the projections of the hypothetical trajectory marked by γ). In other words, the U components of our hypothetical trajectory must be the original homoclinic orbit in the original profile equation

$$U' = F(U, \phi_0; c)$$

without non-local coupling. Last means that the feasible trajectory of point I in backward time must come to the section Σ along the vectors marked by Γ.

Comparing Fig.5.5(a) and Fig.5.5(b), we conclude that for $\mu = 0$ our system displays an inclination flip with respect to the stable manifold. In exactly the same way one can show an inclination flip with respect to the unstable direction while considering the extension of the profile equation by one unstable direction (with $+\sigma$)

$$\begin{aligned} U' &= F(U, \phi_0; c) \\ Y' &= \sigma Y - BU. \end{aligned} \tag{5.22}$$

In this case the same considerations can be applied, keeping in mind that Y becomes now the leading unstable direction of Eq.(5.22) and Fig. 5.5(b) can be used with the reversed directions of the arrows.

5.3.5 Summary: Codimension-4 homoclinic orbit

Summarizing our results for $\mu = 0$, we find a codimension-4 homoclinic orbit in the profile equation for travelling waves in the reaction-diffusion system (5.7) with non-local

coupling given by Eq. (5.8). Here, we present the list of the bifurcations together with the assumptions, under which we find the degeneracies:

1. Inclination flip with respect to the stable manifold (extended equation (5.21)). Assumption: $-\sigma$ is the leading stable eigenvalue of $\mathcal{A}(0)$, i.e. the matrix $\partial_U F(0, \phi_0; c_0)$ has no eigenvalues with real part between $-\sigma$ and 0.

2. Inclination flip with respect to the unstable manifold (extended equation (5.22)). Assumption: σ is the leading unstable eigenvalue of $\mathcal{A}(0)$, i.e. the matrix $\partial_U F(0, \phi_0; c_0)$ has no eigenvalues with real part between 0 and σ.

3. Resonance condition for the leading eigenvalues $\pm\sigma$. Assumption: the matrix A has a specific form, given by Eq. (5.13). This can be violated, for example, by the choice of temporarily inertial non-local coupling like in [93].

4. Existence of the homoclinic orbit itself (existence of solitary pulse in PDE for $\mu = 0$). Assumption: there exists a solitary pulse without non-local coupling.

We would like to stress that the high codimension of the bifurcation at $\mu = 0$ does not depend on the particular system and is solely provided by the non-local coupling. The first two assumptions can be fulfilled by the choice of sufficiently large coupling range, i.e. by the smallness of σ, while the third one follows naturally from the symmetry of the coupling function $e^{-\sigma|y|}$. In this sense the high codimension of the solitary pulse at $\mu = 0$ and the bifurcation to pulse pairs is a generic feature of systems with non-local coupling.

Three of the four bifurcation are unfolded upon switching on non-local coupling by setting $\mu \neq 0$. Each of the found homoclinic bifurcations can produce 2-homoclinic orbits, see Table I and Table II in [34]. Bifurcations to 2-homoclinic orbit for the profile equation (5.14) correspond to the emergence of bound states with 2 pulses with the same velocity in the full PDE system. All three bifurcations were precisely detected numerically in the Oregonator model at $\mu = 0$ by the continuation software AUTO [39].

5.3.6 Stability of bound states

Stability of the bifurcating bound states can be determined in the general framework of the stability of multi-bump pulses [17]. Under assumption of large interpulse distance

the interaction of the pulses within a bound state is weak and can be estimated from the decay properties of the corresponding solitary pulse.

Suppose that we have found a bound state for $\mu = \mu_0$ close to $\mu = 0$. The interpulse distance L_p in the bound state is considered to be large. To simplify our analysis, we assume that the leading eigenvalues of the matrix $\mathcal{A}(0)$ for $\mu = \mu_0$ are given by $\nu^s < 0$ and $\nu^u > 0$, where $\nu^u > -\nu^s$. The last means that the exponential wake behind the pulse decays slower that in the front of it, which is quite often the case if the velocity of the pulse is not zero. The critical spectrum of the bound state with two pulses is then given by two point eigenvalues, one of which is necessarily $\lambda = 0$, representing the translation invariance of the pulse pair.

The second eigenvalue describes the interaction of pulses within a bound state and thus decides upon the stability of the pulse pair. Under the above assumptions on the matrix $\mathcal{A}(0)$, this eigenvalue is given by [14, 17]

$$\lambda_i = -\frac{1}{M}\langle \psi(L_p/2), v(-L_p/2)\rangle,$$

where M is the Melnikov integral for the solitary pulse, $v(z)$ and $\psi(z)$ are the solutions to the linear equations (5.15) and (5.16) for the solitary pulse.

The easiest way to determine the sign of λ_i is to check the stability of periodic pulse trains with interpulse distance L_p. The sign of

$$-\frac{1}{M}\langle \psi(L_p/2), v(-L_p/2)\rangle$$

decides upon the stability of periodic pulse trains as well [16]. Equivalently, the location of the circle of the critical eigenvalues is determined by the above scalar product.

As a result, a pulse pair with interpulse distance L_p is stable if the corresponding spatially periodic pulse train with the same wavelength is stable. For large wavelengths, there is a relation between the slope of the dispersion $c(L)$ and the stability of wave trains, which says that for $\frac{d}{dL}\, c(L) > 0$ the wave trains are stable [15]. Thus it is possible to predict the stability of the bound state from the slope of the dispersion curve for the appropriate periodic pulse trains with the wavelength $L = L_p$.

5.4 Discussion and outlook

In this chapter, we have shown that non-local coupling in the form of exponentially decaying connections between the elements of the medium leads to the emergence of bound

states of pulses. The results of our analysis were obtained under general assumptions on the underlying equations and thus are applicable to a wide class of reaction-diffusion systems under influence of non-local coupling with exponentially decaying strength.

The central point of our analysis was the case where the coupling strength μ was equal to zero. The homoclinic orbit which describes the solitary pulse for $\mu = 0$ was shown to be of codimension-4. Upon switching on non-local coupling, the homoclinic orbit became a generic one of codimension-1. This unfolding of the codimension-4 bifurcation leads to the emergence of N-homoclinics that correspond to bound states in the reaction-diffusion system with non-local coupling. Our results also apply to a non-local coupling with a sufficiently small temporal inertiality τ [93]; in this case the matrix A in Eq. (5.12) is slightly different and the leading eigenvalues of A are not in resonance anymore. We would still have a codimension-3 homoclinic orbit, which can bifurcate to double pulses.

We stress that the high codimension of the bifurcation is provided essentially by the form of the non-local coupling and does not depend on the particular properties of the pulses in the reaction-diffusion system. In our numerical computation with continuation software the predicted bifurcations were accurately detected, which can be considered as a numerical proof of the theoretical analysis. Additionally, in the numerically investigated example the bound state has been shown to be linearly stable, which can be seen as a first step towards real experimental verification of the results.

There are still some open questions about the considered bifurcations. We have shown two inclination flips and resonant homoclinic orbit simultaneously for $\mu = 0$. Both flip bifurcation and resonance condition can produce 2-homoclinics and so far it is not clear which specific bifurcation leads to the emergence of bound states. The interplay of two inclination flip bifurcations with the resonance condition assures an even more intriguing dynamical behaviour than near a codimension-3 point [91, 92].

Chapter 6

Conclusions

In the presented Thesis we theoretically studied the dynamics and stability of solitary pulses and periodic pulse trains in excitable media. Despite the great variety of the particular profiles of pulses, two generic cases can be distinguished: *i*) pulses with oscillations in the tail and *ii*) pulses with monotonous tail. For pulses of both types we report the phenomenon of anomalous dispersion and alternating pulse interaction in dependence on the interpulse distance.

6.1 Pulses with oscillations in the tail

Pulses with oscillatory tails provide a potentially richer dynamics, which can be already seen on the level of profile equations. Such pulses are described by a homoclinic orbit to an equilibrium with complex-conjugate eigenvalues, which provide the oscillations in the asymptotic behavior. Since the works of Shilnikov it was known that such pulses are accompanied by a set of multi-pulses (or, equivalently, bound states in the language of reaction-diffusion systems) and infinitely many periodic solutions.

For reaction-diffusion systems this type of pulses is shown to exist close to the transition between excitable and oscillatory kinetics. In the same time, this is the region of the transition between trigger and phase waves, which are natural spatial solutions for excitable and oscillatory local dynamics, respectively. With the help of model equations, which describe the light-sensitive Belousov-Zhabotinsky reaction, we clearly resolved the transition to the pulses with oscillatory tails and then the transition to phase waves.

Under increase of the "excitability" parameter of the system, the transition from

trigger to phase waves includes the following steps: (*i*) Emergence of tail oscillations behind the solitary pulse. In the same time the dispersion curve of trigger pulse trains becomes oscillatory. (*ii*) Hopf bifurcation in the profile equation, which corresponds to the emergence of undamped tail oscillations of the solitary pulse. The oscillations in the dispersion curve of periodic waves becomes also undamped. This Hopf bifurcation introduces the phase waves with finite velocity.(*iii*) Collision of branches of trigger waves and phase waves and successful disappearance of trigger wave trains in series of saddle-node collisions. The only waves that survive are the phase waves. The point of the collision of trigger and phase waves branches defines the boundary between regimes of trigger waves and phase waves.

The bifurcation parameter which gives us access to different regimes represents the intensity of the applied light illumination in the experiment. This suggests that the found phenomenon can be found in future experiments.

As mentioned above, for the pulses with oscillations in the wake we find wiggly dispersion curve of periodic pulse trains. A new particular feature of this kind of dispersion is the presence of domain of bistability, where two pulse trains with the same wavelength can propagate at different velocities. Two stable solutions are separated by the unstable one. We presented a detailed stability analysis of the coexisting pulse trains, belonging to the same domain of bistability. The possible instabilities of wave trains of wavelength L include: (*i*) period-doubling bifurcation, which can be seen on a periodic domain of length $2L$. (*ii*) Long-wavelength or Eckhaus instability, which is characterized by the change of the curvature sign of spectrum at the origin. (*iii*) A short-wavelength instability, which can be already be seen on periodic domains of length L. This instability is described by the circle of critical eigenvalues detached from the origin.

6.2 Pulses with monotonous tails

Oscillatory tails of pulses are not the only reason for the existence of locking-type phenomena between pulses. Monotonous tails can provide attractive interaction and thus anomalous dispersion as well. In this case, however, the type of interaction does not alternate periodically with the interpulse distance.

In the last part of the Thesis we show that including non-local interaction in the form of long-range coupling between the elements of the medium leads to new features of pulse interaction, including the emergence of bound states and anomalous dispersion.

Physically the phenomenon can be understood as the interplay between activating and inhibiting type of non-local coupling, which is controlled by the sign of the coupling strength μ. The emergence of bound states and anomalous dispersion was analytically proven to occur precisely at $\mu = 0$.

More detailed theoretical considerations base on the analysis of the profile equation, where we analytically showed that the solitary pulse at $\mu = 0$ undergoes a certain bifurcation of a high codimension. Unfolding of this bifurcation (turning on the non-local coupling) leads to the emergence of N-pulses (or bound states). In the same time the dispersion of periodic pulse trains demonstrate an overshoot, followed by an anomalous part with negative slope. We calculated the spectra of periodic solutions close to the overshoot and revealed the fine details of the stability of pulse trains. It turned out that the pulse trains become unstable through a long-wavelength instability prior to the period doubling. However, the period-doubling instability can be relevant if we consider the system on a relatively small domain with a length of several wavelengths of the pulse train.

The results of the last chapter are applicable to the wide class of reaction-diffusion systems since we have proven the bifurcation to N-pulses to be model-independent. The only assumptions were on the exponential decay of the coupling function and the broadness of the non-local coupling field. The results of the analysis can be applied to non-local coupling with a small temporal inertiality, which makes the codimension of the bifurcation be smaller by one.

6.3 Suggestions for further studies

Concerning non-local coupling, there is a plethora of possible further investigations, both theoretically and experimentally. To the best of our knowledge, the dynamics of spiral waves in excitable media under non-local coupling (or, equivalently, with a strongly diffusive species) has not been studied. We can speculate that the presence of another spatial scale can drastically modify the dynamics of spiral waves. In the radial direction the non-local field should slowly approach some limit state, corresponding to the non-local field over a plane wave. If we could tune the parameters of the system so that the asymptotic state of the non-local field suppresses the propagation of the spiral fronts, it were possible to create localized spiral waves on homogeneous background.

A possible two-dimensional study is also interesting for the case of oscillatory pulse

tails. Winfree [18] has already demonstrated theoretically the coexistence of alternating spiral waves due to the oscillations in the pulse tail, but the phenomenon of velocity locking was not considered.

One of the experimental challenges might be the uncovering of the small oscillations behind the pulse in the realistic Belousov-Zhabotinsky reaction. The experiments in the laboratory of group of Prof. Engel showed some indirect tips to the existence of those small-amplitude oscillations, but there is still no convincing evidences on that.

Appendix A

Group velocity of periodic wave train and its spectrum

Here, our aim is to show that the slope of the dispersion curve $c(L)$ which we will call here *group velocity* of the wave train, is equal to the first derivative of the essential spectrum $\lambda(i\gamma)$ at the origin

$$-c_g = \frac{d}{dL}c(L) = \frac{d}{d\gamma}\mathrm{Im}\,\lambda(\gamma)\Big|_{\gamma=0}.$$

The derivation is an adapted first-order version of the analogous proof in [94]. Another difference is that we use the formulation of dispersion in terms of wavelength L and phase velocity c instead of wave number k and frequency ω as in [94].

We consider wave trains, i.e. periodic solutions to the profile equation

$$DU'' + cU' + F(U) = 0, \qquad ' = \partial_z$$

cast as a first-order system

$$u' = f(u; c), \qquad 0 < z < L \tag{A.1}$$

where

$$u = \begin{pmatrix} U \\ V \end{pmatrix}, \quad f = \begin{pmatrix} V \\ D^{-1}[-cV - F(U)] \end{pmatrix}. \tag{A.2}$$

The linearization around the wave train, given by

$$DV'' + cV' + F_U(U)V = \lambda V \tag{A.3}$$

can be written as a first order system as well

$$v' = A(z;\lambda)v \tag{A.4}$$

with the matrix A is given by

$$A(z;\lambda) = \partial_u f(u(x);c) + \lambda B, \qquad B = \begin{pmatrix} 0 & 0 \\ D^{-1} & 0 \end{pmatrix}. \tag{A.5}$$

We note from Eq. (A.2) and Eq. (A.5) that

$$\partial_c f = -Bu', \quad ' = \partial_z. \tag{A.6}$$

We can reformulate the eigenvalue problem (A.5) with the help of the operator

$$\mathcal{T}(\lambda) \quad : \quad v \longmapsto \frac{dv}{dz} - A(\cdot;\lambda)v \tag{A.7}$$

in the following form

$$\mathcal{T}(\lambda)v = 0.$$

Later on we will need a solution ψ of the adjoint problem

$$\mathcal{T}^*(\lambda)\psi = 0.$$

We recall that λ is in the essential spectrum of the wave train if, and only if, the boundary-value problem

$$\begin{aligned} v' &= A(z;\lambda)v, \qquad 0 < z < L \\ v(L) &= e^{i\gamma}v(0) \end{aligned} \tag{A.8}$$

has a solution for some $\gamma \in \mathbb{R}$.

Typically, periodic wave trains live in families on the dispersion curves $c = c(L)$. We rescale the co-moving coordinate by introducing a new coordinate $x = z/L$. From now on we have

$$' := \partial_x = L\partial_z.$$

The profile equation reads then

$$\frac{1}{L}u' = f(u;c), \qquad 0 < x < 1 \tag{A.9}$$

and the linearized problem Eq. (A.8)

$$\begin{aligned} &\frac{1}{L}v' = A(x;\lambda)v, \qquad 0 < x < 1 \\ &v(1) = e^{i\gamma}v(0), \end{aligned} \tag{A.10}$$

where we omitted the rescaling of γ. With $v = e^{i\gamma x}w$ we obtain from Eq. (A.10)

$$\begin{aligned} &\frac{1}{L}w' = \left[A(x;\lambda) - \frac{i\gamma}{L}\right]w, \\ &w(1) = w(0). \end{aligned} \tag{A.11}$$

For the operator $\mathcal{T}(\lambda)$ we obtain then

$$\mathcal{T}(\lambda) \quad : \quad v \longmapsto \frac{1}{L}\frac{dv}{dx} - A(\cdot;\lambda)v + \frac{i\gamma}{L}v, \quad A = \partial_u f(u(x;L);c(L)) + \lambda B \tag{A.12}$$

With the substitution $u = u(x;L)$, we take the first derivative of Eq. (A.9) with respect to L

$$\frac{1}{L}\partial_L u' - \frac{1}{L^2}u' = \partial_u f(u(x;L),c(L))\,\partial_L u + \partial_c f(u(x;L),c(L))\,\frac{d}{dL}c(L),$$

which we rewrite with the help of the operator $\mathcal{T}(\lambda)$ from Eq. (A.12)

$$\mathcal{T}(0)\,\partial_L u = \frac{1}{L^2}u' + \partial_c f(u(x;L),c(L))\,\frac{d}{dL}c(L). \tag{A.13}$$

Next, we substitue $w = w(x;\gamma)$ and take the first derivative of Eq. (A.11), evaluating it at $\gamma = \lambda = 0$

$$\frac{1}{L}\partial_\gamma w' = \partial_u f(u(x;L);c(L))\,\partial_\gamma w + \frac{d}{d\gamma}\lambda(\gamma)\,Bw + \underbrace{\lambda B\,\partial_\gamma w}_{=0} - \frac{i}{L}w - \underbrace{\frac{i\gamma}{L}\partial_\gamma w}_{=0},$$

which again can be reformulated with the operator $\mathcal{T}(\lambda)$ (see Eq. (A.12)) as

$$\mathcal{T}(0)\,\partial_\gamma w = \frac{d}{d\gamma}\lambda(\gamma)\,Bw - \frac{i}{L}w. \tag{A.14}$$

We note that the functions on the right-hand sides of Eq. (A.13) and Eq. (A.14) belong to the range of the operator $\mathcal{T}(0)$. This means that their product with a function ψ from the null-space of the adjoint operator $\mathcal{T}^*(0)$ must vanish:

$$\begin{aligned} &\langle\psi, \frac{1}{L^2}u' - \frac{d}{dL}c(L)\,Bw\rangle = 0, \\ &\langle\psi, \frac{d}{d\gamma}\lambda(\gamma)\,Bw - \frac{i}{L}w\rangle = 0, \end{aligned} \tag{A.15}$$

where we used Eq. (A.6) with $\partial_z = L^{-1}\partial_x$

$$\partial_c f(u(x;L);c(L)) = -\frac{1}{L}Bu'$$

together with $w(x;0) = u'(x;L)$. Eliminating $\langle \psi, Bw\rangle$ from Eq. (A.15) and using the normalization

$$\langle \psi, u'\rangle = 1,$$

we obtain

$$\frac{d}{dL}c(L) = \frac{d}{d\gamma}\mathrm{Im}\,\lambda(\gamma)\Big|_{\gamma=0},$$

which means that the sign of the slope of the dispersion curve $c(L)$ coincides with the orientation of the curve of the essential spectrum at zero.

Appendix B

Law of Mass Action

Suppose that we have a reversible chemical reaction with N reagents $R_j, j = 1, \ldots, N$ and M products $P_j, j = 1, \ldots, M$, given by

$$\sum_j^N \alpha_j R_j \rightleftharpoons \sum_j^M \beta_j P_j,$$

where α_j and β_j are natural numbers that denote the number of molecules of reagents and products involved in a single reaction step.

The rates of the forward and backward reactions are then given by [95]

$$\begin{aligned} [\text{forward rate}] &= k_1 \prod_j^N R_j^{\alpha_j}, \\ [\text{reverse rate}] &= k_{-1} \prod_j^M P_j^{\beta_j}. \end{aligned} \tag{B.1}$$

The above formulae show that the rate of the reaction is directly proportional to the product of the n-th orders of the reagent concentration. Physically it means that the rate of the reactions depend on the probability of (nearly) simultaneous collision of the corresponding number of the reagents molecules.

For the following hypothetic reaction

$$A + 2B \to C$$

the rate would be proportional to the concentration of A and to the square of the concentration of B, i.e.

$$[\text{forward rate}] = k_1 [N_A][N_B]^2. \tag{B.2}$$

The constant k is determined by the conditions like temperature, pressure and so on. We can immediately write down the differential equation, describing the temporal evolution of the concentration of the reagent A:

$$\frac{d}{dt}[N_A] = k_1[N_A][N_B]^2.$$

From Eq. (B.1) we can derive the condition for the stationary non-equilibrium state

$$[\text{forward rate}] = [\text{reverse rate}],$$

which reads

$$\frac{k_1}{k_{-1}} = \frac{\prod_j^N R_j^{\alpha_j}}{\prod_j^M P_j^{\beta_j}} = \text{const.}$$

The above equation is the statement of the *law of mass action*. In words it means: when a reversible reaction has attained equilibrium, the reaction quotient[1] remains constant.

[1]The *reaction quotient* is the ratio of molar concentrations of the reactants to those of the products, each concentration being raised to the power equal to the coefficient in the equation.

Bibliography

[1] I. Farkas, D. Helbing, and T. Vicsek, *Mexican waves in an excitable medium*, Nature **419**, 131, 2002.

[2] A. S. Mikhailov, *Foundation of Synergetics i: Distributed Active Systems*, Springer Berlin, 1991.

[3] M.C. Cross and P. C. Hohenberg, *Pattern formation outside of equilibrium*, Rev. Mod. Phys. **65**, 851–1112, 1993.

[4] J. J. Tyson, *What everyone should know about the Belousov-Zhabotinsky reaction*, Lecture Notes in Biomathematics (S.A. Levin, ed.), vol. 100, Springer, New York, 1994, pp. 569–587.

[5] A. M. Turing, *The chemical basis of morphogenesis*, Philos. Trans. R. Soc. London B **237**, 37–72, 1952.

[6] V. Castets, V. Dulos, J. E. Boissonade, and P. De Kepper, *Experimental evidence of a sustained standing Turing-type nonequilibrium chemical pattern*, Phys. Rev. Lett **64**, 2953–2956, 1990.

[7] M. Falcke, *Reading the patterns in living cells - the physics of* Ca^{2+} *signaling*, Advances in Physics **53**, 255, 2004.

[8] A. Hodgkin and A. Huxley, *A quantitative description of membrane current and its application to conduction and excitation in nerve*, J. Physiol **117**, 500–544, 1952.

[9] Richard Fitzhugh, *Impulses and physiological states in theoretical models of nerve membrane*, Biophysical Journal **1**, 445–466, 1961.

[10] J. Nagumo, S. Arimoto, and S. Yoshizawa, *An active pulse transmission line simulating nerve axon*, Proc. IRE **50**, 2061–2070, 1964.

[11] G. K. Moe, W. C. Rheinbolt, and J. A. Abildskov, *A computer model of atrial fibrillation*, Amer. Heart J. **67**, 200–220, 1964.

[12] Alexander Panfilov and Arkady Pertsov, *Ventricular fibrillation: evolution of the multiple-wavelet*, Phil Trans. R. Soc. Lond. **359**, 1315–1325, 2001.

[13] Yu. A. Kuznetsov, *Elements of applied bifurcation theory*, Springer Berlin, 1995, 1998, 2004.

[14] Björn Sandstede, *Handbook of Dynamical Systems, v. 2 (edt. by B. Fiedler)*, North-Holland, 2002.

[15] Michal Or-Guil, Ioannis G. Kevrekidis, and Markus Bär, *Stable bound states of pulses in an excitable medium*, Physica D **135**, 154–174, 2000.

[16] Björn Sandstede and Arnd Scheel, *On the stability of periodic travelling waves with large spatial period*, J. Diff. Eq. **172**, 134–188, 2001.

[17] B. Sandstede, *Stability of multiple-pulse solutions*, Trans. Amer. Math. Soc. **350**, 429–472, 1998.

[18] A. T. Winfree, *Alternative stable rotors in an excitable medium*, Physica D **49**, 125–140, 1991.

[19] C. Elphick, E. Meron, J. Rinzel, and E. A. Spiegel, *Impulse patterning and relaxational propagation of excitable media*, Jour. Theor. Biol. **146**, 249–268, 1990.

[20] J. Christoph, M. Eiswirth, N. Hartmann, R. Imbihl, I. Kevrekidis, and M. Bär, *Anomalous dispersion and pulse interaction in an excitable surface reaction*, Phys. Rev. Lett. **82(7)**, 1586–1589, 1999.

[21] V. K. Vanag and I. R. Epstein, *Packet waves in a reaction-diffusion system*, Phys. Rev. Lett. **88**, 088303, 2002.

[22] N. Manz, S. C. Müller, and O. Steinbock, *Anomalous dispersion of chemical waves in a homogeneously catalyzed reaction system*, J. Phys. Chem. A **104**, 5895, 2000.

[23] N. Manz, C. T. Hamik, and O. Steinbock, *Tracking waves and vortex nucleation in excitable systems with anomalous dispersion*, Phys. Rev. Lett. **92**, 248301, 2004.

[24] H. U. Bödeker, A. W. Liehr, T. D. Frank, R. Friedrich, and H.-G. Purwins, *Measuring the interaction law of dissipative solitons*, New J. of Phys. **6**, 62, 2004.

[25] R. J. Field and R. M. Noyes, *Oscillations in chemical systems IV. Limit cycle behavior in a model of a real chemical reaction*, J. Amer. Chem. Soc. **60**, 1877–1884, 1974.

[26] P. Glandsdorff and I. Prigogine, *Thermodynamic theory of structure, stability and fluctutations*, Wiley, New York, 1971.

[27] G. Nicolis, Advan. Chem. Phys. **19**, 209, 1971.

[28] J. J. Tyson, *Some further studies of nonlinear oscillations in chemical systems*, J. Chem. Phys. **58**, 209, 1973.

[29] R. J. Field, E. Körös, and R. M. Noyes, *Oscillations in chemical systems II. Through analysis of temporal oscillations in the bromate-cerium-malonic acid system*, J. Amer. Chem. Soc. **94**, 8649–8664, 1972.

[30] H.-J. Krug, L. Pohlmann, and L. Kuhnert, *Analysis of the modified complete oregonator accounting for oxygen sensitivity and photosensitivity of Belousov-Zhabotinsky reaction*, J. Phys. Chem. **94**, 4862–4865, 1990.

[31] Morten Brøns and Kedma Bar-Eli, *Canard explosion and excitation in a model of Belousov-Zhabotinsky reaction*, J. Phys. Chem. **95**, 8706–8713, 1991.

[32] J.J. Tyson and J.P. Keener, *Singular perturbation theory of travelling waves in excitable media (a review)*, Physica D **32**, 327, 1988.

[33] B. Sandstede and A. Scheel, *Defects in oscillatory media: toward a classification*, IAM J. Appl. Dyn. Sys. **3**, 1–68, 2004.

[34] Björn Sandstede, *Constructing dynamical systems having homoclinic bifurcation points of codimension two*, J. Dyn. Diff. Eq. **9**, 269, 1997.

[35] S. N. Chow, B. Deng, and B. Fiedler, *Homoclinic bifurcation at resonant eigenvalues*, J. Dyn. Diff. Eq. **2(2)**, 177–244, 1990.

[36] S. Nii, *N-homoclinic bifurcation for homoclinic orbits changing their twisting*, J. Dyn. Diff. Eq. **8**, 549–572, 1996.

[37] E. Yanagida, *Branching of double pulse solutions from single solutions in nerve axon equations*, J. Diff. Eq. **66**, 243–262, 1987.

[38] Björn Sandstede, *Verzweigungstheorie homokliner verdopplungen. PhD thesis, Uuniversity of Stuttgart*, 1993.

[39] E. Doedel, R.C. Paffenroth, A.R. Champneys, T.F. Fairgrieve, Yu.A. Kuznetsov, B.E. Oldeman, B. Sandstede, and X. Wang, *AUTO2000: Continuation and bifurcation software for ordinary differential equations (with HOMCONT)*, Concordia University, Montreal, 2002.

[40] L. Shilnikov, *Some cases of generation of periodic motions from singular trajectories*, Mat. Sbornik **61(103)**, 443–466, 1963.

[41] L. Shilnikov, *A case of existence of a countable number of periodic motions*, Soviet. Math. Dokl. **6**, 163–166, 1965.

[42] J. Neimark and L. Shilnikov, *A case of generation of periodic motions*, Soviet. Math. Dokl. **6**, 305–309, 1965.

[43] B. Deng, *The Shilnikov problem, exponential expansion, strong λ-lemma, c^1-linearization, and homoclinic bifurcation*, J. Diff. Eq. **79**, 189–231, 1989.

[44] P.Glendinning and C.Sparrow, *Local and global behaivour near homoclinic orbits*, J. Stat. Phys **35**, 645–696, 1984.

[45] R. Gardner, *Spectral analysis of long wavelength periodic waves and applications*, J. Reine Angew. Math **491**, 149–181, 1997.

[46] J.D.M. Rademacher, B. Sandstede, and A. Scheel, *Computing absolute and essential spectra using continuation, preprint.*

[47] Björn Sandstede and Arnd Scheel, *Absolute and convective instabilities of waves on unbounded and large bounded domains*, Physica D **145**, 233, 2000.

[48] J.Rademacher, *Private communications*, 2004.

[49] J. D. M. Rademacher, *Geometric relations of absolute and essential spectra of wave trains*, preprint.

[50] P. Wheeler and D. Barkley, *Computation of spiral spectra*, SIADS **5**, 157–177, 2006.

[51] Raymond Kapral and Kenneth Showalter (eds.), *Chemical Waves and Patterns*, Kluwer Academic Publishers, 1995.

[52] C. Elphick, Ehud Meron, and E. A. Spiegel, *Spatiotemporal complexity in travelling patterns*, Phys. Rev. Lett. **61(5)**, 496–499, 1988.

[53] Oliver Steinbock, *Excitable front geometry in reaction-diffusion systems with anomalous dispersion*, Phys. Rev. Lett. **88**, 228302, 2002.

[54] C. van Oss, A. V. Panfilov, P. Hogeweg, F. Siegert, and C. J. Weijer, *Spatial pattern formation during aggregation of the slime mould* dictyostelium discoideum, J. Theor. Biol. **181**, 203–213, 1996.

[55] J.-M. Flessels, A. Belmonte, and V. Gaspar, *Dispersion relation for wave in the Belousov-Zhabotinsky reaction*, J. Chem. Soc., Faraday Trans. **94**, 851, 1998.

[56] Chad T. Hamik, Niklas Manz, and Oliver Steinbock, *Anomalous dispersion and attractive pulse interaction in the 1,4-Cyclohexanedione Belousov-Zhabotinsky reaction*, J. Phys. Chem. **105**, 6144–6153, 2001.

[57] M.G.Zimmerman, S.Firle, M.Natiello, M.Hildebrand, M.Eiswirth, M.Bär, A.K.Bangia, and I.G.Kevrekidis, *Pulse bifurcation and transition to spatiotemporal chaos in an excitable reaction-diffusion model.*, Physica D **110**, 92–104, 1997.

[58] M. Or-Guil, J. Krishnan, I. G. Kevrekidis, and M. Bär, *Pulse bifurcations and instabilities in an excitable medium: Computation in finite ring domains*, Phys. Rev. E **64**, 046212, 2001.

[59] G. Röder, *Diploma thesis, Technische Universität Berlin*, 2005.

[60] G. Röder, G. Bordyugov, M. Falcke, and H. Engel, *In preparation*, Phys. Rev. E, 2006.

[61] Martin Falcke, Michal Ol-Guil, and Markus Bär, *Dispersion gap and localized spiral waves in a model for intracellular ca^{2+} dynamics*, Phys. Rev. Lett. **84(20)**, 4753–4756, 2001.

[62] Y. Kuramoto, *Chemical Oscillations, Waves, and Turbulence*, Springer Berlin, 1984.

[63] Wiktor Eckhaus, *Studies in nonlinear stability theory, springer tracts in natural philosophy*, Springer-Verlag, Berlin, 1965.

[64] A. C. Newell and J. A. Whitehead, *Finite bandwidth, finite amplitude convection*, J. Fluid. Mech. **38**, 279, 1969.

[65] P. Ortoleva and J. Ross, *Phase waves in oscillatory chemical reaction*, J. Chem. Phys **58**, 5673–5680, 1973.

[66] Edward J. Reusser and Richard J. Field, *The transition from phase waves to trigger waves in a model of the Zhabotinskii reaction*, Journal of the American Chemical Society **101(5)**, 1063–1071, 1979.

[67] Rubin R. Aliev and Vadim N. Biktashev, *Dynamics of the oscillation phase distribution in the bz reaction*, J. Phys. Chem **98**, 9676–9681, 1994.

[68] C. P. Schenk, P. Schütz, M. Bode, and H.-G. Purwins, *Interaction of self-orginized quasiparticles in a two-dimensional reaction-diffusion system: The formation of molecules*, Phys. Rev. E **57**, 6480–6486, 1998.

[69] M. Bode, A. W. Liehr, C. P. Schenk, and H.-G. Purwins, *Interaction of dissipative solitons: Particle-like behaviour of localized structures in a three-component reaction-diffusion system*, Physica D **161**, 45–66, 2002.

[70] G. Bordiougov and H. Engel, *Oscillatory dispersion and coexisting stable pulse trains in an excitable medium*, Phys. Rev. Lett. **90(14)**, 148302, 2003.

[71] John Ross, Stefan C. Müller, and Christian Vidal, *Chemical Waves*, Science **240**, 460–645, 1988.

[72] J.Rademacher, *Phd thesis, university of minnesota*, 2004.

[73] Björn Sandstede and Arnd Scheel, *Absolute versus convective instability of spiral waves*, Phys. Rev. E **62(6)**, 7708, 2000.

[74] R. Gardner, *On the structure of the spectra of periodic travelling waves*, J. Math. Pures Appl. **72**, 415–439, 1993.

[75] Martin Krupa, Björn Sandstede, and Peter Szmolyan, *Fast and slow waves in the FitzHugh-Nagumo equation*, J. Diff. Eq. **133**, 49–97, 1997.

[76] P. Hirschberg and E. Knobloch, *Šil'nikov-Hopf bifurcation*, Physica D **62**, 202–216, 1993.

[77] A. R. Champneys and A. J. Rodriguez-Luis, *The non-transverse Shil'nikov-Hopf bifurcation: uncoupling of homoclinic orbits and homoclinic tangencies*, Physica D **128**, 130–158, 1999.

[78] N. Manz and O. Steinbock, *Dynamics of excitation pulses with attractive interaction: Kinematic analysis and chemical wave experiments*, Phys. Rev. E. **70**, 066213, 2004.

[79] M. Abeles, *Corticonics*, Cambridge University Press, England, 1991.

[80] G.B. Ermentrout and J.D. Cowan, *A mathematical theory of visual hallucination patterns*, Biological Cybernetics **34**, 137–150, 1979.

[81] J. Christoph and M. Eiswirth, *Theory of electrochemical pattern formation*, Chaos **12**, 215, 2002.

[82] F. Plenge, H. Varela, and K. Krischer, *Asymmetric target patterns in one-dimensional oscillatory media with genuine nonlocal coupling*, Phys. Rev. Lett. **94**, 198301, 2005.

[83] Mauricio Barahona and Louis M. Pecora, *Synchronization in small-world systems*, Phys. Rev. Lett. **89**, 054101, 2002.

[84] Daniel M. Abrams and Steven H. Strogatz, *Chimera states for coupled oscillators*, Phys. Rev. Lett. **93**, 174102, 2004.

[85] Shinichiro Shima and Yoshiki Kuramoto, *Rotating spiral waves with phase-randomized core in nonlocally coupled oscillators*, Phys. Rev. E **69**, 036213, 2004.

[86] Yoshiki Kuramoto, Dorjsuren Battogtokh, and Hiroya Nakao, *Multiaffine chemical turbulence*, Phys. Rev. Lett. **81**, 3543–3546, 1998.

[87] Ernesto Nicola, *PhD thesis, Technische Universität Dresden*, 2001.

[88] Ernesto M. Nicola, Michal Or-Guil, Wilfried Wolf, and Markus Bär, *Drifting pattern domains in a reaction-diffusion system with nonlocal coupling*, Phys. Rev. E **65**, 055101, 2002.

[89] M. Hildebrand, H. Skødt, and K. Showalter, *Spatial symmetry breaking in the Belousov-Zhabotinsky reaction with light-induced remote communication*, Phys. Rev. Lett. **87**, 088303, 2001.

[90] Ernesto M. Nicola, Markus Bär, and Harald Engel, *Wave instability induced by nonlocal spatial coupling in a model of the light-sensitive Belousov-Zhabotinsky reaction*, Phys. Rev. E **NN**, accepted, 2006.

[91] A.J. Homburg and B. Krauskopf, *Resonant homoclinic flip bifurcations*, J. Dyn. Diff. Eq. **12**, 749–774, 2000.

[92] B. E. Oldeman, B. Krauskopf, and A. R. Champneys, *Numerical unfoldings of resonant homoclinic flip bifurcations*, Nonlinearity **14**, 597, 2001.

[93] Dan Tanaka and Yoshiki Kuramoto, *Complex Ginzburg-Landau equation with nonlocal coupling*, Phys. Rev. E. **68**, 026219, 2003.

[94] A. Doelman, B. Sandstede, A. Scheel, and G. Schneider, *The dynamics of modulated wave trains*, preprint.

[95] *http://scienceworld.wolfram.com/chemistry/lawofmassaction.html*.